

2009

Prospects for Large-Scale Energy Storage in Decarbonised Power Grids

INTERNATIONAL ENERGY AGENCY

SHIN-ICHI INAGE

WORKING PAPER

INTERNATIONAL ENERGY AGENCY

The International Energy Agency (IEA), an autonomous agency, was established in November 1974. Its mandate is two-fold: to promote energy security amongst its member countries through collective response to physical disruptions in oil supply and to advise member countries on sound energy policy.

The IEA carries out a comprehensive programme of energy co-operation among 28 advanced economies, each of which is obliged to hold oil stocks equivalent to 90 days of its net imports. The Agency aims to:

- Secure member countries' access to reliable and ample supplies of all forms of energy; in particular, through maintaining effective emergency response capabilities in case of oil supply disruptions.
- Promote sustainable energy policies that spur economic growth and environmental protection in a global context – particularly in terms of reducing greenhouse-gas emissions that contribute to climate change.
 - Improve transparency of international markets through collection and analysis of energy data.
 - Support global collaboration on energy technology to secure future energy supplies and mitigate their environmental impact, including through improved energy efficiency and development and deployment of low-carbon technologies.
 - Find solutions to global energy challenges through engagement and dialogue with non-member countries, industry, international organisations and other stakeholders.

IEA member countries:

Australia
Austria
Belgium
Canada
Czech Republic
Denmark
Finland
France
Germany
Greece
Hungary
Ireland
Italy
Japan
Korea (Republic of)
Luxembourg
Netherlands
New Zealand
Norway
Poland
Portugal
Slovak Republic
Spain
Sweden
Switzerland
Turkey
United Kingdom
United States



International
Energy Agency

© OECD/IEA, 2009
International Energy Agency
9 rue de la Fédération
75739 Paris Cedex 15, France

Please note that this publication is subject to specific restrictions that limit its use and distribution. The terms and conditions are available online at www.iea.org/about/copyright.asp

The European Commission also participates in the work of the IEA.

Prospects for Large-Scale Energy Storage in Decarbonised Power Grids

Shin-ichi Inage

Summary of Key Points

This paper focuses on the potential role that large-scale energy storage systems can play in future power systems. The starting point and basis for simulations is the Energy Technology Perspectives 2008 (ETP) BLUE scenario for power supply (IEA, 2008). According to the scenario, increased use of renewable energy and nuclear technologies can play an important role in reducing CO₂ emissions dramatically in the power sector. Through the increased use of these technologies, the use of fossil fuel powered plants, and consequent CO₂ emissions, will be reduced. Wind power and solar power provides 12% and 11% of global electricity generation by 2050 in the BLUE Map scenario. Variable output renewable technologies such as wind and solar are not dispatchable. With large shares of these technologies, steps would need to be taken to ensure the continued reliable supply of electricity.

While related issues include voltage and frequency variations, inter alia, this report focuses on frequency stability. Constant balance of demand and supply is essential to achieve this, and, in the majority of today's power systems, mid load technologies such as coal and gas and in some cases hydro, play the chief role in this regard. The main focus of this paper is to investigate the storage growth and total global storage capacity needed between 2010 and 2050, to assist in the balancing of power systems with large shares of variable renewables.

Variable renewable energies are associated with weather-related power output variations, which consist of short term variations on a scale of seconds to several minutes, superimposed on long term variation on the scale of several hours. Frequency change depends on the short-term variation, therefore this report focuses on short-term variations.

Although the output of individual wind or solar plants can vary considerably, wide geographical dispersal of wind power and PV plants reduces the net variation of many plants as seen by the system as a whole. The net output variation of renewables is an important parameter in this analysis. To date, the impact of this smoothing effect varies from region to region. If the outputs of individual wind and PV plants are uncorrelated, the extent of variation decreases with the inverse square root of the overall number of plants. On the other hand, over relatively small areas with large numbers of wind and PV plants, plants may show strong correlation with each other. In such situations a significant net variation will remain.

The extent to which a power system can accommodate variations in supply is governed to a large extent by its flexibility - a measure of how fast and how much the system can quickly increase or decrease supply or demand, to maintain balance at all times. A range of measures exist to increase the flexibility of power systems, and thus the extent to which they can accommodate variable renewables. This paper looks at one of these measures - storage.

Another option is to interconnect among adjacent power systems. For instance, in Western Europe (WEU), interconnected power grid and electricity trading play an important role.

Flexible power plants such as gas and hydro can act as reserves to provide for deficits in wind power generation across the interconnected area, while at the same time the geographic smoothing effect is increased because the total area is larger. At present, in Denmark, where the average share of wind power is approximately 20%, effective balancing of supply and demand is facilitated through electricity trade with other Scandinavian countries.

However, taking for example a cluster of interconnected systems lying under a single weather system, all with a high share of variable renewables, trade of electricity may not be relied upon for fast access to additional electricity during low wind / solar periods, nor to dispose of surpluses, because deficits and surpluses among all such systems will coincide to a large extent. Moreover, reduced flexible power plant capacity over the entire region in 2050, due to partial displacement by renewables and nuclear, as seen in the BLUE Scenario, may lead to a lack of flexible reserves. To provide for such cases, internal solutions are needed to be in place. Balance will not be maintained by interconnectors alone, and system designers and operators should look at additional measures such as energy storage, as well as load leveling and plug-in electric vehicles (the latter are not the focus here).

By way of illustration, the analysis estimated the required capacity of energy storage in WEU. Recent measurements of wind power variation in WEU show that the maximum net variability over 10-15 minutes is 6-12% and the average variability is perhaps 20-30% of that value. The analysis shows that if a 5% net variation were to be maintained then even at the high wind and solar shares projected for 2050 under the ETP BLUE scenario, no energy storage capacity would be required in the WEU. However, in areas in which the smoothing effect is limited, net output variation larger than 5% would be seen in some parts of WEU. Simulations of wind power variation levels between 5% and 30% yield estimates of energy storage capacity in the WEU ranging from 0GW to 90GW in 2050. The balance between the demand and the supply was calculated for every 0.1 hr (i.e., 6 minutes). To estimate energy storage worldwide, net variations were assumed as 15% and 30%. Simulations undertaken suggest that worldwide energy storage capacity ranging from 189GW to 305GW would be required. Under smaller variations, the capacity will decrease as in the WEU case. Rather than specific numerical values, it is the relative amounts of storage against net variability that is most important. Therefore high quality assessment of the net variation, taking into account the output of power plants across the entire system as well as demand variation, is fundamental to accurate identification of required storage capacities.

As mentioned above, as each storage system has different specifications, the optimal arrangement of these systems depends on circumstances in individual countries. In Annex 1, the current technical potential of NaS cells, pumped hydro, redox flow cells, Compressed Air Energy Storage (CAES), electric double-layer capacitors, Li-ion batteries, Superconducting Magnetic Energy Storage (SMES) and flywheel systems is reviewed. Reducing costs of such storage technologies may be a key to expanding the use of energy storage technologies to keep pace with the growth of variable renewables.

<p>The views expressed in this Working Paper are those of the author(s) and do not necessarily represent the views or policy of the International Energy Agency or of its individual Member countries. As this paper is a Work in Progress, designed to elicit comments and further debate, comments are welcome, directed to the author at shin-ichi.inage@iea.org.</p>

TABLE OF CONTENTS

Summary of Key Points.....	1
INTRODUCTION	5
1. BACKGROUND INFORMATION	7
2. GENERAL CHARACTERISTICS OF THE POWER GRID.....	13
3. POWER QUALITY	15
4. ENERGY STORAGE SYSTEMS	17
5. PROSPECTS OF ENERGY STORAGE GROWTH	21
6. CONCLUSIONS AND RECOMMENDATIONS.....	37
7. REFERENCES	39
ANNEX 1: BRIEF REVIEW OF ENERGY STORAGE SYSTEMS.....	43
ANNEX 2: NUMERICAL ALGORITHMS	84
ANNEX 3: COMPARISON WITH OTHER SCENARIOS	89

INTRODUCTION

Renewable energy is a key technology in the effort to reduce CO₂ emissions. The *Energy Technology Perspectives 2008* (IEA, 2008) BLUE Map scenario estimates that renewables could contribute as much as 21% of the reductions in energy-related CO₂ emissions called for by 2050. Electricity, unlike other energy carriers, can only be stored in large quantities in rare circumstances, and always in other forms such as chemical, potential, or thermal energy. As a consequence, electricity supply and demand must always be balanced simultaneously. The need to ensure supply that matches demand under all circumstances poses particular challenges for variable renewable power options such as wind and solar generation, whose supply heavily depends on season, time and weather conditions.

A number of strategies exist to deal with the challenges of variability and demand-supply balance presented by variable renewables, including having a backup supply capacity based on storable fuels such as fossil fuels or biomass, ensuring a wider regional dispersion of variable renewable plants to cancel the variability among sites, and developing technologies that can produce more controllable electricity across a wider range of weather conditions. Further interconnections between grids and energy storage resources can also enhance the grid's ability to deal with stability problems.

In addition, as renewable capacity increases, the net variability in the combined output of many variable renewables is smoother than the output of individual renewable power plants. To accurately evaluate the relationship between high penetration of renewables and energy storage, this “smoothing effect” must be considered.

This report describes the development of a simplified algorithm to determine the amount of storage that compensates for short-term net variation of wind power supply and assesses its role in light of a changing future power supply mix. It also examines the range of options available to power generation and transmission operators to deal with variability. This will be a valuable input to the complex topic of determining the necessary amount of storage capacity required over time in power systems with a high share of variable generation sources.

The discussion in this paper focuses on the technical characteristics of relatively large-scale energy storage options to be applied to renewables and their potential role in power systems. The starting point is the *Energy Technology Perspectives 2008*, BLUE Map scenario of power supply.

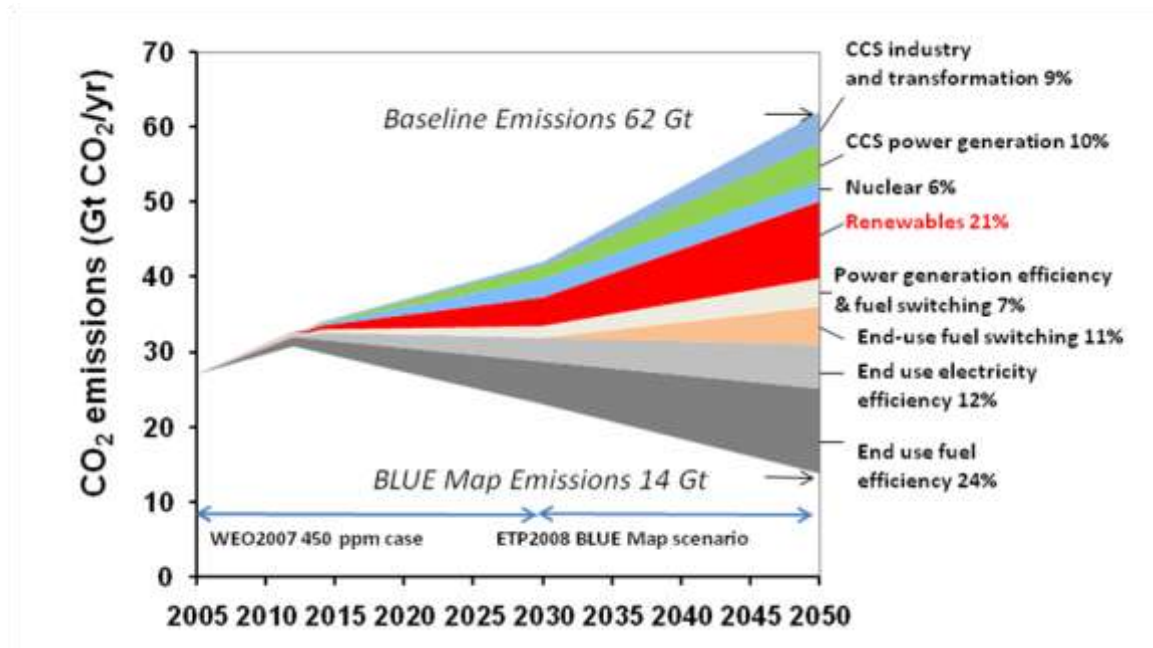
The following questions are addressed:

- What energy storage capacities will be needed under the BLUE Map scenario in different parts of the world?
- What influence does the smoothing effect have on determining the required storage capacity?
- How can the role of storage options in the electricity system be properly assessed?
- What are the current and future characteristics of energy storage technology options?
- What is the future role of energy storage systems, given the potential of competing strategies to deal with variability?

1. BACKGROUND INFORMATION

The BLUE Map scenario defined by IEA, aims to cut energy-related CO₂ emissions in half between 2005 and 2050. Figure 1 shows CO₂ reduction based on the BLUE Map scenario. Renewables account for 21% of the total global CO₂ emission mitigation target in 2050. This contribution comes on top of significant renewable growth in the Baseline scenario. For example, the share of renewables in power generation rises to 46% in 2050, compared with around 19% today. The bulk of the growth of renewables is based on variable renewable supply options: wind, solar and hydro power each grows to around 5000TWh. Given the high share of variable renewables in the total global power supply, power system planning faces an emerging challenge that will require engineering solutions to maintain electricity quality. A power supply based on variable renewables will always be subject to weather conditions.

Figure 1: CO₂ reduction during 2005-2050 based on the BLUE Map scenario



Source: IEA, 2008.

To maintain electricity quality, balancing the demand and supply is essential. Middle load, usually supplied by natural gas combined-cycle plants, can play an important role in balancing the demand and supply, and can also serve as backup capacity in case of a renewable power supply shortfall.

A much higher share of renewable power with variable generation will raise a number of engineering issues in the future:

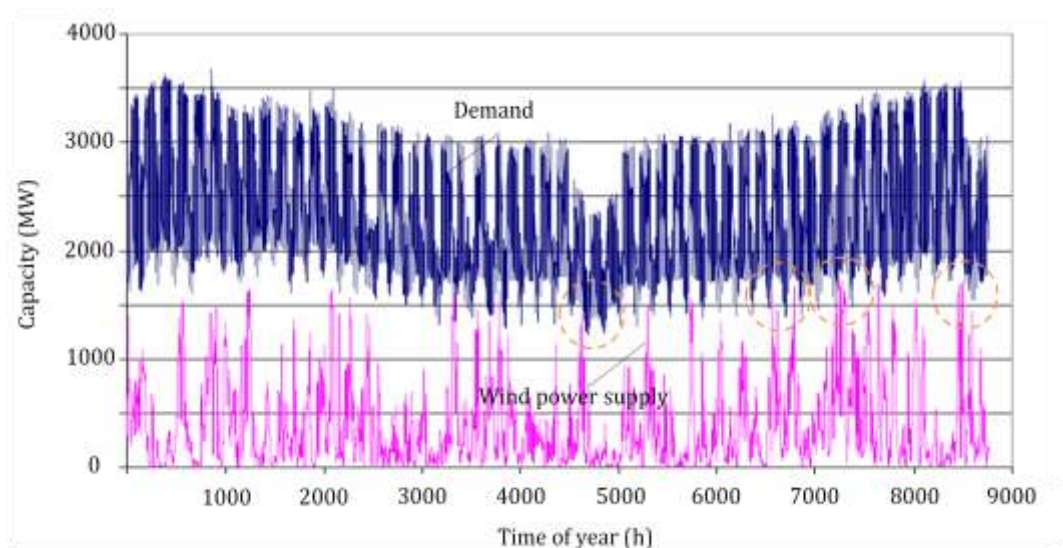
- 1) Short-term variation: variability on the scale of seconds or minutes will cause larger deviations of power system frequency.
- 2) Hourly variation: variability on the scale of hours will increase the difficulty of hourly generation dispatch and unit commitments, and influence the electricity trade between power systems.
- 3) Longer-term variation: variability on the scale of days or months, which influences the stable supply of wind power

Hourly and long-term variations are relatively forecastable, because they depend on overall weather conditions. Therefore, they might be absorbed by flexible generation capacity, transmission interconnection, and load leveling. On the other hand, short-term variations are quite random and difficult to forecast. Under a high share of renewables, both variations should be discussed, but this working paper focuses on short-term variations of power system frequency. Several possibilities are explored to maintain electricity quality, particularly energy storage technologies.

The variability characteristics of solar, wind and impoundment hydro power vary substantially from season to season, day to day, time to time. Wind turbines may be shut off during storm conditions that could last for hours. Wind speeds may fall to zero or very low levels over large areas for days. Solar power is not generated at night (although thermal storage can address some of the diurnal variation) and insolation levels may be significantly reduced in winter, especially at higher latitudes. Solar power may also fluctuate depending on cloud levels and the moisture content of the air. Finally, hydro power may be absent in dry years, depending on the water inflow (glaciers or rainfall). These different variability characteristics require different types of response strategies.

Existing regional grids with high shares of variable renewable do not always provide a relevant reference for a future power system with high shares of renewables. The reason is that such grids do not operate as islands; rather, they are well connected to other grids that stabilize their operation. This is the case for Denmark and Northern Germany. Figure 2 compares demand and supply of wind power in Denmark during 2001.

Figure 2: Example of the demand and supply of wind power in Denmark in 2001



Source: P. Sørensen, 2004.

In that year, the demand and supply of wind power corresponded fairly closely. When excess power was available, it could be exported through interconnections with Norway, Sweden and Germany. Conversely, power could be imported in periods of shortfall. Therefore, in Denmark, no counter measure would be needed to mitigate short-term and long-term variations, despite an anticipated greater share of wind power. Interconnectors provide a key short- and medium-term option to deal with the variability of renewable power generation, but will not be

sufficient to deal with large grids on a continental scale with high renewables penetration, as in the BLUE Map scenario.

A severe drop of wind power in Germany during a one-week period in 2004 was reported in Wind Report 2005, e-on Netz GmbH. The data indicate that the difference between the maximum and minimum power available reached 6000MW, and that the maximum drop rate was approximately 16MW/min.

This suggests that wind power capacity can come online and offline at a rate of about 3% per minute. This is a much slower rate than that of a single wind turbine, where total capacity can come online or offline on a time scale of seconds. In comparison, a natural gas combined-cycle (NGCC) generator can come online and offline at a maximum rate of 8% per minute. This suggests that the variability of distributed renewables can be lessened through proper spatial distribution.

Figure 3 shows the concept of an interconnection grid and electricity trading. Thermal power plants in Area 2 absorb excess wind power produced in the area on the left, and conversely supply power to the area on the left with wind power fall short. In this system, the availability of sufficient thermal power plant capacity in Area 2 and enough interconnection capacity between both areas are essential. To promote this system, a greater investment in the grid would be required as renewable power increases.

Figure 4 shows the relationship between wind power supply and the net trade in western Denmark in 2006. The graph demonstrates that net trading is strongly correlated with the wind power supply as the concept of Figure 3 is put into practice.

In the BLUE Map scenario, the share of renewable power in the generation mix increases significantly while the share of power from thermal plants declines. Therefore, insufficient thermal power plant capacity remains to absorb renewable power variations. The concept of Figure 3 is not applicable.

Figure 3: Balancing demand and supply through the interconnected grid. In the top figure, surplus wind power supply is exported through the grid, while in the bottom figure power is imported.

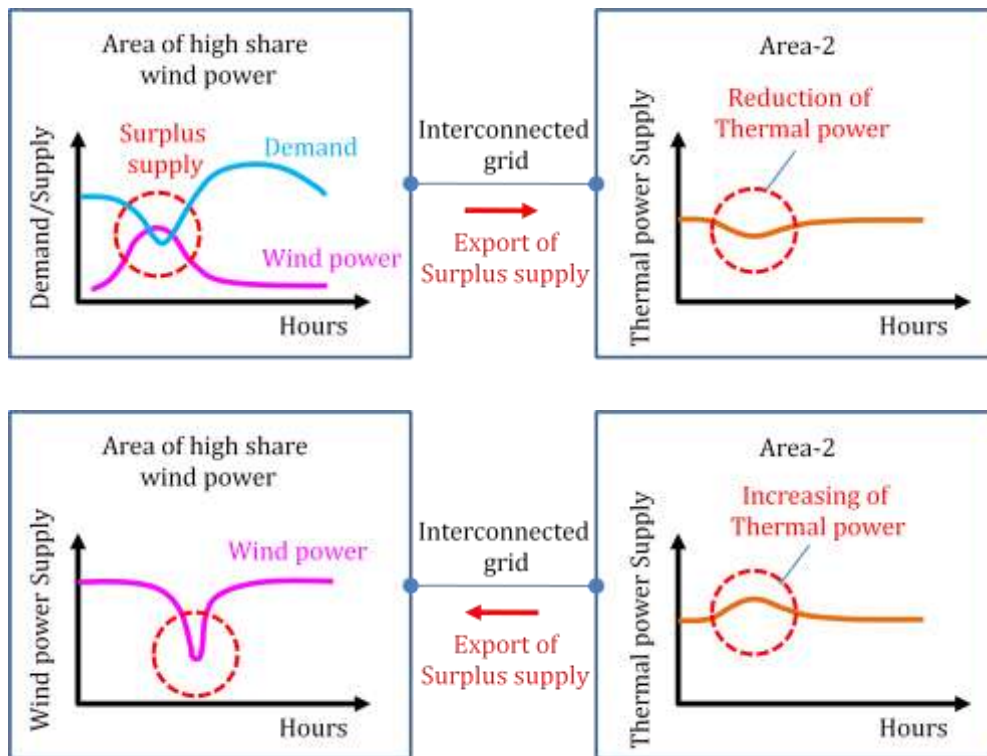
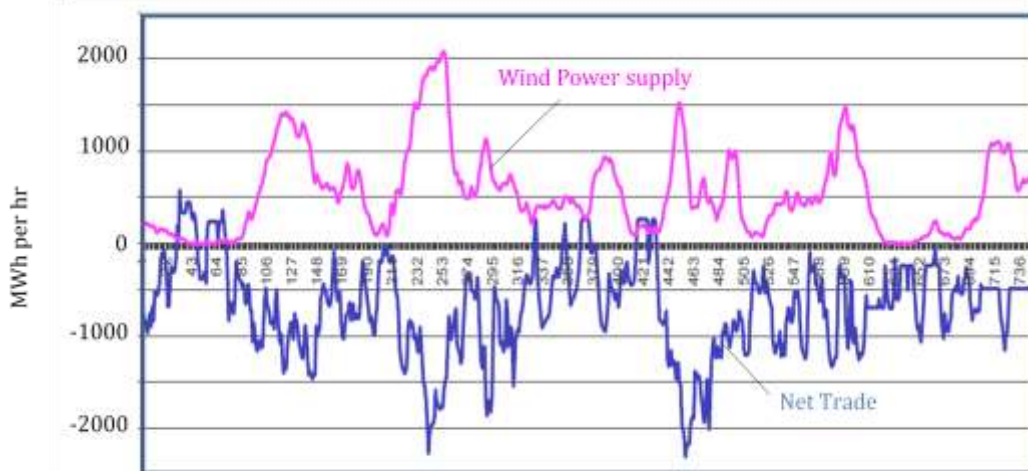


Figure 4: Comparison of the wind power supply and net trade in western Denmark at 2006



Source: H. Sharman, 2007.

An interesting case of a power system with a high proportion of wind power is found in Spain and Portugal on the Iberian Peninsula. In 2008, there was a day when the share of wind power in the total power supply reached 23% in Spain. This high proportion created power quality problems that have since been resolved through better interconnections within Spain. In addition, Spain has significant pumped hydropower capacity that can mitigate power supply variations during the operation.

For this working paper, a new numerical simulation method has been developed to estimate the necessary storage capacity for a given amount of variable renewables, taking into account other solutions such as backup capacity, interconnectors and spatial distribution of renewable power generation options.

This analysis focuses on the BLUE Map scenario, whose framework condition of halving emissions has a dramatic impact on power systems. Such a system structure is radically different than that of the Baseline scenario. However, total power supply investment costs are not significantly higher than in the Baseline scenario because of substantial end-use efficiency efforts that reduce electricity demand and mitigate the power supply investment needs.

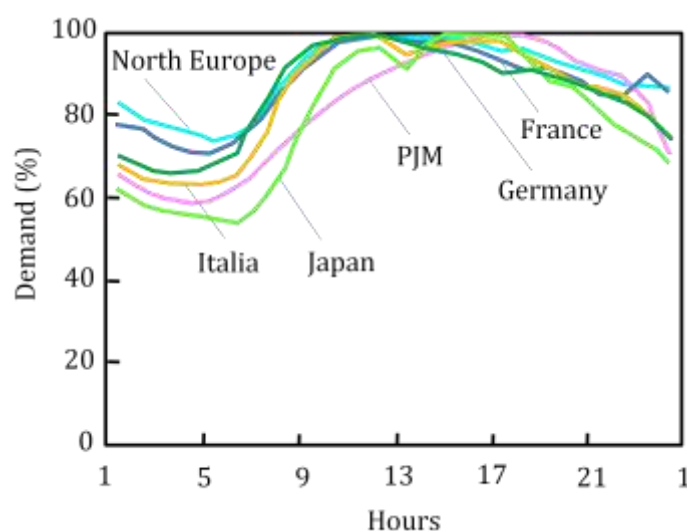
2. GENERAL CHARACTERISTICS OF THE POWER GRID

Grid Operation and Load Curves

Load duration curves can be split into base and peak loads. Base loads are generated by plants whose output is difficult to change; they therefore operate most of the time at full capacity. Base loads are generally served by either high-efficiency fossil-fired or nuclear reactor power plants with low production cost. Peak loads are usually served by natural gas combined-cycle plants, gas turbine generation, or hydropower plants that can change their output in a short time, although with high production cost.

Daily load curves for six electricity systems are shown in Figure 5. Each load curve represents the day of the year with the maximum load variation and is normalized by the maximum load, which is equal to 100%. In Japan, the peak demand ranges from 50% to 100% of maximum. However, in North Europe, PJM (Mid-Central Atlantic region of the U.S.), Italy, France and Germany, the difference is much smaller. The different load curve shapes depend on climate conditions (e.g. for air conditioning), lifestyle, and demand structure (e.g. industry demand is often flat when plants operate full time).

Figure 5: Comparison of daily load curves

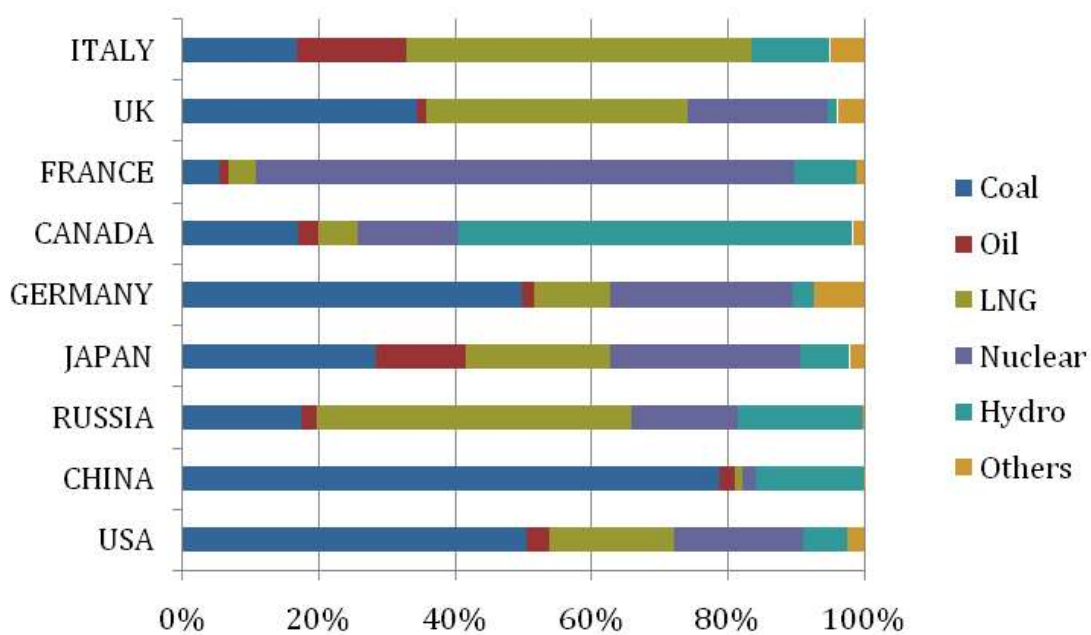


Source: IEEJ (*The Institute of Energy Economics, Japan*), 2005.

In Japan, the large load variations are met by a number of peak load stations such as pumped hydro and thermal power fueled by natural gas or oil. In particular, natural gas combined-cycle and pumped hydro plants are suitable for following the short cycle of demand variation. Variable renewable power generation options may or may not be suited to match fluctuating demand. For example, solar PV supplies broadly match air conditioning demand, since air conditioning is needed on hot days when the sun shines. Wind power may match such demand less favorably, since it depends on only wind speed that can be independent of air temperature.

For countries with comparatively small demand variations, a high share of coal or nuclear-based load stations may be acceptable. The mixes of power generation resources found in different countries are compared in Figure 6. These shares are a result of demand structure, energy resources, technology availability and energy policy strategy. Note that in France, Germany, Japan, China and the United States, the total share of base load contributed by coal and nuclear power ranges from 50% to 90%, which will limit their potential to increase the share of variable renewables.

Figure 6: Comparison of power generation mix



Source: IEA Electricity Information, 2006.

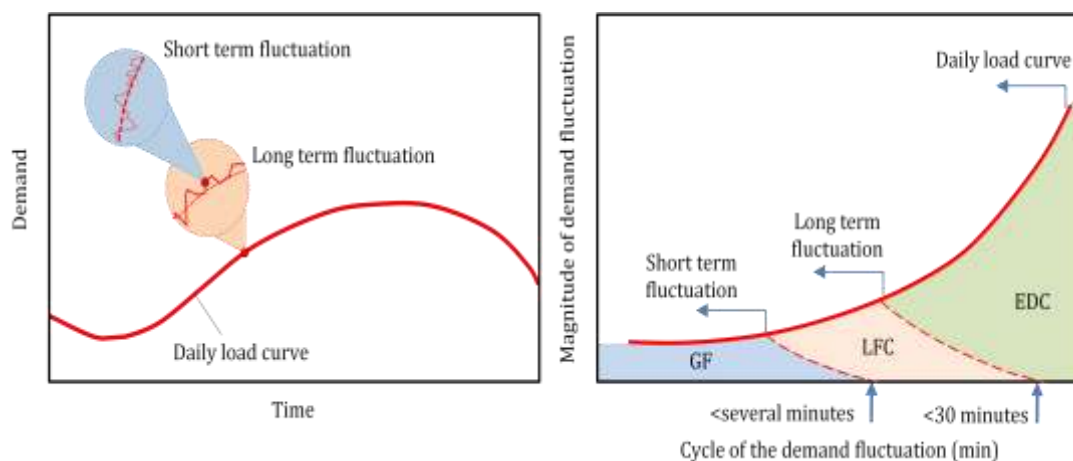
3. POWER QUALITY

While related issues include voltage and frequency stability, inter alia, this working paper limits itself to the issue of frequency stability in systems with increasing shares of variable renewable generation assets.

As shown in Figure 5, electricity demand constantly changes. The actual demand variations consist of the superposition of short-term and long-term variations, which depend on each user's situation. Without a balance of demand and supply, frequency is not stable. Frequency falls when demand exceeds supply and rises when supply exceeds demand. Therefore, the power supply must be completely balanced to produce stable power system frequency.

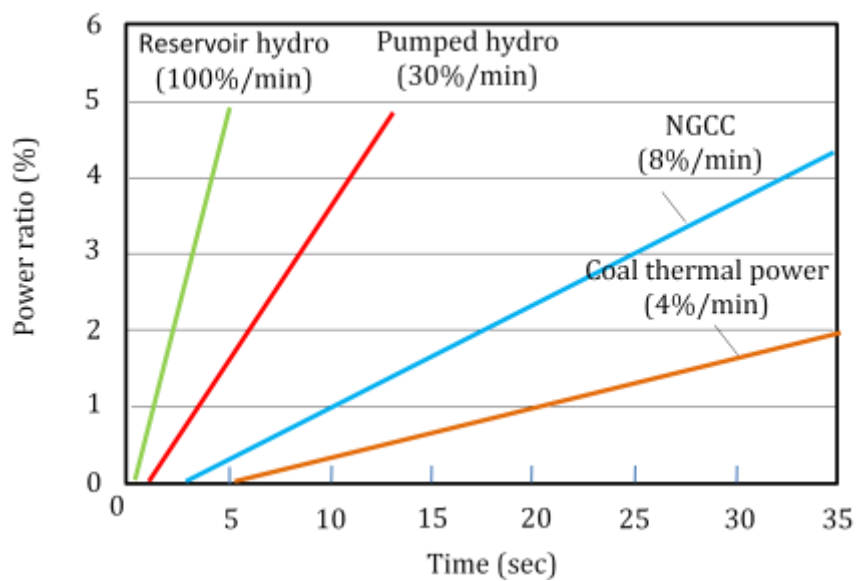
Middle load power plants have a control system to minimize the frequency change. To balance the load between supply and demand, hydro and thermal power plants modify their output through governor-free (GF) controls for short-cycle demand variations. For an intermediate cycle, a load frequency control (LFC) system is used. For a long cycle, an economic load dispatching control (EDC) system controls the balance. Figure 7 compares the time scales and functions of the three different frequency control techniques.

Figure 7: Comparison of frequency controllers



Electric frequency is controlled within a small deviation: for example, in Japan the standard is 0.2-0.3Hz; in the U.S. it is 0.018-0.0228Hz; and in the European UCTE it is 0.04-0.06Hz. As renewables increase, the potential for fatal frequency changes grows, since such generators rarely have frequency control systems and can produce large variations in output as weather conditions change. Figure 8 compares the adjustable load rates of several types of power plants. General hydro plants have the fastest response times, able to change from full power to zero and vice versa within one minute. On the other hand, coal thermal power plants respond comparatively slowly. Using a suitable combination of these power plants yields the optimal frequency. As mentioned in Section 1, hourly and long-term variations are reacted by EDC, while short-term variation that is quite random should be absorbed by LFC or GF.

In existing power systems with a low share of renewables, the total capacity of resources needed to support frequency regulation is adequate. However, with a high share of variable renewables, a shortage of regulation capacity is anticipated.

Figure 8: Comparison of the adjustable load rates of four power plants

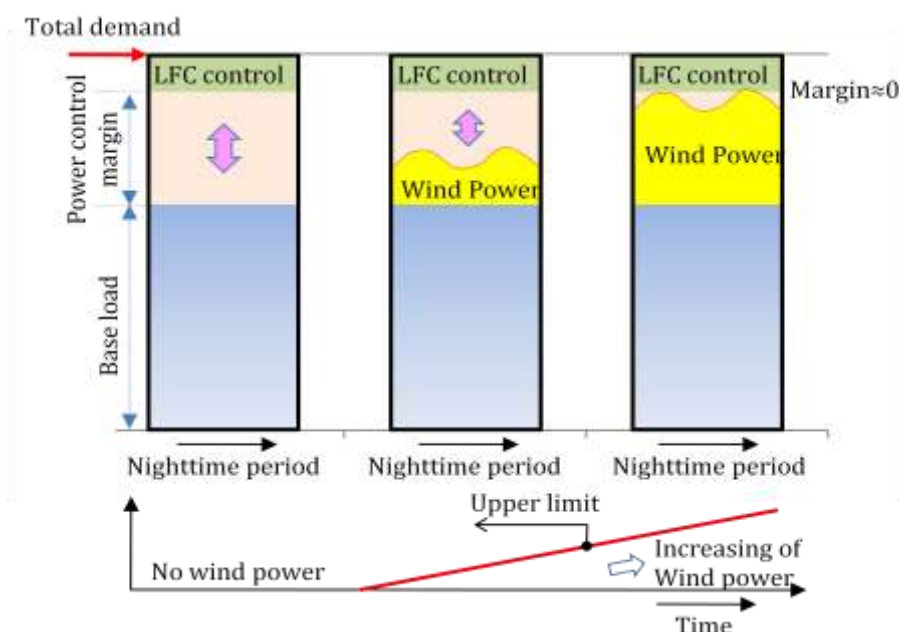
Source: Japanese Wind Power Association, 2004.

4. ENERGY STORAGE SYSTEMS

System-Related Issues under Massive Deployment of Renewables

Electricity demand decreases at night. Base load generation, such as that supplied by nuclear power plants and large-scale thermal power plants with coal-firing boilers, are unsuited to controlling supply. Therefore, certain power control margins are maintained in the grid. As the proportion of wind generation increases, those power control margins will decrease (Figure 9).

Figure 9: Influence of wind power on power control margin at night



The wind power variation consists of the superposition of short-term variations on the scale of seconds to several minutes, and long-term variations that occur over several hours. Wind turbines will be distributed geographically throughout individual countries. In that case, power variations from different turbines in different areas should be slightly correlated, while the cumulative generation of all the turbines should have less net variation than an individual turbine or groups of turbines in a given area. This is the wind farm smoothing effect, which can be observed on many scales. In the present simulation, the smoothing effect was focused throughout the assessment area. As shown in Figure 10, such a smoothing effect would be noticeable given a combination of wind generators distributed in non-correlated areas. Figure 11 shows actual data that demonstrate the smoothing effect in Germany. In Germany, power variations for individual wind turbines were clearly greater than net variations observed in a group of wind farms and for all German wind farms. For instance, the net variation of several countries in Western Europe ranges from 5.5 to 11%, while the net variation of several areas in the US ranges from 24% to 35%.

Even with smoothing effect, the short- and long-term net variations will remain, even though the magnitude will be lower than in the case of each wind turbine. These net variations influence the balancing of demand and supply. To mitigate short-cycle demand variations, as described above, the governor-free (GF) operations of hydro and thermal power plants would be applied. For intermediate-cycle variations the load frequency control (LFC) system would be used, while for long-cycle variations an economic load dispatching control (EDC) would be used.

Figure 10: Wind farm smoothing effect on net power variation

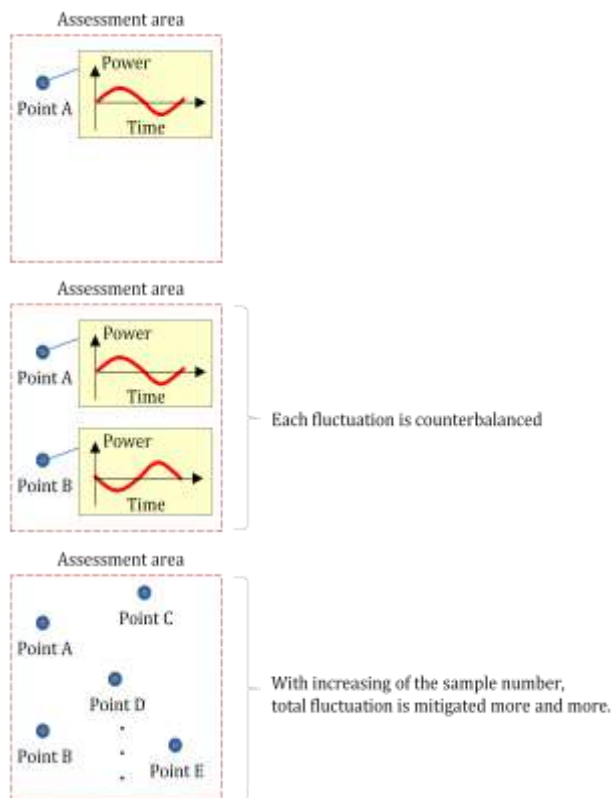
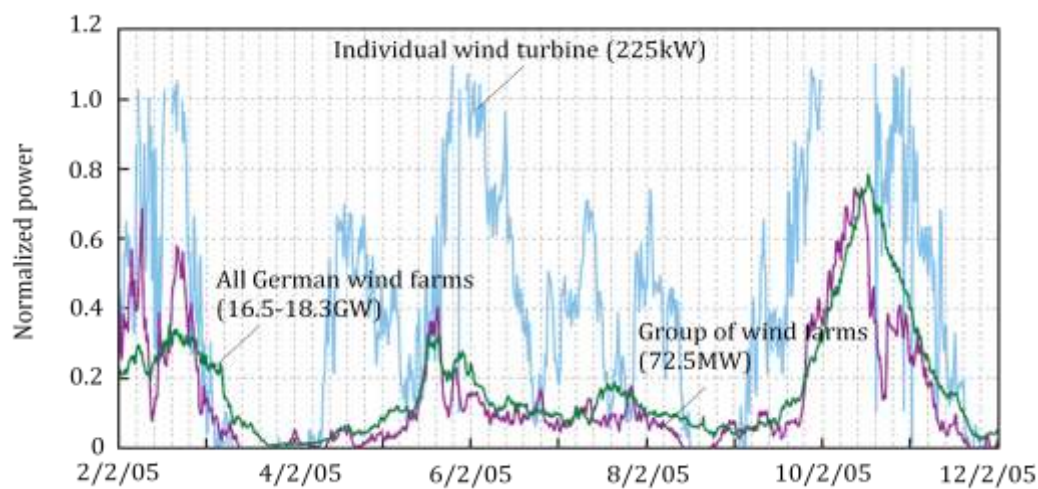


Figure 11: Smoothing effect of wind power in Germany.



Source: IEA, 2008c.

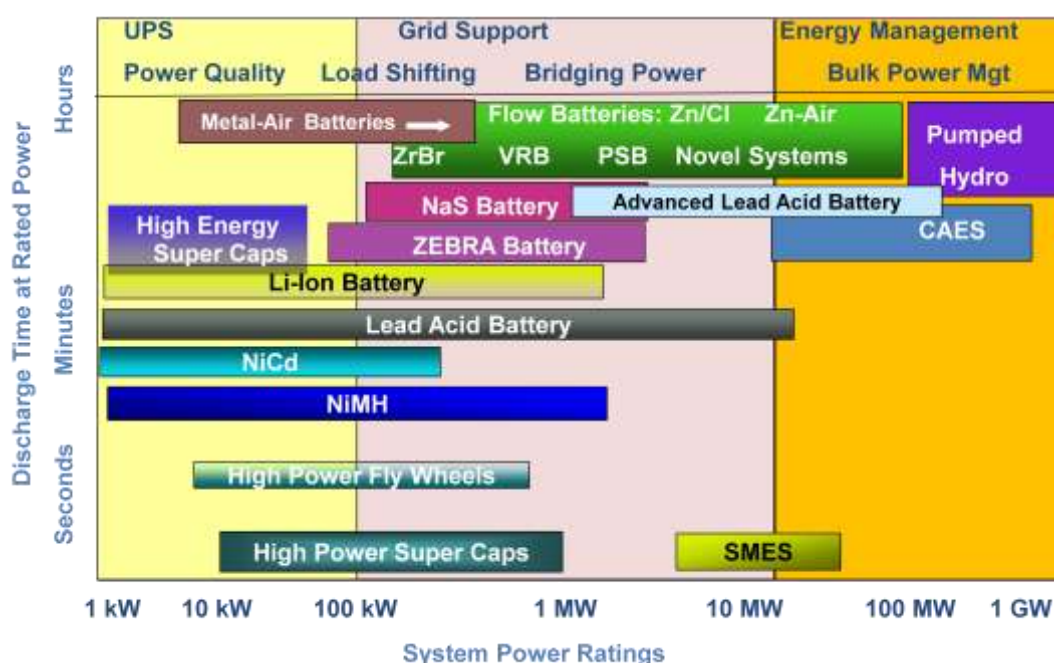
On the other hand, with a higher share of renewables, which is equivalent to a lower share of thermal power, the installed capacity of wind generation might be limited by the balance between the power control margin and total supplies of wind power without any counter measures.

Characteristics of Energy Storage Systems

The essential characteristics of an energy storage system are: 1) Storage properties, which include energy density, output density, energy storage efficiency, storage scale and charge/discharge times. 2) Operation properties, which include start-and-stop times, load response, partial load feature, lifetime, and reliability. 3) Safety, location, construction time and lead time.

The significance of the above characteristics depends on the purposes of use and type of utility. Complete evaluations based on economic and environmental considerations are required before reaching a final decision on purchase and deployment. General features of several energy storage systems are compared in Figure 12.

Figure 12: Comparison of energy storage technologies



Source: EPRI, 2008.

Specifications are compared in Table 1. Annex 1 reviews NaS cell, pumped hydro, redox flow cell, compressed air energy storage (CAES), electric double-layer capacitor, Li-ion batteries, superconducting magnetic energy storage (SMES) and flywheels, and provides their latest status.

The existing energy storage capacity of 100GW worldwide mainly consists of pumped hydro plants. Pumped hydro has a successful and reliable operating history of more than 50 years. There are many options among electricity storage systems, with different specifications including, in particular, discharge times. The best choice of energy storage systems are indicated for many purposes and areas. In the next chapter, the energy storage capacity required to achieve the BLUE Map scenario will be evaluated.

Thermal energy storage, in which energy produced by a generator or solar power plant is stored as heat, should also be mentioned. It can play an important role, particularly in the use of large-scale solar thermal plants. However, as the main purpose of this working paper is to estimate the influence of the high penetration of renewable power on electricity quality, this energy storage option is not addressed.

Table 1: Comparison of specifications of typical energy storage systems

Storage Type	Power	Duration of Discharge	Efficiency (%)	Lifetime	Total Capital Cost (USD/kW)
CAES (100-300 MW, Underground)	15-400 MW	2-24 hrs	54 (Eff _{NG} =1)* 76(Eff _{NG} =0.54)* 88(Eff _{NG} =0.39)*	35 years	600-750
Pumped Hydro	250 MW >1 GW	12 hrs	87	30 years	2700-3300 Upgrade:300**
Li Ion	5 MW	15 min to several hrs	90 (DC)	15 years	4000-5000
Lead Acid	3-20 MW	10 sec to several hrs	75-80 (DC) 70-75 (AC)	4- 8 years	1740-2580
NaS	35 MW	8 hrs	80-85 (DC)	15 years	1850-2150***
VRB Flow Cell	4 MW	4-8 hrs	75-80 (DC) 63-68 (AC)	10 years	7000-8200
ZnBr Flow Cell	40-100 kW, 2 MW	2-4 hrs	75-80 (DC) 60-70 (AC)	20 years	5100-5600
High Power Flywheel	750-1650 kW	15 sec to 15 min	93	20 years	3695-4313
ZEBRA	<10 MW	Up to 8 hrs	80-85 (DC)	Over 1500 cycles shown	1500-2000***
Fe/Cr Flow Battery	<10 MW	2-4 hrs	50-65	20 years	200-2500***
Zn/Air	20 kW-10 MW	3-4 hrs	40-60	a few hundred cycles	3000-5000***
SMES	1-3 MW	1-3 sec	90	>30,000 cycles	380-490
SMES****	100 MW-200 MW	100 sec (MWh) 0.5-1h (100MWh) 5-10 hr (GWh)	90	>30,000 cycles	700-2000
Ultra capacitors	10 MW	Up to 30 sec	90	>500,000 cycles	1500-2500

*For CAES, the following round-trip efficiency is usually used:

$$\eta = \frac{1.0 \text{ kWh}}{(4220/3600) * \text{Eff}_{NG} + 0.67}$$

where Eff_{NG} is 1.00 for natural gas, 0.54 for NGCC, 0.385 for simple GT. When Eff_{NG} =1.00, and the round-trip efficiency is equivalent to the conventional energy efficiency.

** Based on an interview for manufacturers

*** Projected

****Estimated by RASMES (Research Association of SMES, Japan)

5. PROSPECTS OF ENERGY STORAGE GROWTH

Estimation of the Necessary Storage Capacity to Mitigate Power Variations due to Wind Power

Objectives

There are four main objectives in simulating the prospects for energy storage growth:

- 1.) To establish a methodology to estimate the influence of a high share of renewables.
- 2.) To estimate the storage capacity necessary to balance electricity demand and supply in a grid with a high share of renewables.
- 3.) To estimate the regional differences in renewable power output and variability.
- 4.) To predict storage growth during 2010-2050 and total global storage needs.

The starting point is the generation mix used in the BLUE Map scenario of ETP 2008. This generation mix was calculated using the ETP MARKAL model, which regards the natural gas combined-cycle (NGCC) for the middle load as backup capacity when variable renewables generate less power. Demand can be met by either the backup capacity or by energy storage. However, the rate at which backup capacity can be brought online is limited, while stored electricity is available almost instantaneously.

Analysis conditions

Table 2 shows the ETP 2008 generation mix of the Western Europe (WEU) in 2010 and 2050, as described in the BLUE Map scenario. The sum of PV and wind power rises to 30% of total power generation in 2050. Total annual demands are 3161TWh and 4647TWh in 2010 and 2050, respectively.

Table 2: *The electricity generation mix in WEU in the BLUE Map scenario, 2010 and 2050*

Power generation type	Shares(2010)	Shares(2050)
Base load	35.6%	37.5%
PV power	0.1%	4.6%
Wind power	9.8%	25.4%
Middle load	54.5%	32.5%

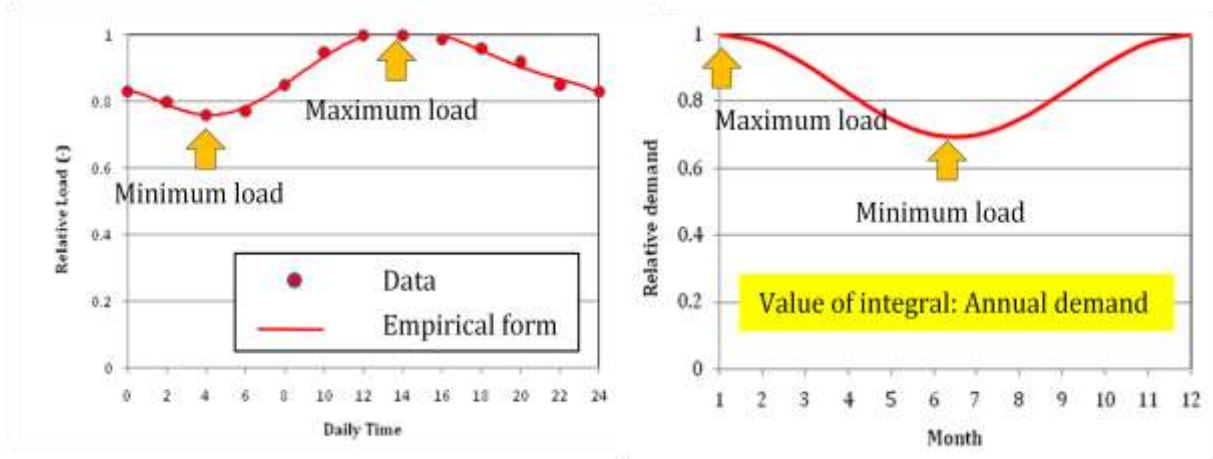
Figures 13 and 14 show the daily and annual load curves in WEU. The curves were normalized to the maximum daily and annual demand, respectively. The daily load curve has its minimum and maximum demands at 04:00 and 14:00, respectively, while the annual load curve has its maximum and minimum demands in winter and summer, respectively. The area below the load curve in Figure 14 is equivalent to the annual demand. This simulation focuses on prospects for 2050, applying the existing functional forms of the daily and annual load curves as is.

Modeling Approach

Since the focus of this study is the short-term variation of wind power, the balance between the demand and the supply was calculated for every 0.1h (i.e., 6 minutes). To simulate the balance between demand and the supply, the base load, PV power, wind power and the middle load are modeled separately.

Figure 13 (left): Daily load curve in WEU

Figure 14 (right): Annual load curve in WEU

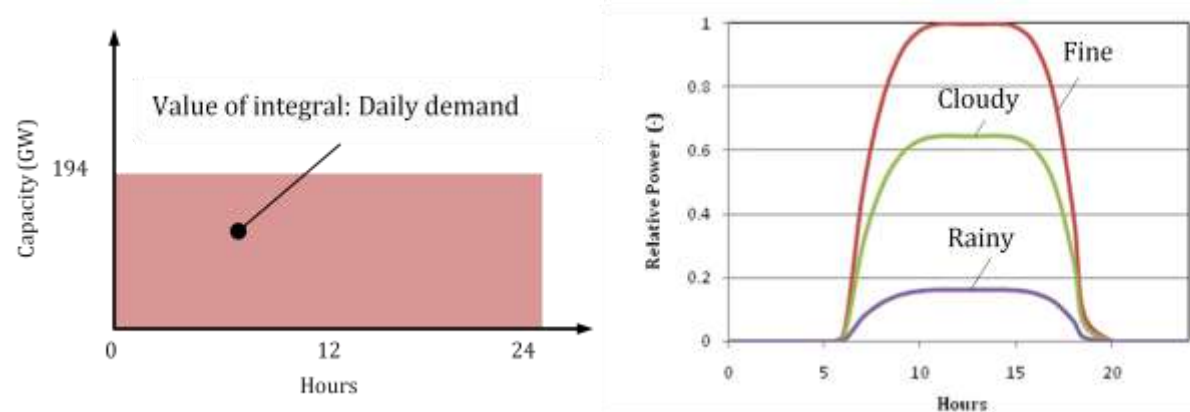


1) Base load model

Base load includes power supplies from nuclear reactor plants, coal-fired plants, and diversion hydropower plants. In this simulation, the base load operation was modeled as a constant 200GW. The colored area in Figure 15 indicates the necessary base load power generation.

Figure 15 (left): Base load operation curve

Figure 16 (right): PV normalized operation curve: f_{PV}



2) Solar PV power model

Figure 16 shows the normalized operation curves of PV power. The PV option supplies power from 06:00 to 18:00, with output dependent on the weather. Three weather patterns were considered. The weather patterns of each day were estimated using a uniform random number X based on weather probability data for fine, cloudy and rainy days (P_f , P_{cl} and P_r , respectively):

$$\text{Fine weather: } X > 1 - P_f$$

$$\text{Cloudy weather: } 1 - P_f > X > 1 - P_f - P_{cl} \quad (1)$$

$$\text{Rainy weather: } 1 - P_f - P_{cl} > X$$

P_f , P_{cl} and P_r were assumed to be 0.80 (80%), 0.17 (17%) and 0.03 (3%), respectively.

With this operational curve, the power supply from PV was given by:

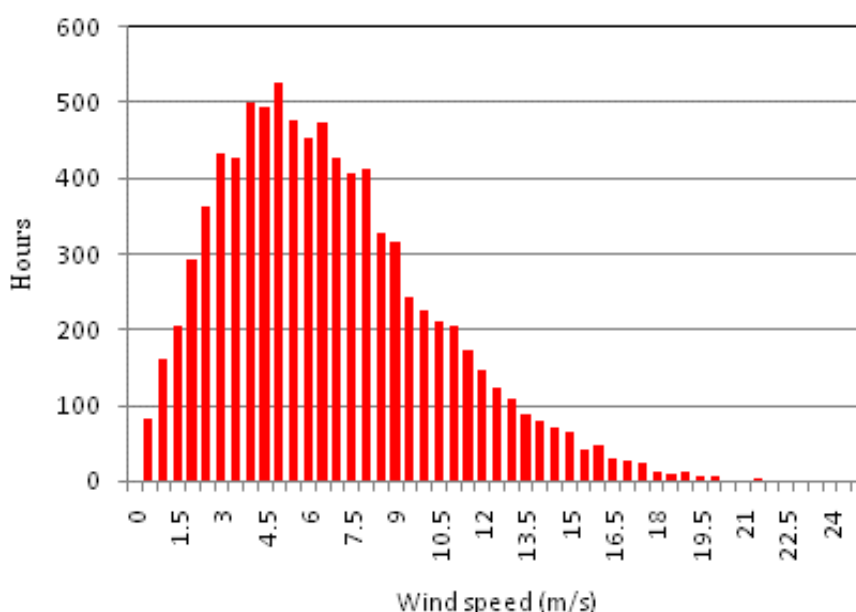
$$P_{PV} = C_{PV} \cdot f_{PV} \cdot \Delta T \quad (2)$$

where C_{PV} is a constant which was set to satisfy the PV share, f_{PV} is a normalized operation curve (Figure 16), and ΔT is time mesh. More detail on f_{PV} is provided in Annex 2. Since the main focus was the effect of wind power, the PV power variation was not considered. Therefore, the effect of the weather only affected estimates of the overall PV power capacities.

3) Wind power model

An approach similar to that used for PV power was applied to wind power. Figure 17 shows an example of actual wind speed distribution data from New Mexico, United States. The curve suggests that the distribution is quite similar to a Weibull distribution. Therefore, the wind speed was simulated by a random number based on a Weibull distribution.

Figure 17: Actual wind speed distribution

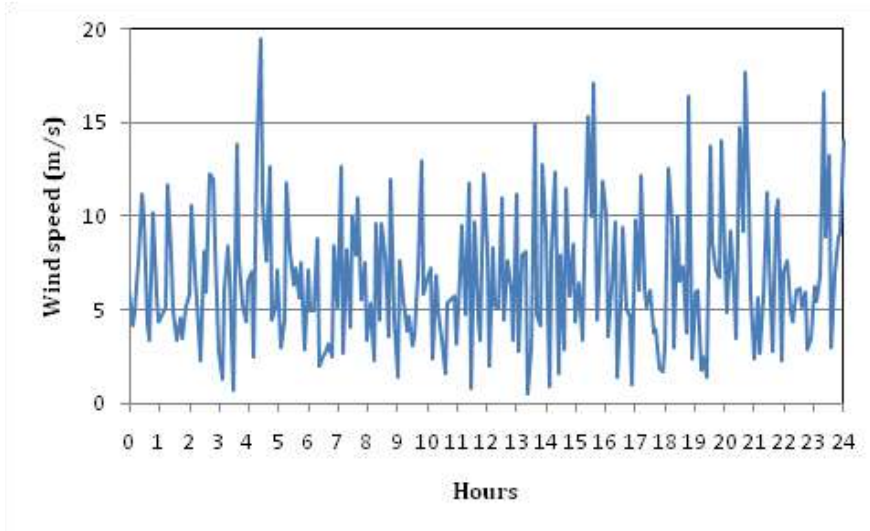


Source: IEA, based on data from Lee Ranch, Sandia National Laboratories, 2003.

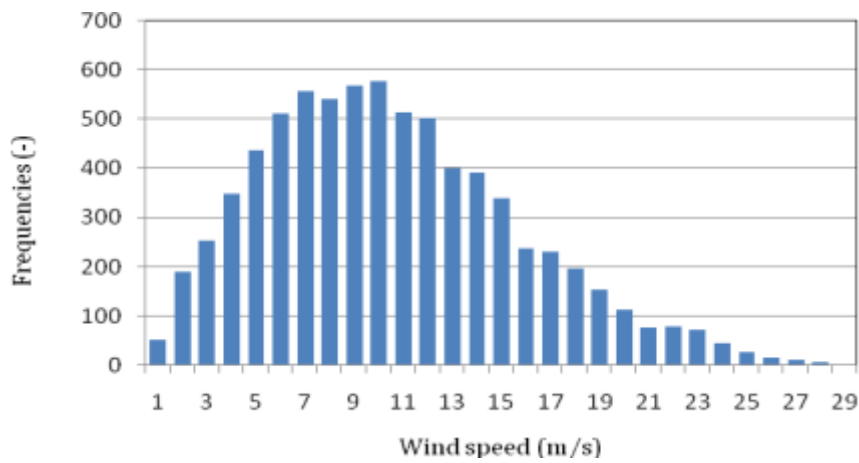
This approach assumes that wind speeds can vary significantly over short time periods; the impact of this assumption needs to be assessed in greater detail. For the data of Figure 17, the average wind speed was 8m/s. Figure 18 (top) shows the trend for simulated wind power. Variations in wind speed were simulated using random numbers based on the Weibull distribution. To evaluate the use of random numbers, the distribution of wind power was simulated, and an example is shown in Figure 18 (bottom). The distribution was quite similar to the Weibull distribution and actual data observed in the field.

Figure 19 shows the operational curve of a wind turbine, which was assumed in simulation. The cut-in and cut-out wind speeds were assumed to be 3m/s and 26m/s, respectively. The power generation capacity was assumed constant at speeds from 13 to 26 m/s. In the speeds from 3 to 13m/s, wind power generation was proportional to the cube of the wind speed.

Figure 18: Simulated wind speed distribution

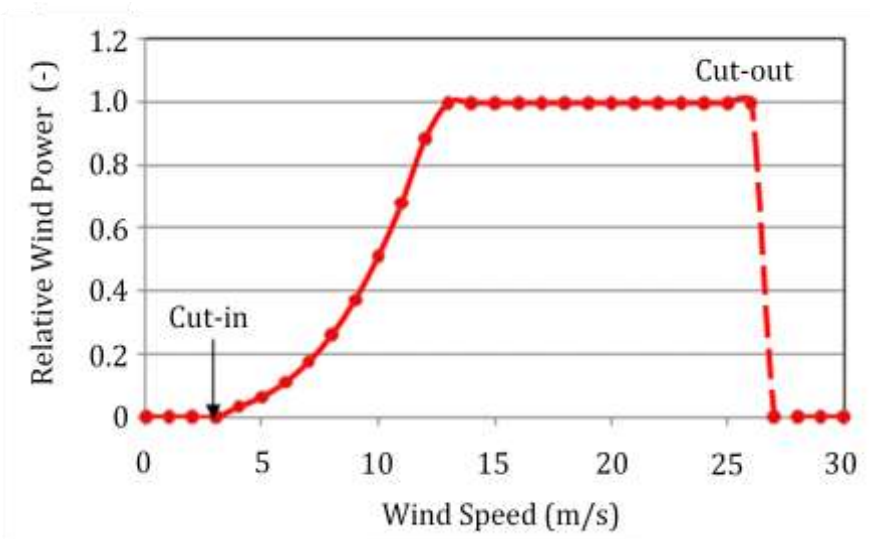


a) Trend of the simulated wind power (average wind speed: 8m/s)



b) Distribution of the simulated wind power

Figure 19: Normalized operational curve of a wind turbine



With this operational curve, the power supplied was expressed as:

$$P_W = C_W \cdot f_w \cdot \Delta T \quad (3)$$

where C_W is a constant, f_w is a normalized operation curve of wind power (Figure 19), ΔT is time mesh. More detail on f_w is provided in Annex 2. C_W was set to satisfy the share of wind power estimated in the BLUE Map scenario. With random wind speeds, the operational curve simulates a fluctuating wind power supply. When wind speed exceeds the cut-out speed of 26 m/s, the wind power supply immediately becomes zero.

As described in Chapter 4, to estimate the net variations of wind power, the smoothing effect plays an important role. In this calculation, the smoothing effect was simulated by the sum of several wind powers as follows,

$$P_{W(S.E)} = \frac{\sum P_{W(i)}}{m}, \quad (4)$$

where, $P_{W(S.E)}$ is the wind power with the smoothing effect, $P_{W(i)}$ is the i -th wind power, and m is the numbers of samples. The net variation of $P_{W(S.E)}$ will be expected to decrease as the number of wind power sources increases. In order to account for the smoothing effect of wind turbines, the supply of wind power was averaged for 10 to 35 sampled wind speeds.

Figure 20 shows the simulated trend of wind power supplies with 35 (left) and 10 (right) samples based on equation (4). In both case, the time-averaged supply was assumed to be 130 GW. As is evident, 35 samples exhibit less variation than 10 samples. In fact, the variation ratio for 35 samples is 15%, compared to 30% for 10 samples. This shows the importance of the smoothing effect on net power variation with geographically distributed wind power generators.

Figure 20: Comparison of simulated wind power with different sample numbers, for 35 samples (left) and 10 samples (right)

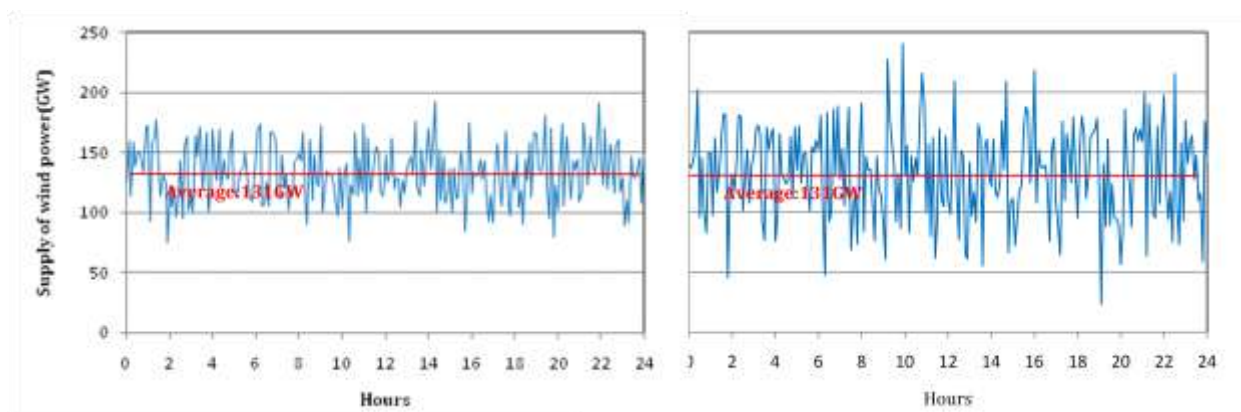
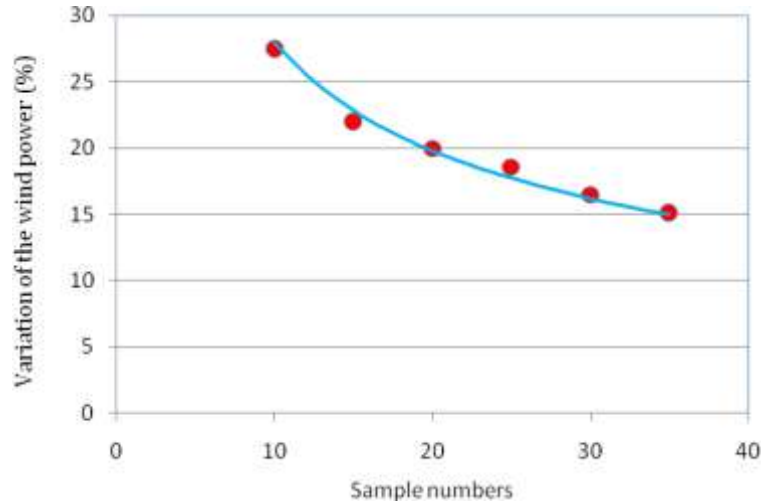


Figure 21 shows the relationship between the number of samples and the variability of cumulative wind power for several sample number. Net variation decreased with increasing numbers of samples. As is well known, if a set of random numbers are independent of each other, the variation of the average value generally decreases with the inverse square root of the sample number. The blue line in Figure 21 is the fitted curve based on the square root of the sample numbers. The simulated results indicate that the smoothing effect depends on this generalization of the law of large numbers. The net variation is dependent on the number of wind turbines and their correlation. If wind speeds in an area are quite independent each other, the net variation will decrease as area increases.

On the other hand, if the wind speeds are associated each other, the smoothing effect would not be effective. Actually, the smoothing effect might be smaller than the ideal case, which

should decrease with the inverse square root of the number of sites. Making the most of the smoothing effect is the key to reducing net power variations.

Figure 21: *The relationship between number of samples and net variation*



4) Middle load model

Middle load generation resources include natural gas combined-cycle (NGCC) plants, simple gas turbines, and impoundment hydropower plants. The middle load supply is estimated based on the balance of demand and supply as follows:

$$\text{Supply of the middle load} = \text{Demand} - (\text{Base load} + \text{PV power} + \text{Wind power}) \quad (5)$$

In this simulation, if the term (Base load + PV power + Wind power) exceeded demand, the excess supply was omitted from the supply of the wind power (representing a shutdown or braking of wind turbines).

5) Middle load operation model to mitigate power variation

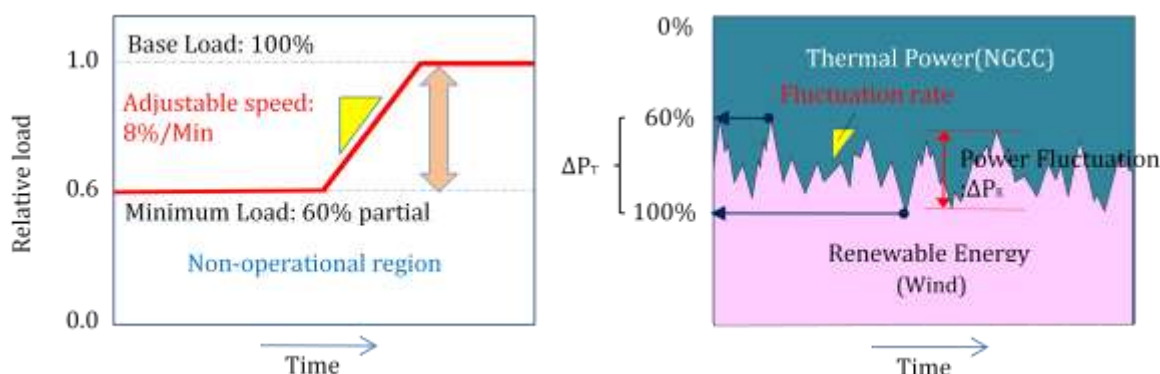
The middle load plays an important role in balancing demand and supply. In this simulation, the middle load was provided by NGCC plants. On a time scale of hours, the supply of the middle load was assumed to be controlled by the start and stop of each constituent NGCC plant. However, on a time scale of minutes, mitigation of short-term net power variations depends on the adjustable speed and operational load of each NGCC plant. An NGCC can be operated flexibly in the range of 60% to 100% of its full rated capacity (Figure 22), with an adjustable speed of about 8%/min for each NGCC plant. Figure 23 conceptually shows how middle load plants mitigate the net power variations due to wind power.

To absorb the net power variation, the following conditions should be satisfied:

$$\Delta P_T > \Delta P_R, \quad (6)$$

$$\text{Adjustable speed of NGCC} > \text{Fluctuation rate of the wind power}, \quad (7)$$

where ΔP_T is (Full load - 60% load), and ΔP_R is (maximum net variation - minimum net variation) of the wind power. If the conditions of equations (6) and (7) in the simulated balance of demand and supply are satisfied, the middle load can cope with the variability. If this is not the case, some countermeasures would be needed. In the present simulation, as variation on the scale of 0.1 h was assumed, the condition of equation (7) was automatically satisfied, since during that time an NGCC will be able to achieve up to 48% adjustability (6 min \times 8%/min). The adjustability is larger than (Full load - 60% load).

Figure 22 (left): Adjustable-speed rate and operational load range of NGCC**Figure 23 (right):** Combining variable renewable with NGCC

Simulation Results

In Western Europe, the effect of a high share of renewables is most pronounced during the minimum demand period of a year, as described in Figure 14. Therefore, the following calculation was performed under the conditions likely to be found in June or July.

1) Balance in 2010

Figure 24 shows the time-averaged balance of demand and the supply for one day in the year 2010. This simulation was performed assuming a 15% net variation ratio. Since the shares of PV and wind power are still small, the share of the middle load is a comparatively large component of the daily load curve.

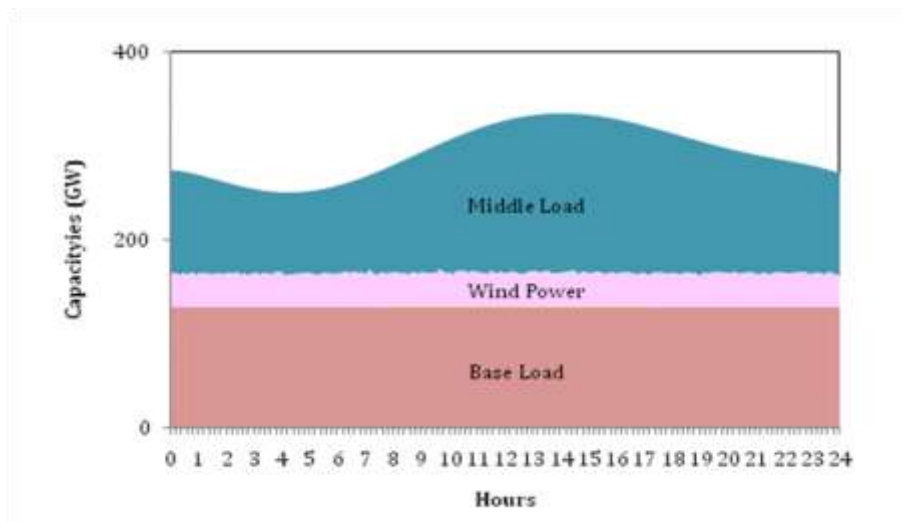
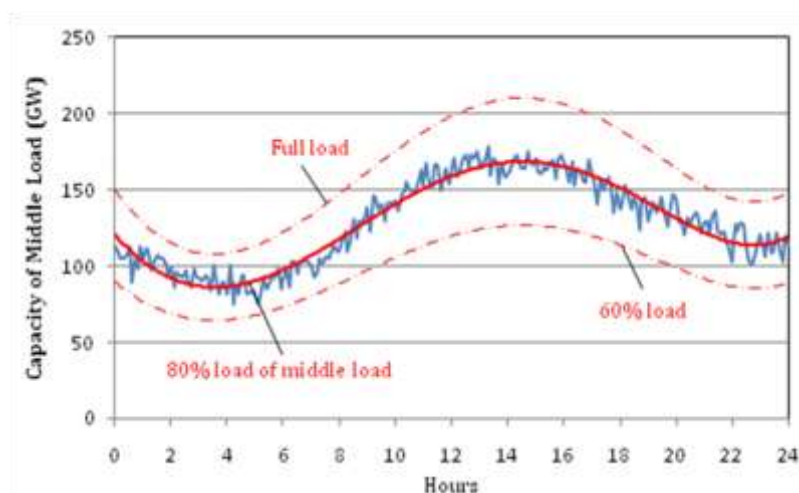
Figure 24: Time-averaged results in 2010 (net variation ratio: 15%)

Figure 25 shows the trend of the middle load supply during a typical day among the calculated 30 days. The middle load supply varies every 0.1h, in accordance with the net variation of the wind power supply. The average middle load supply is indicated by the red solid line, which also represents the 80% load factor. The full load and 60% load are indicated by dotted lines. This figure suggests that the net power variation due to wind power is smaller than the margin given by the “60% load to (full load-60%)” window for middle load operations.

Figure 25: Daily trend of simulated middle load in summer 2010

This indicates that the penetration of wind power anticipated for WEU in 2010—a share that is not much different than current PV and wind power capacity—is quite feasible without any countermeasures.

2) Balance in 2050

Figure 26 plots the balances of demand and supply for two typical days in June with minimum demand. In this simulation, 10 and 35 sample numbers were used, so that the net variation ratios of wind power were approximately 30% and 15%, respectively. Figure 26 left is the fine weather case, and Figure 26 right is the rainy weather case. As the shares of PV and wind power are expected to be much higher in 2050 than they are in 2010, renewable power variations play a much more important role.

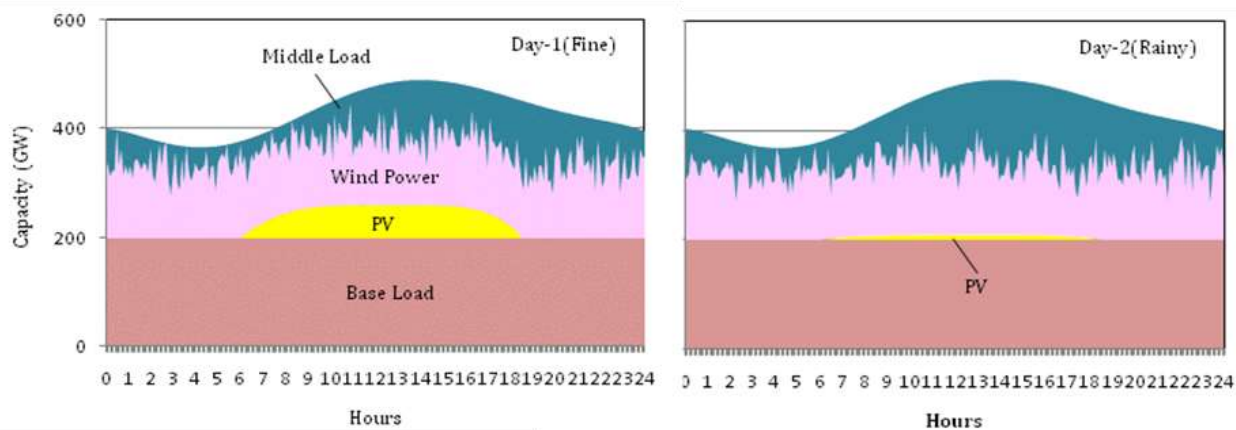
Figure 26: Daily balance of demand and supply on two typical days in 2050: a fine weather case (left) and rainy weather case (right) (net variation ratio: 15%)

Figure 27 shows the time-averaged results for 30 days. Compared with the results for 2010 shown in Figure 24, the share of the middle load is much less. Especially in June, with its daily minimum load, the share of the middle load plants is quite low. Even if the demand and supply seem to be balanced in the time-averaged results, the feasibility of the balance would depend on the relationship between wind power variations in the short term and the margin of the middle load on individual days.

Figure 27: Time-averaged results in 2050 (net variation ratio: 15%)

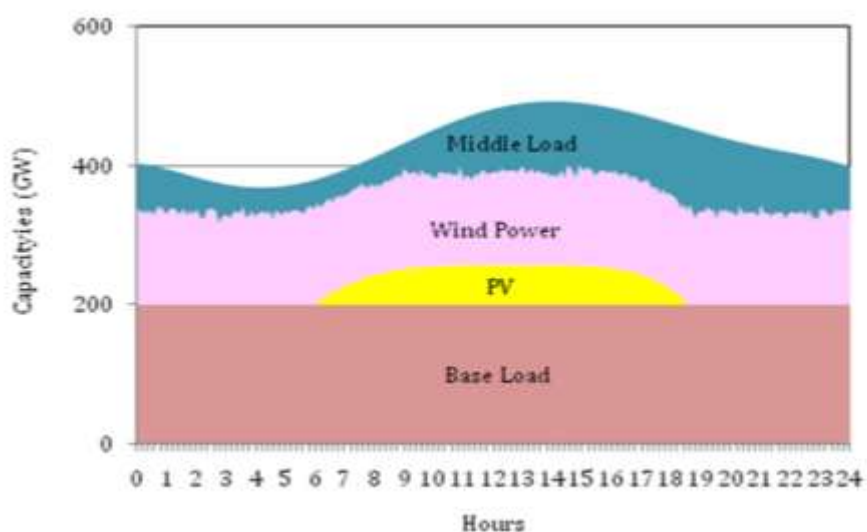


Figure 28 plots the middle load variations on a typical day among 30 days. The lines in Figure 28 are analogous to those in Figure 25. The left and right sides of Figure 28 illustrate the cases of 35 and 10 samples, respectively. Both cases show large excess power variations that exceed the margin of middle load operation. Therefore, operation on such a day would not be feasible without countermeasures.

Figure 28: Daily trends of middle load in typical two days under the minimum load curve in WEU, with net variation ratios of 15% (left) and 30% (right).

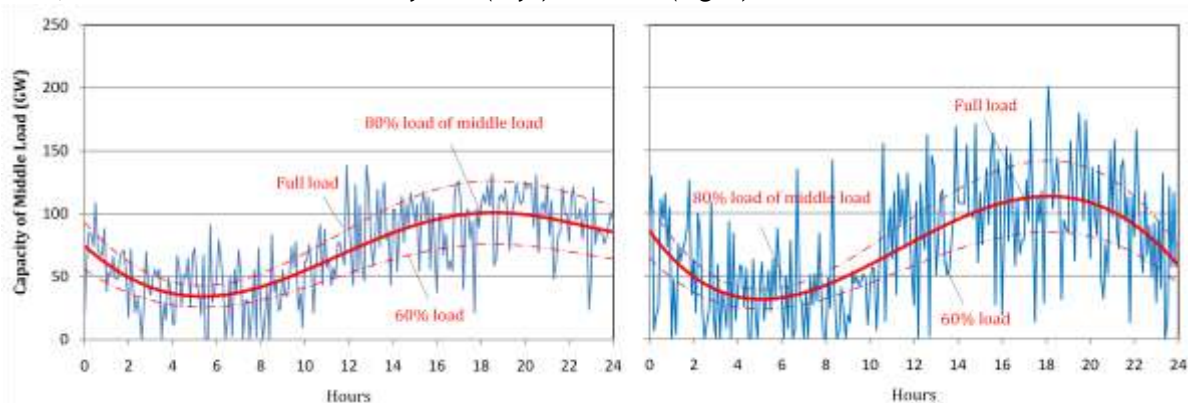


Figure 29 shows the upper and lower excess compensation requirements in Figure 28. The zero of the vertical axis in Figure 28 left is the base load for the upper excess power variation, while the zero in Figure 28 right is 60% load for the lower excess power variation shown in Figures 28 left and right, respectively. The maximum magnitudes of the net variation are 55GW and 98GW with two different smoothing effect parameters, which cannot be absorbed by middle load plants and must be compensated by other measures. This indicates that to absorb this excess power, energy storage capacities of 55 to 98GW will be required.

Figure 29: Excess capacities in a typical day, with net variation ratios of 15% (left) and 30% (right)

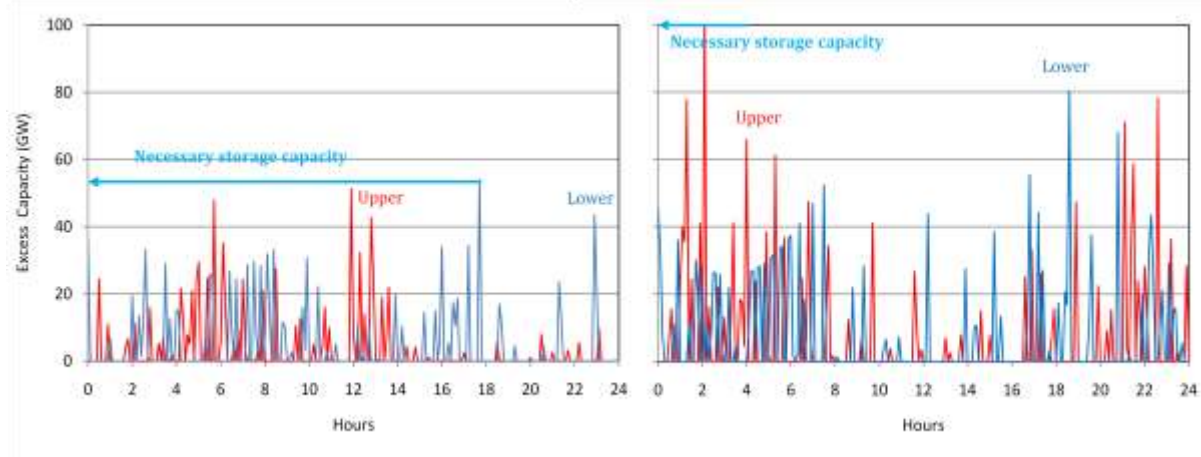


Figure 30 compares the relationship between the net variation of wind power and the necessary storage capacities for 2010, 2015 and 2050 in WEU. In 2050, wind generation variation ratios between 10% and 30% correspond to necessary storage capacities from 40GW to 100GW. Since 33GW of energy storage capacity already exists in WEU, mainly in the form of pumped hydro, new storage capacity of 7 to 67GW would be required to mitigate net power variations due to variable renewables through 2050. Reliable estimation of needed storage capacity depends on the accuracy of the estimate of wind power variability. As described above, installing more wind power is expected to reduce net variation due to the smoothing effect of a widely distributed wind power supply. Therefore, accurate measurement and analysis of the smoothing effect should be carried out for the areas of interest in the near future. It should be fully understood that the present results are only a framework for such an evaluation.

Figure 30: The relationship of net wind power variation and necessary storage capacities

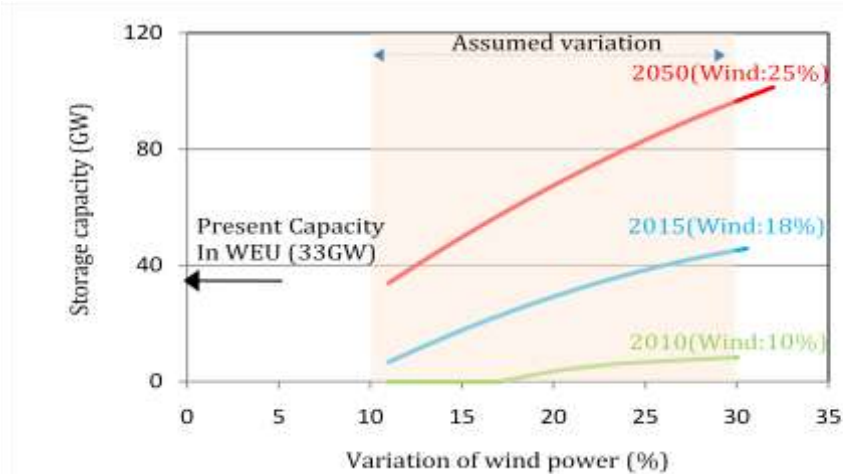
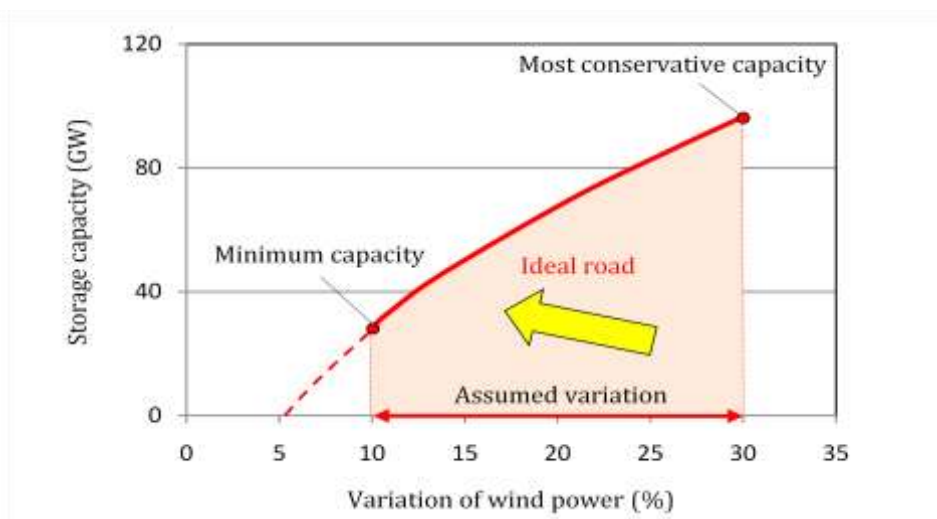


Figure 31 shows the ideal road for increasing energy storage in WEU. As described above, the necessary energy storage capacity strongly depends on the variation, with net variation ratios from 10% to 30% corresponding to storage capacity changes from 30 to 90GW. Taking the best advantage of the smoothing effect is the key to reducing the amount of energy storage capacity needed. To that end, wind power variability must be accurately measured. By way of illustration, the analysis estimated the required capacity of energy storage in WEU. Recent measurements of wind power variation in WEU show that the maximum variability in 10-15 minutes is 6-12% and the average variability is perhaps 20-30% of that value. The analysis shows that if 5% net variation were to be maintained even at the high shares projected for 2050, no energy storage capacity would be required in WEU. However, in areas in which the

smoothing effect is limited, net output variation larger than 5% of current small variation levels in WEU would be seen.

Figure 31: *The ideal road of increasing energy storage in WEU toward 2050*



The present simulation was also applied to important regions of the world based on the BLUE Map scenario for the period 2010 to 2050. Figure 32 compares the necessary storage capacities in four major regions. The net variation ratio of wind power was assumed to be 15%. Each country/region has its own storage capacity needs, which depend on the shapes of daily and annual load curves and the share of PV power and wind power in their generation mixes.

In the Former Soviet Union (FSU) the shares of PV and wind power are expected to be quite low in 2050, so no energy storage capacity is needed. That represents a situation similar to WEU in 2010. In China, where large total capacities of wind power are expected, the necessary storage capacity will also be large. On the other hand, the magnitude of the total energy to be mitigated is not high, as the share of the middle load is relatively large compared to that of other countries.

At minimum demand periods in Japan and the United States, the supplies of (wind power + base load) or (wind power + base load + PV) are expected to occasionally exceed demand. In that event, this simulation assumes curtailment of the upper excess supply. Energy storage will be useful to allow full utilization of the excess supply.

Figure 32: Comparison of the load curves and necessary storage capacity for Japan, China, the United States, and Former Soviet Union at 2050 (net variation ratio: 15%)

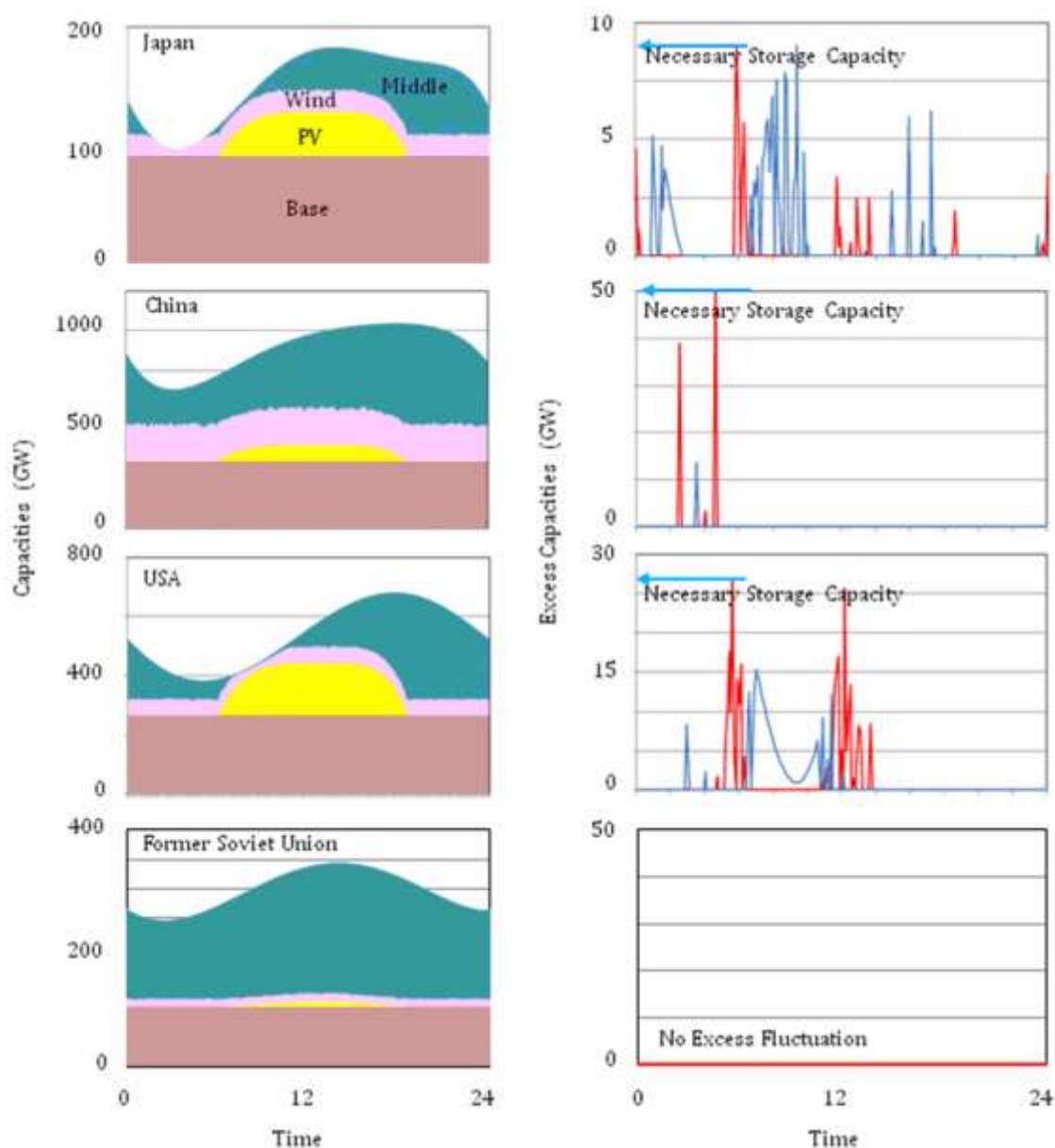
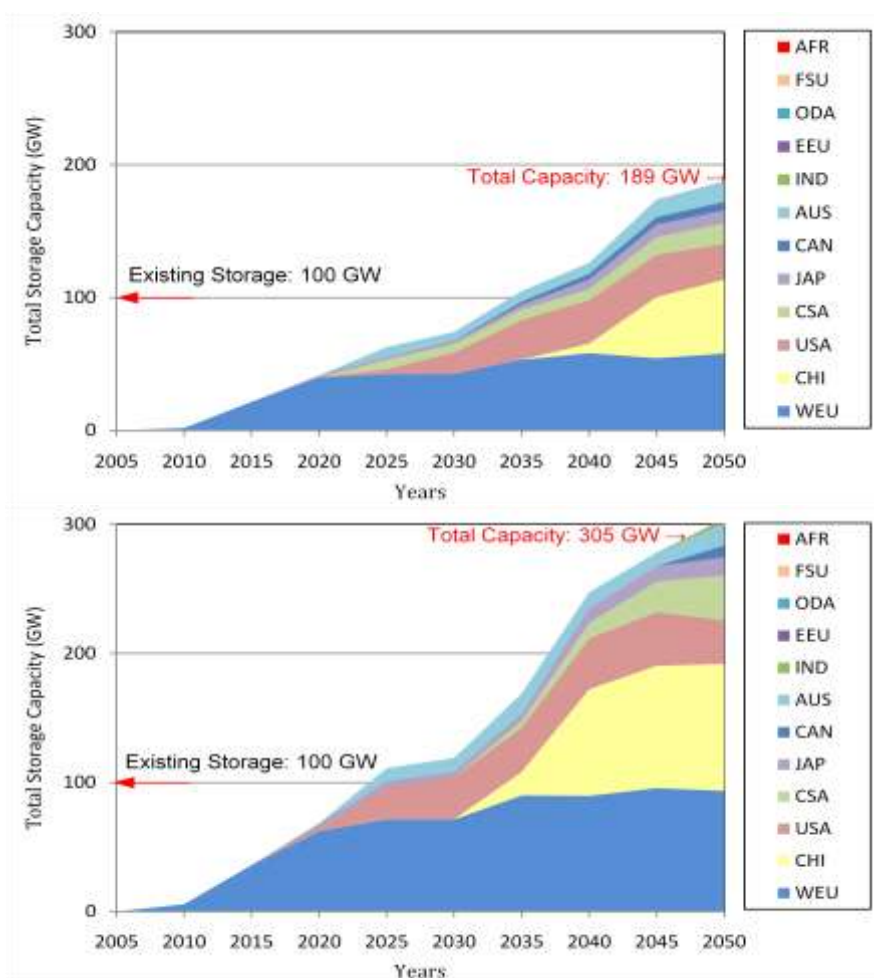


Figure 33 shows the growth in energy storage capacities required worldwide from 2010 to 2050 to achieve the BLUE Map scenario. As described, the total storage capacity needed heavily depends on the net variation ratio of the wind power. As a result, the storage required ranges from 189GW to 305GW, corresponding to net variation ranging from 15% to 30%. Under smaller variation, the capacity will decrease as in WEU case. As the existing storage capacity is 100GW worldwide, consisting mainly of pumped hydro storage installed in the last 40 years, the amount of additional storage capacity required is about 89 to 205GW. IEA's *Energy Technology Perspectives* estimates the required energy storage capacity as 500GW, larger than the range derived in this simulation. However, that estimate did not consider the effect of net wind power variation. Through the present simulation, the importance of the variation was offered as a new insight. To determine the required energy storage capacity with a high accuracy, further measurement and analysis are essential. Rather than specific numerical values, it is the relative amounts of storage against net variability that is most important. Therefore high quality assessment of the net variation, after taking into account the output of power plants across the entire system as well as demand variation, is fundamental to accurate identification

of required storage capacities. The objective is not to identify dedicated storage capacity for individual technologies or power plants.

Figure 33: Growth of necessary energy storage capacity worldwide during 2010-2050, with net variation ratios of 15% (top) and 30% (bottom).

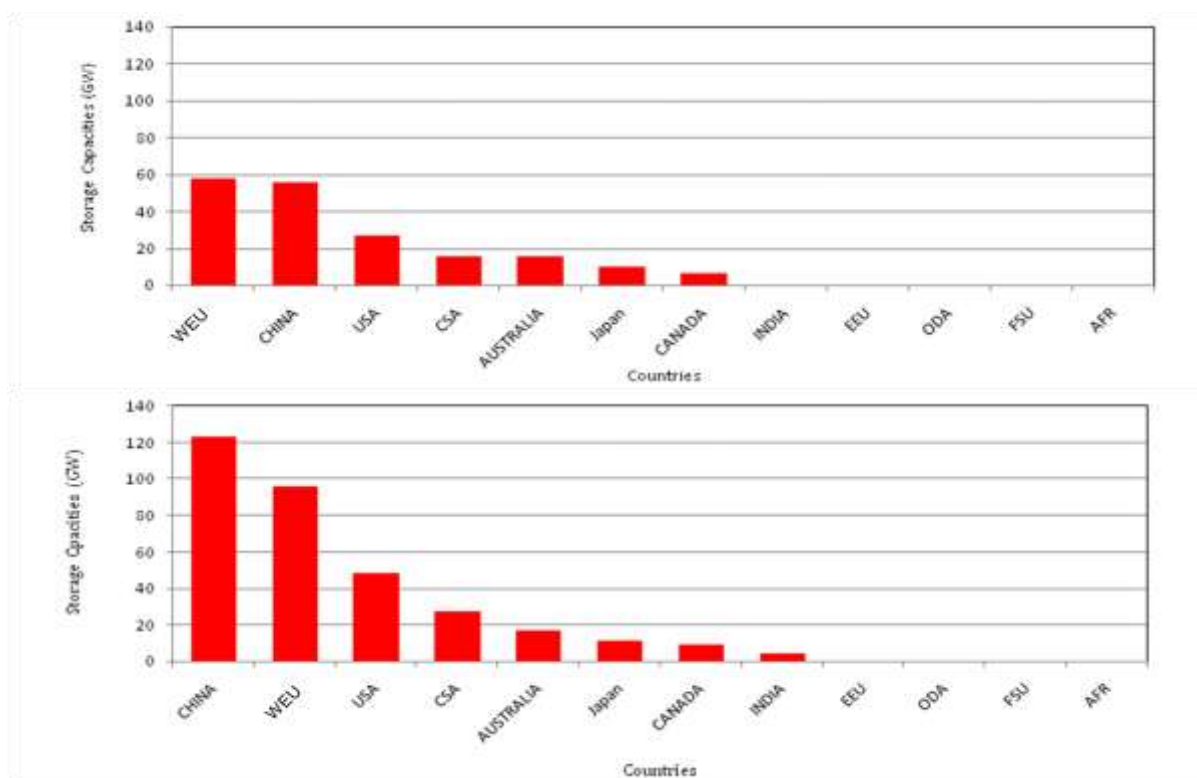


WEU: Western Europe, CHI: China, CSA: Central South America, JAP: Japan, AUS: Australia, IND: India, EEU: Eastern Europe, FSU: Former Soviet Union, AFR: Africa

Deployment of an additional 89 to 205GW of energy storage capacity seems to be possible toward 2050. On the other hand, existing energy storage mainly consists of pumped hydro storage systems used to level the demand against the base load. Therefore, energy storage capacity is also required to shift energy supply from low demand periods at night to peak demand periods in the daytime. However, the main purpose of future storage will be mitigating net power variations due to wind power supplies. Suitable capacity and energy densities should be determined in individual countries.

Figure 34 compares required storage capacities in various countries in 2050. As mentioned above, predicting accurate estimates in each area requires measurement and analysis of the net variation in each area. Appropriate geographical distribution of the wind power is expected to reduce the net variation.

Figure 34: Comparison of the necessary energy storage capacity in 2050, with net variation ratios of 15% (top) and 30% (bottom)



The optimal arrangement of energy storage depends on situations of individual countries. CAES is an effective option for the United States, Western Europe and China, which have suitable salt mines in which compressed air can be stored. On the other hand, secondary batteries will be effective in countries that have no salt mines, such as Japan. In Japan in particular, large-scale wind farms are very unlikely to be implemented. In that case, secondary batteries operating with individual wind turbines will play an important role.

In countries with large wind farm potential, large-scale energy storage systems such as pumped hydro and CAES will be suitable. It will be especially important to effectively utilize pumped hydro, which has 100GW of capacity worldwide. In a typical pumped hydro plant, pumps are operated at night at a constant rotational speed to pump water from a low reservoir to a higher one, which makes pumped hydro generally unsuitable for absorbing net wind power variations. That would require the use of adjustable-speed pumped hydro, which will be described in Annex 1. As the cost of upgrading pumped hydro is approximately 300 USD/kW, implementing adjustable-speed pumped hydro will play an important role.

Among the secondary batteries, breakthrough technologies for the cost reduction will be required. Even NaS batteries, which have adequate performance characteristics, are more expensive than pumped hydro and CAES. If Li-ion batteries play an important role in the form of electricity storage for electric vehicles (EVs) and plug-in hybrid vehicles, their cost might decrease with volume efficiency. On the other hand, the specifications of Li-ion battery for EVs and power grids are quite different, and current efforts to develop and promote Li-ion batteries for EVs may not be applicable to energy storage use. For Li-ion batteries in power grid applications, manganese will be applied to the positive electrode. As manganese is cheaper than cobalt, which is the material now used for the positive electrode, Li-ion batteries intended for power grids will have a large potential to reduce cost.

In the case of SMES, the superconducting magnet has proven its operational performance in the field of nuclear science. This energy storage technology, that is unusual in that it stores

electricity in its original form instead of converting it to another form such as chemical or potential energy, has excellent properties and shows enormous promise.

In conclusion, it is reemphasized that this study suggests only a framework for assessing the need for energy storage against variations of wind power generation based on the Blue Map scenario. As the share of wind power in WEU and China is higher than that in other areas, they will require the larger storage capacities of 50-100GW, depending on the penetration level and the net variation ratio. According to Figures 29 and 32, WEU experiences variations all day, while in China excess variations appears during the minimum demand period in the morning. In both countries, different specifications for storage would be required despite their similar storage capacity needs. In WEU, pumped hydro, CAES and secondary battery systems, which can store powers for several hours, would be suitable. On the other hand, in China, pumped hydro and flywheel systems would be suitable. As a future alternative, SMES could also prove suitable.

For such large capacity areas as WEU and China, the owners of small-scale wind power systems and large-scale storage systems would be different. To mitigate power variations due to wind power, the problem then is: who operates the large-scale storage systems? Specific frameworks for operating the storage systems would be required, especially in WEU. In Japan, wind turbine owners are obligated to use energy storage to mitigate the net variation by regulation.

From the present simulation results, the following conclusions may be drawn:

- 1.) The necessary energy storage capacity to mitigate wind power variation depends on the net variation ratio of the wind power generation. In the world in 2050, the necessary capacity was estimated to be from 189 to 305GW, corresponding to net variation of 15% to 30%, resulting in a need for an additional worldwide energy storage capacity of between 89 and 205GW. To achieve the BLUE Map scenario, these capacities are essential.
- 2.) Since the capacity depends on the net variation of the wind power, monitoring and analysis of the net variation is essential.
- 3.) The necessary capabilities are important factors in high-penetration areas of wind power generation like WEU, China and the United States.
- 4.) Since the owners of wind power systems and large-scale storage systems will be different, specific frameworks to operate the storage systems, such as ancillary service agreements, would be required.

6. CONCLUSIONS AND RECOMMENDATIONS

In this working paper, energy storage systems were reviewed and a simulation study based on the BLUE Map scenario was carried out. A new algorithm was developed (see Annex 2) for evaluating large-scale power systems and optimising grid stabilization needed when using variable renewables. The following results were obtained:

1.) By way of illustration, the analysis estimated the required capacity of energy storage in WEU. Recent measurements of wind power variation in WEU show that the maximum variability of 10-15 minutes is 6-12% and the average variability is perhaps 20-30 % of that value. Simulations of wind power variation levels between 5% and 30% yield estimates of energy storage capacity in WEU ranging from 0GW to 90GW in 2050. The analysis shows that if a 5% net variation were to be maintained even at the high shares projected for 2050, no energy storage capacity would be required in WEU. However, in areas in which the smoothing effect is limited, net output variation larger than 5% of current small variation levels in WEU would be seen.

2.) The energy storage capacity needed to mitigate net variations due to variable renewables is largely dependent on variations of the wind power supply. The necessary worldwide storage capacity ranges from 189 to 305GW, corresponding to net variation ratios from 15% to 30%. These capacities are an integral part of the power system in the BLUE Map scenario. Rather than specific numerical values, it is the relative amounts of storage against net variability that is important. Therefore high quality assessment of the net variation, after taking into account the output of power plants across the entire system as well as demand variation, is fundamental to accurate identification of required storage capacities. The objective is not to identify dedicated storage capacity for individual technologies or power plants.

3.) Since the necessary capacity depends on the net variation of wind power, monitoring and analysis of the net variation of wind power generation is key. Strategies should be developed to minimize the net variation and minimize storage investment needs.

4.) Western Europe, China and the United States are in particular need of significant storage capacities, as those countries will be expected to have the highest shares of renewables. Pumped hydro capacity of about 100GW is presently available. Pumped hydro plants located in Europe, North America, and Japan have been developed to match stable base load and day/night demand variations. This capacity can be put to good use to deal with variability caused by renewable power supplies.

Further, the following recommendations address security standards:

1.) It is preferable that wind power generation resources be distributed to maximize the smoothing effect, which is the key to reducing net variation of the wind power supply.

2.) Since the necessarily capacities of energy storage depend on the net variation of wind power, measuring methods and analytical systems should be established by individual countries or groups of countries. Through an accumulation of these efforts, the necessary countermeasures should be determined.

3.) Since the owners of wind power systems and large-scale energy storage systems would be different entities, specific frameworks such as ancillary service agreements to operate the storage facilities will be required.

4.) The necessary capacity and operating characteristics of energy storage depends on the share of renewables in individual countries. The number of storage options should be increased. In particular, it is expected that SMES, lithium-ion batteries, and adjustable-speed pumped hydro systems will be significant factors in the power grids of the future.

7. REFERENCES

CHAPTER 1

e-on Netz GmbH (2005), “Wind Report 2005”,
http://www.countryguardian.net/EON_Netz_Windreport2005_eng.pdf.

IEA (International Energy Agency) (2008), *Energy Technology Perspectives 2008: Scenarios & Strategies to 2050*, OECD/IEA, Paris.

Sharman, Hugh (2007), “As Denmark Doubles Renewable Energy to 30% by 2025”,
<http://www.leonardo-energy.org/Files/denmarkvrb.pdf>.

Sørensen, Paul (2004), “System integration of wind turbines in Denmark”, IEA Topical Expert Meeting on System Integration of Wind Turbines.

CHAPTER 2

IEA (2006), *IEA Electricity Information 2006*, OECD/IEA, Paris.

IEEJ (The Institute of Energy Economics, Japan) (2005), *Energy*, 2005-8, pp.85-87.

CHAPTER 3

Japanese Wind Power Association (2004), “Counter measure of electricity frequency change (in Japanese)”,
<http://www.meti.go.jp/committee/downloadfiles/g40422a50j.pdf>.

Rastler, Dan (2009), “Overview of energy storage options for the electric enterprise”, EPRI, United States.

CHAPTER 4

IEA (2008c), *Empowering Variable Renewables: Options for Flexible Electricity Systems*, Paris.

CHAPTER 5

DOE, (US Department of Energy) (2006) “Cost, and Performance Trends: 2006, Energy Efficiency and Renewable Energy”, Annual Report on U.S. Wind power Installation, DOE, United States.

Lee, Ranch (2003), Sandia National Laboratories,
<http://www.sandia.gov/wind/other/LeeRanchData-2002.pdf>.

Tohoku Electric Power Co., Inc. (2006), “Estimation of potential of interconnected wind power in Tohoku power grid (in Japanese)”,
<http://www.meti.go.jp/committee/materials/downloadfiles/g50426a21j.pdf>.

Wind Energy Report Germany (2006), IEST, Kassel.

ANNEX 1

Aguro, Katsutoshi, *et al.* (2008), “Rich operation experiences and new technologies on adjustable speed pumped storage systems in Japan”, A1-101, CIGRE, Paris, France.

Bacon power Corporation, FACT SHEET (2009), “Frequency Regulation and Flywheels”
http://www.beaconpower.com/files/Flywheel_FR-Fact-Sheet.pdf.

Barpanda, PraBeer and Amatucci, Glenn G. (2001), “Faradaic and non-faradaic reaction mechanisms in carbon- iodine nanocomposite electrodes for asymmetric hybrid super capacitors”, *J. Electrochem. Soc.*, No. 148, A930.

Bonk, Josh, *et al.* (2009), “Comparison of hydraulic and mechanical responses measured in model and prototype of a low specific speed pump turbine”, *BG Hydraulic and Mech Responses*, Paper 66 - 4 February 2009.

Buenoa, Celia and Carta, J.A. (2006), “Wind powered pumped hydro storage systems, a means of increasing the penetration of renewable energy in the Canary Islands”, *Renewable and Sustainable Energy Reviews* 10, pp.312-340.

Bullough, Chris, *et al.* (2004), “Advanced adiabatic compressed air energy storage for the integration of wind energy”, *Proceedings of the European Wind Energy Conference, EWEC 2004*, pp. 22-25.

Crotogino, Fritz, *et al.* (2001), “Huntorf CAES: more than 20 years of successful operation”, *Crotogino and Huntorf CAES Compressed Air Energy Storage. pd*, KE2003H03c, Spring 2001 Meeting Orlando, Florida, United States.

EA Technology (2004), “Review of electrical energy storage technologies and systems and of their potential for the UK”, Contract Number: DG/DTI/00055/00/00.

EPRI (Electric Power Research Institute (2009), “Advanced Compressed Air Storage Demonstration”, Project ID: 1018785, EPRI, Palo Alto, CA.

EPRI (2009), “Utility Scale Mobile Energy Storage System Field Demonstration”, Project ID: 067247, EPRI, Palo Alto, CA.

ESA (Energy Storage Association) (2009),
http://www.electricitystorage.org/site/technologies/li-ion_batteries/.

Gaines, Linda and Cuenca, Roy (2000), “Costs of Lithium-Ion Batteries for Vehicles”, DOE, ANL/ESD-42, United States Department of Energy, United States.

Green, Michael A. and Strauss, Bruce P. (2008), *IEEE Transactions on Applied Superconductivity*, Vol. 18, No. 2.

Hatamiya, Shigeo, *et al.* (2007), “An experimental and analytical study on the advanced humid air turbine system”, *International Conference on Power Engineering 2007*. pp. 290-296.

Hennessy, Tim (2007), “Storage Options in Planning”, Profiled evidence Report No. 8 of GEC-Pembina-OSEA.

Holzman, David C. (2007), “The flow batteries put wind energy in the Bank”, *Environmental Health Perspectives*, Vol. 115.

Ichimura, Masahiro (2004), “Next-generation lithium ion batteries (in Japanese)”, *Technical report of NTT Building Technology Institute*.

IHA (International Hydropower Association) White Paper (2003), “The role of hydropower in sustainable development”.

Ise, Toshihumi and Sato, Hiroshi (2003), “Magnet power supply with SMES in the DC link for large accelerator”, *Proceedings of the 14th Symposium on Accelerator Science and Technology*, Tsukuba, pp.90-92.

Ise, Toshihumi, *et al.* (2002), “Magnet power supply with net power variation compensating function using SMES for high intensity synchrotron”, *IEEE Transaction on Applied Superconductivity*, Vol.13, pp.1814-1817.

Ishii, Yoshito, *et al.*, (2006), “Anode Material for High Energy Density Rechargeable Lithium-Ion Battery”, *Hitachi Chemical Technical Report*, No.47, pp.29-32.

Laforgue, Alexis, *et al.* (2001), “Hybrid supercapacitors based on activated carbons and conducting polymers”, *J. Electrochem. Soc.*, 148, A1130.

Lako, Paul (2002), “Learning and diffusion for wind and solar”, Energy Research Centre of the Netherlands, (ECN), ECN-C--02-001.

Langen, Christian, *et al.* (2009), “Solar European Industry Initiative”, European Photovoltaic Industry Association.

Matsukawa, Toshiaki, *et al.* (1987), *IEEE Trans. Energy Conv. EC-2*, pp. 262.

Mc COY Power Report 2008 (2008).

Nakabayashi, Takashi (2004), “Performance of large electric power equipment and future view large capacity battery system: sodium sulfur battery” (in Japanese), *Plasma Fusion Res.* Vol.80, No.7 pp.563-567.

Naoi, Katsuhiko and Simon, Patrice (2008), “New materials and new configurations for advanced electrochemical capacitors”, *The Electrochemical Society Interface*, pp. 34-37.

Negishi, Akira, Nozaki, Ken, and Kaneko, Hiroko (1999), “Electrolyte of vanadium redox flow battery for load levelling (in Japanese)”, *Technical Report of National Institute of Advanced Industrial Science and Technology*, Vol.63., pp.27-35.

Nishida, Takehiko, *et al.* (2004), “Development of power storage system applying Li-ion batteries (in Japanese)”, *MHI Technical Report*, Vol. 41 No.5.

Nomura, Shinichi, *et al.* (2002), “Variations of force-balanced coils for SMES”, *IEEE Transactions on Applied Superconductivity*, 12 (1), pp.792-795.

Okamura, Michio (2001), “Electric double-layer capacitor system and electricity storage (in Japanese)”, *Nikkan kogyo shinbun sha*, 2001, ISBN 4526047139.

Okumura, Hiroshi, *et al.* (2009), “Successful upgrading of pumped hydro at the Blenheim Gilboa pumped hydro”, *BG Hydraulic and Mech Responses 4-2-2009*, pp.67.

RASMES (Research Association of Superconducting Magnetic Energy Storage), <http://www.rasmes.com/>.

Rojas, Alex (2003), "Flywheel energy matrix systems: today's technology, tomorrow's energy storage solution" Conference Proceedings, Battcon 2003, Vol. 1.

Sato, Hiroshi, et al. (2003), "Compensation of load variation of power supply system for large accelerator using SMES", Proceedings of the 2003 Particle Accelerator Conference, Portland, Oregon, pp.755-757.

Schinker, Robert B., et al. (2008), "New Utility Scale CAES Technology: Performance and Benefits (Including CO₂ Benefits)", EPRI, Product ID 1016901.

Schneuwly, Adrian, et al. (2002), "Ultracapacitors, the New Thinking in the Automotive World", *White paper*, Maxwell Technologies.

Schoenung, Susan M., et al. (1991), "Design performance and cost characteristics of high temperature superconducting magnetic energy storage" *IEEE Transactions on Magnetics*, Vol. 27, No. 2.

Shimada, Ryuichi (2004), "Performance of large electric power equipment and future view kinetic energy storage (flywheel, compressed air energy storage) (in Japanese)", *J. Plasma Fusion Res.* Vol.80, No.7, pp.572-577.

Shimada, Takakazu, et al. (1980), 3-MJ magnet for superconductive energy storage, *Advances in Cryogenic Engineering*, No. 25, pp.98-104.

UL 1642, ISBN 1-55989-829-1, "Lithium Batteries",
<http://img1.zyzhan.com/5/20090519/633783482645312500.pdf>.

Vadasz, Peter (1999), Compressed air energy storage: optimal performance and techno-economical indices, *Int. J. Applied Thermodynamics*, Vol.2, (No.2), pp. 69-80.

Water Power Year Book 2008 (2008).

Yoshio, Akira, et al. (2004), "Development of a lithium-type advanced energy storage device", *J. Electrochem. Soc.*, 151(12) A2180.

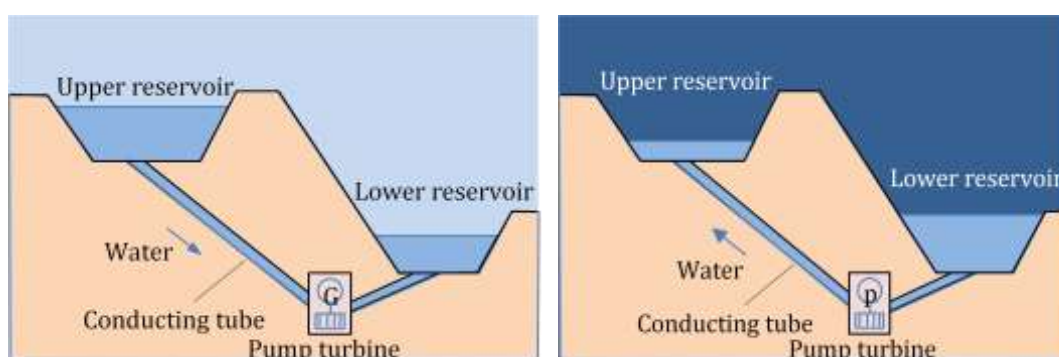
ANNEX 1: BRIEF REVIEW OF ENERGY STORAGE SYSTEMS

Pumped Hydro

Concept

Pumped hydro systems are today the most widely applied energy storage technology, with about 100 GW installed worldwide. Their principle is explained in Figure A.1. The pump turbine is the key device. In periods of discharging (usually during daytime), the system generates power just like a conventional hydropower plant. In periods of charging (usually during night), water is pumped from a lower reservoir to an upper reservoir. In some designs, a single machine operates as a turbine and as a pump; in other cases, two separate machines are installed.

Figure A.1: Principle of pumped hydro storage systems, showing discharge during the day (left) and charge during the night (right).



Structure

Pumped hydro systems are classified as mixed pumped hydro or simple pumped hydro structures. The former are operated with a large reservoir, which has a larger effective storage capacity based on a natural source of water. As a result, it can operate during high water seasons. In dry seasons, the pumped hydro structure can provide support to meet load. The 200 to 400MW class systems are generally preferred.

The simple pumped hydro structure has only an artificial reservoir, so charging it with water is essential. To meet peak load during a short period, 1000 to 2000MW class capacities are generally preferred. The discharge time is 6-10h.

Features

Pumped hydro systems are suitable for large capacity energy storage, as described above, and have long lifetimes of over 40 years. Their efficiency is approximately 70% as shown in the following equation.

$$\eta = \eta_c \cdot \eta_d = \left[\eta_p \cdot \eta_M \left(\frac{H - \Delta H_p}{H} \right) \right] \cdot \left[\eta_t \cdot \eta_G \left(\frac{H - \Delta H_t}{H} \right) \right] \quad (\text{A.1})$$

$$\approx [0.92 \times 0.98 \times 0.93] \times [0.92 \times 0.98 \times 0.93] \approx 0.70$$

η_c : charging efficiency, η_d : discharging efficiency, η_p : pumping efficiency, η_t : turbine efficiency, η_M : motor efficiency of generator/motor, η_G : generator efficiency of generator/motor, H : head, ΔH_p : loss head of water way in pumping operation, ΔH_t : loss head of water way in turbine operation

The response time of pumped hydro is several minutes, which makes it easy to provide power conditioning. When a generating unit is in stand-by operation after it starts operation and is connected to the power grid, it takes only about 60 seconds to transition from zero to full output. Pumped hydro systems are suitable for following short-cycle power demand variation with governor-free operation.

However, when a single-speed unit is operating in the pumping mode, input power can not be changed because it is determined solely by the pumping head—that is, the difference in water elevation of the upper and lower reservoirs. Consequently, the conventional single-speed unit does not work to stabilize grid frequency in the night time. However, an adjustable-speed unit that can rapidly change input power can contribute to stabilizing the grid frequency as described below.

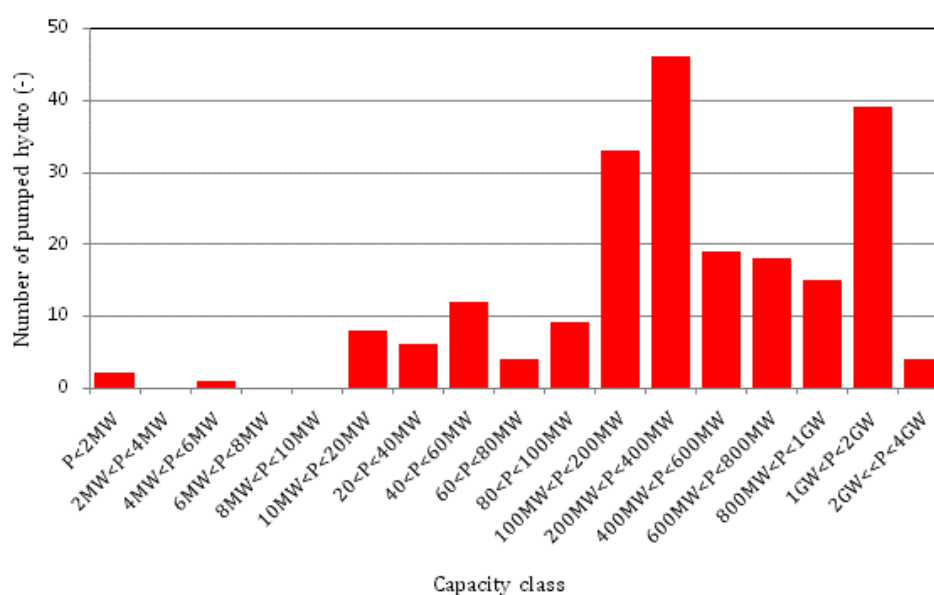
In addition to the above, some pumped hydro units of both single-speed and variable-speed types can operate in a condenser mode for the purpose of tuning the phase difference or the reactive power of the power grid. In the condenser mode operation the water of the runner/inpeller chamber is depressed downward by compressed air in order to reduce stirling power loss caused by a spining runner.

Technical status

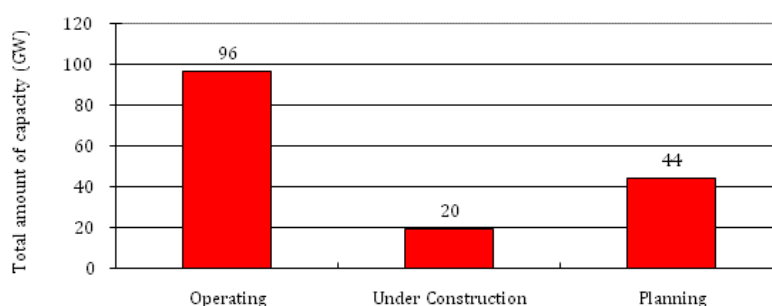
The first pumped hydro system was built in 1892, and the technology is very reliable and mature. The world's largest plant is the 2710MW pumped hydropower plant at Bath County, Virginia, United States. The number of pumped hydro power plants from 1960-2007 are shown by power classification in Figure A.2. The 100 to 400MW and 1 to 2GW class systems are the mainstays of pumped storage power plants.

Generally, each pumped hydro plant consists of two to eight pump turbine units. Worldwide, in 2007 the total capacity of operating pump turbines was 96GW, with 20GW under construction and another 44GW in the planning stage, as shown in Figure A.3. Figure A.4 summarizes the history of installed pumped hydro capacity and cumulative capacity per year. In the twenty years from 1970 to 1990, the total capacity of operating pump turbine units worldwide increased from 12 to 75GW, which means that an average of 3GW per year of pump turbine capacity was installed in this period.

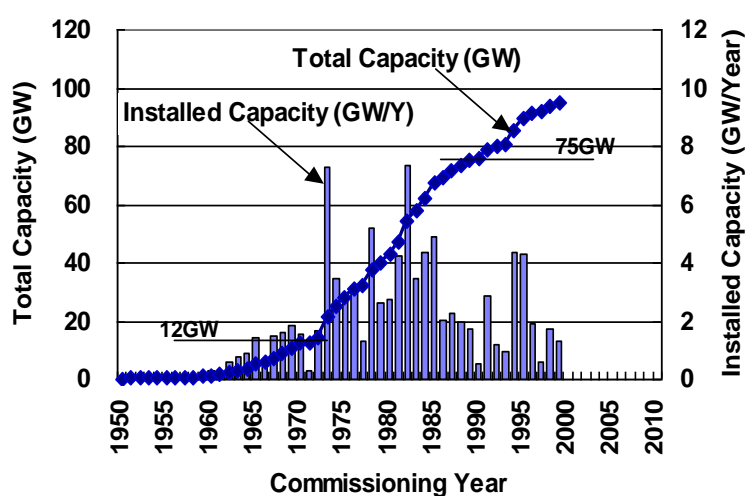
Figure A.2: Relationship between number of pumped hydro systems and capacities



Source: IEA, based on data from Mc COY report 2008, (2008).

Figure A.3: Total capacity of pump turbines worldwide

Source: IEA, based on data from Mc COY report 2008, (2008).

Figure A.4: Installed capacity of pump turbines worldwide

Source: IEA, based on data from Mc COY report 2008, (2008).

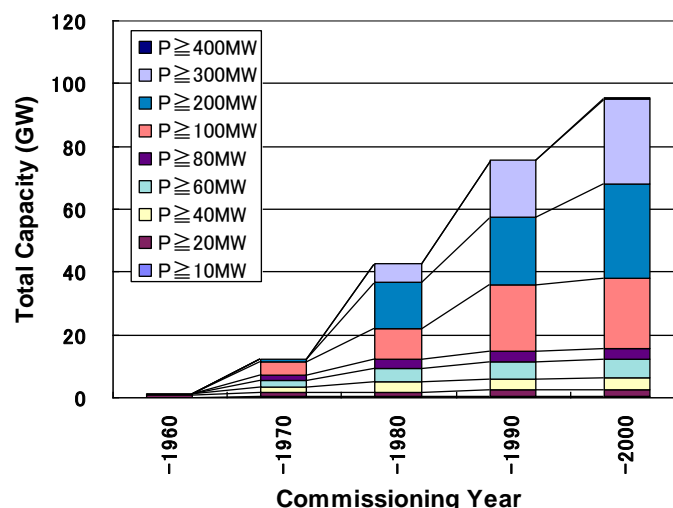
The historical change of unit capacity as part of the total capacity of pumped hydro systems is shown in Figure A.5. Large capacity units with pump turbines of over 100MW of have been installed since the 1970s and account for about 80% of the total number of operating pump turbines at present. The tipping point of this trend of installing larger capacity units coincided with the development of the high-head pump turbine provided for the Numappara Power Station (Japan) in 1973, which had a head of more than 500 meters.

The energy density of the water in a pumped hydro plant increases as the pump turbine head increases, as shown in the following equation:

$$E = \frac{\int P dt}{\rho V} = gH \quad (\text{A.2})$$

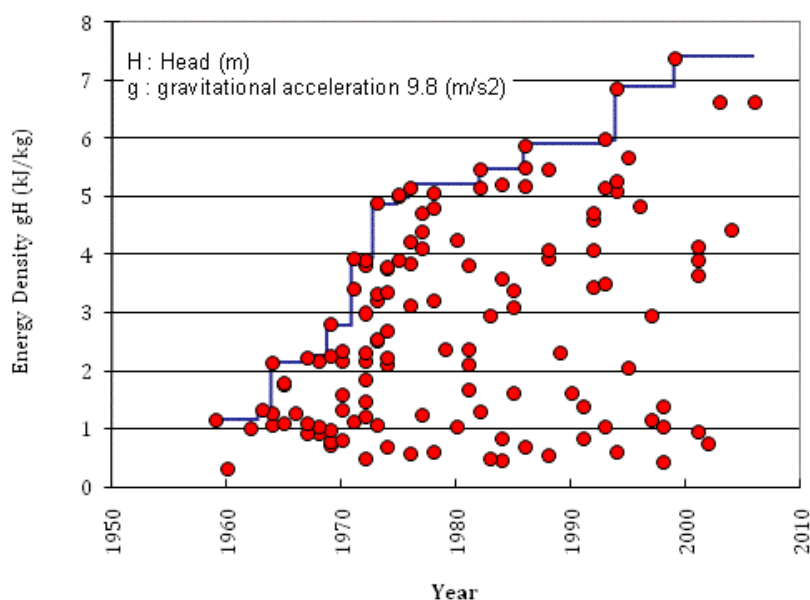
where E is specific energy or energy density of water (J/kg), P is power (W), ρ is water density (kg/m^3), V is volume of water (m^3), g is gravitational acceleration (m/s^2), and H is pump turbine head (m). Consequently, relatively small-volume water reservoirs and relatively compact pump turbines are required for high-head pumped hydro units, which have a large amount of energy stored in the upper reservoir. This feature of high-head pumped hydro has led to the use of higher and larger pump turbines in order to make the storage system more cost-effective. The historical change worldwide in the energy density gH (kJ/kg) of operating water for pump turbines is shown in Figure A.6.

Figure A.5: Composition of unit capacity



Source: IEA, based on data from Mc COY report 2008, (2008).

Figure A.6: Energy density of pumped hydro storage over time

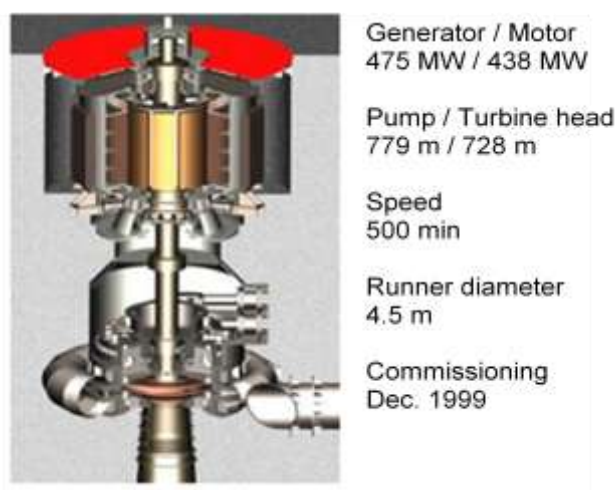


Source: IEA, based on data from Mc COY report 2008, (2008).

In 1999, the world's highest pump turbine unit, with a pumping head of 779m and turbine output of 412MW, was commissioned in Kazunogawa Pumped Storage Power Station (Japan). Figure A.7 shows a three-dimensional CAD sectional drawing of the pump turbine.

Cost status

For new facilities, the current capital cost of pumped hydro is 2700-3300USD/kW (EPRI, 2009). As described above, pumped hydro storage is a mature technology with no experience curve efficiency expectations. Operation and maintenance costs are approximately 90-160USD/kW. The capital cost to upgrade facilities is 600-3000USD/kW. Details of cost are given in Table A.1.

Figure A.7: 700m- 400 MW class pump turbine

Source: Hitachi Ltd., 2008.

Table A.1: Detail of cost for pumped hydro

Dam	30%
Chanel	21%
Generator	15%
Civil engineering	9%
Others	25%
Total	100%

Operational status

More than 200 pumped hydro plants are operating worldwide. There are few technical bottlenecks and it is the most mature and reliable technology among large-scale energy storage systems.

Production status

As noted earlier, the installed capacity of pump turbines from 1950-2000 is shown in Figure A.6. In this period, total capacity has grown to more than 90GW. Shipments have been decreasing gradually after a peak was recorded in 1982. The primary reasons for this trend might be difficulties in finding a suitable location, environmental resistance to the dams and reservoirs needed for pumped hydro storage systems, and competition with cheap natural gas.

The most attractive proposition is upgrading and modernizing old facilities. As shown in Figure A.4, pump turbine units accounting for more than half of the total capacity were installed more than 30 years ago. Upgrades would include increasing the capacity and efficiency of existing units.

Regulatory status

Pumped hydro storage systems comply with regulations similar to those governing conventional hydro power plants. From this viewpoint, significant barriers to growth are difficulties involving siting and environmental resistance.

Future Scenarios

As an initial strategy for expanding pumped hydro capacity, upgrading and efficiency improvement are suitable. For future pumped hydro systems, the following alternatives are investigated.

Strategic addition of pumping capacities

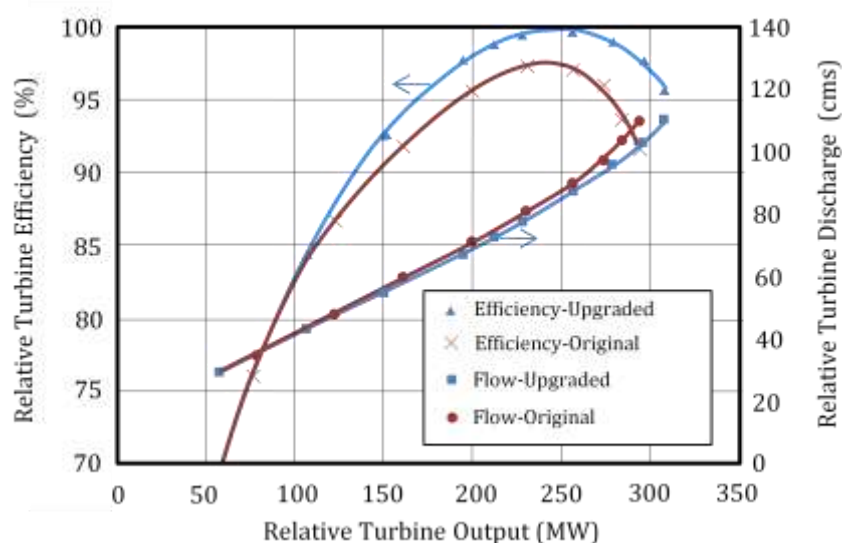
In the reversible pump of a conventional pumped hydro plant, the capacity of the pump is smaller than the capacity of the water turbine. Therefore, the water pumping process requires more time than the generation process. To make the most of pumped hydro, speeding up the pumping process during periods of reduced-rate power availability is advisable.

The strategic addition of pumping capacity is type of upgrading solution. However, in such an upgrading case, damage to the turbine runner, such as cracking, has been reported.

One successful example of upgrading a pumped hydro plant is the Blenheim Gilboa pumped storage project in New York State. Figure A.8 compares the performance of the original and upgraded pump turbines when operating as turbines. Efficiency was increased significantly and the new operating range, based on equivalent pulsations, vibrations and other parameters, is 140MW to 290MW.

The strategic addition of pumping capacity is an important option for increasing efficiency and turbine discharge.

Figure A.8: Comparative Performance of Original and Upgraded Pump/Turbines



Source: H. Okumura et al., 2009.

Seawater pumped hydro

Pumped hydro that utilizes seawater as an operating fluid has been investigated. An aerial view of seawater pumped hydro is shown in Figure A.9. This 30MW plant, located at Okinawa, Japan has 136m head, 26m³/s discharge, and 546,000m³ artificial effective storage.

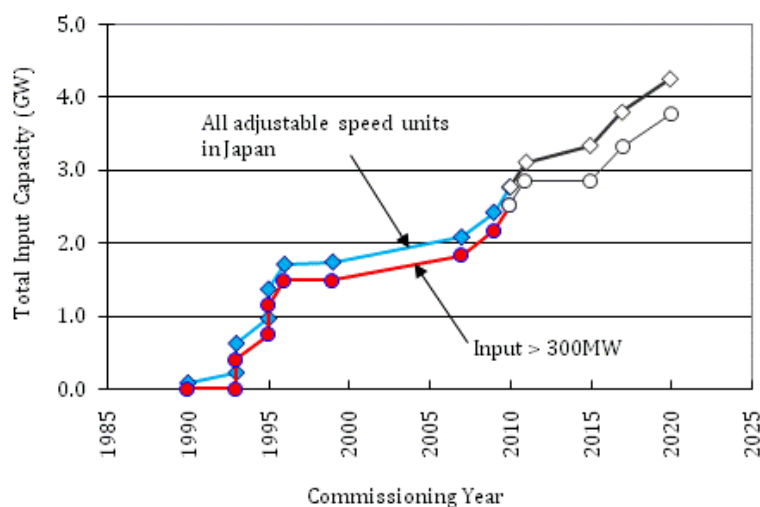
A seawater pumped hydro plant has the following advantages:

- 1) It is comparatively easy to find an appropriate location for the plant because the vast ocean is utilized as the lower reservoir.
- 2) They can attain up to 80% efficiency because of the short waterway length, which reduces the hydraulic losses by 93% to 98% (c.f. equation (A.4)).

Figure A.9: *Aerial view of seawater pumped hydro*

Source: J-Power, 1999.

An adjustable-speed unit (as described below) is used with the seawater pumped hydro plant in Figure A.10. If renewable energy plants such as wind or solar power stations with enough capacity were to be built nearby, even with large output variations, renewable energy supplies could be used for charging the seawater in the upper reservoir.

Figure A.10: *Growth of adjustable speed pumped hydro*

Source: K. Aguro et al., 2008.

Table A.2 compares the costs between the conventional pumped hydro plant and the seawater pumped hydro plant. For corrosion prevention measures, the cost of the pump turbine increases. As an overall cost, 15% increase of is estimated.

Table A.2: *Comparison of relative cost (BOP = balance of plant)*

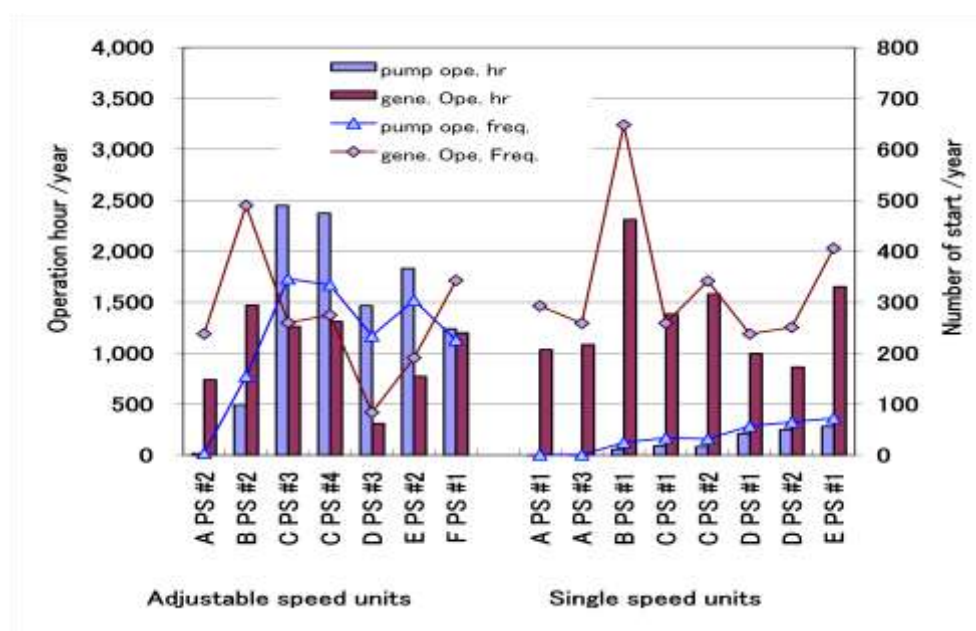
Devices	Conventional pumped hydro	Seawater pumped hydro
Pump turbine	1.0	1.54
Generator motor		1.0
Main transformer and BOP		1.62
Total	3.62	4.16

Adjustable-speed pumped hydro

Because the pump turbine uses a turbo impeller, both the rotational speed and the pumping head determine the input of the pump turbine. Therefore, when operating at a certain pumping head, a single-speed pump turbine driven by a synchronous motor cannot vary the input. In contrast, an adjustable-speed pump turbine that is driven by an adjustable speed motor can vary the input. This feature enables tuning of the grid frequency at night as well as the use of fluctuating renewable wind or solar energies to pump water to the upper reservoir.

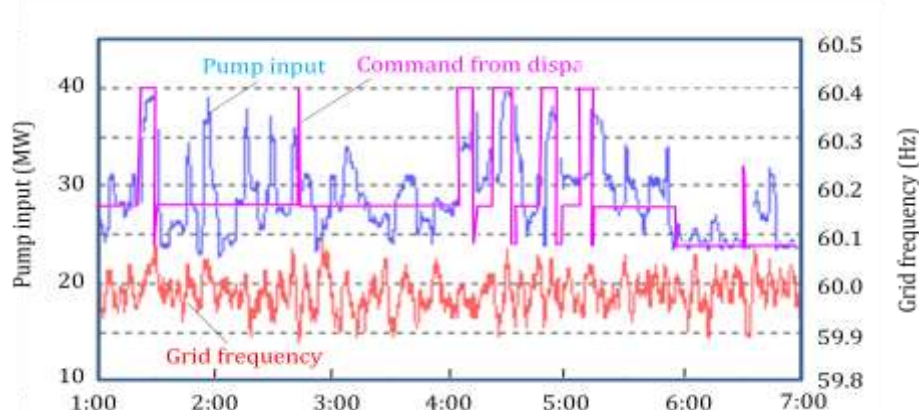
Adjustable-speed pumped hydro units have been installed in Japan since the 1990s, as shown in Figure A.11. The majority have capacities of over 300MW input. The principal feature of the adjustable-speed units is that the input power is adjustable when carrying out automatic frequency control (AFC) while charging the energy in the upper reservoir. This operation is frequently required to adjust the speed of units during light load periods such as the middle of night and holidays. Consequently, the pump operating hours are much longer for capacities over 300 MW input. Operational hours are also much longer for adjustable-speed units than for single-speed units, as shown in Figure A.12. In addition, pump starts are much more frequent for variable-speed units than for single-speed units.

Figure A.11: Operation of adjustable-speed pump



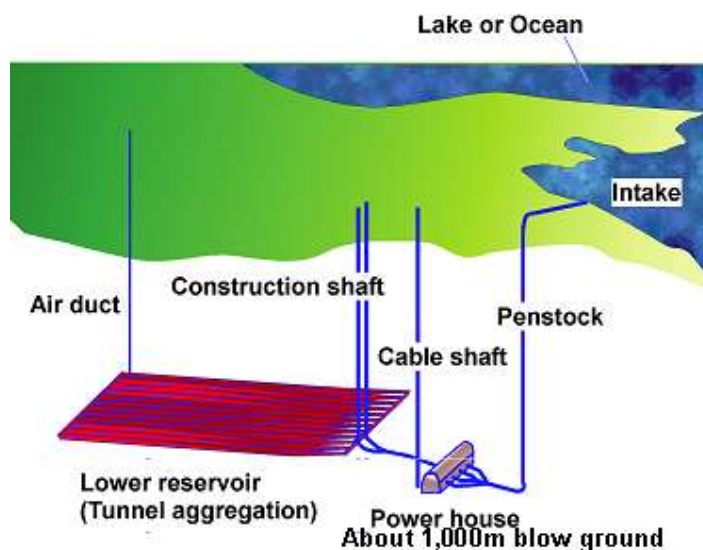
Source: K. Aguro et al., 2008.

Pumped hydro power plants are important facilities in the power grid, They are more efficient and stable than coal-fired thermal power plants and nuclear reactor power plants, which are alternatives to oil for supplying base load electricity. Economical difficulties due to lack of appropriate locations that satisfy environmental, topographical, and geological conditions are significant challenges. Underground reservoir systems are expected to be a solution to such difficulties.

Figure A.12: AFC plus governor free operation in pumping mode

Source: K. Aguro et al., 2008.

For conventional pumped hydro plants, both the upper and the lower reservoirs are constructed above ground. In contrast, underground pumped hydro systems are of two types: fresh-water underground pumped hydro systems that utilize artificial underground tunnels as the lower reservoir and a natural lake as the upper reservoir; and seawater underground pumped hydro systems that utilize artificial underground tunnels as the lower reservoir and the ocean as an upper reservoir. A sketch of the underground pumped hydro system is shown in Figure A.13.

Figure A.13: Sketch of underground pumped hydro

Both types of underground pumped hydro plants retain the features of the conventional pumped hydro and have the following extra features:

- 1.) Reduce the impact on the above-ground environment, such as the natural scenery.
- 2.) Preserve the ecological system of raptor species.
- 3.) Expand the range of plant location choice by relaxing the restrictions on topographical conditions.
- 4.) Reduce transmission costs by installing the pumped hydro plant nearer the site of electricity consumption.

Compared to conventional pumped hydro plants, underground pumped hydro plants have been conceived to be more practical facilities for the future.

The Agency of Natural Resources and Energy of Ministry of International Trade and Industry (MITI) in Japan investigated the following items for five years from 1997 to 2002 as part of an effort to realize underground pumped hydro schemes:

- 1.) Rational design and construction of an underground pumped hydro power station that utilizes space deep underground, aiming for more economical efficiency.
- 2.) Development of a pump turbine for use with seawater and establishment of technologies for casting, forging, rolling and welding a new stainless steel that can withstand seawater.
- 3.) Design of a generator motor to be used for an ultra-high-head pump turbine.
- 4.) Development of instruments for surveying geological conditions deep underground (1000m).
- 5.) Development of geological research and evaluation methods for deep underground environments.
- 6.) Environmental evaluation of the impact of a deep underground pumped hydro power plant.

Projected specifications of the plant are as follows.

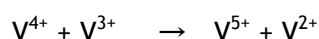
Output	maximum 2000MW
Generating hours	7h
Effective head	800m (7.8 kJ/kg)
Static head	830m (freshwater plan), 850m (seawater plan)
Maximum flow volume	296m ³ /s
Upper reservoir	35m (available depth for freshwater plan)
Lower reservoir	30m (available depth)
Submergence	90m
Effective storage	8,000,000m ³

Vanadium Redox Flow Cell

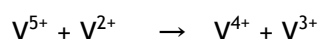
Concept

The principle of the vanadium redox flow cell is shown in Figure A.14. In a diluted sulphuric acid solution in which vanadium is dissolved, the valences of vanadium vary with charge and discharge as follows:

- 1) Charge:



- 2) Discharge:



By recirculating the flow of electrolyte, large capacity systems can be realized in which much electric power is stored.

Figure A.14: Principle of redox flow cell

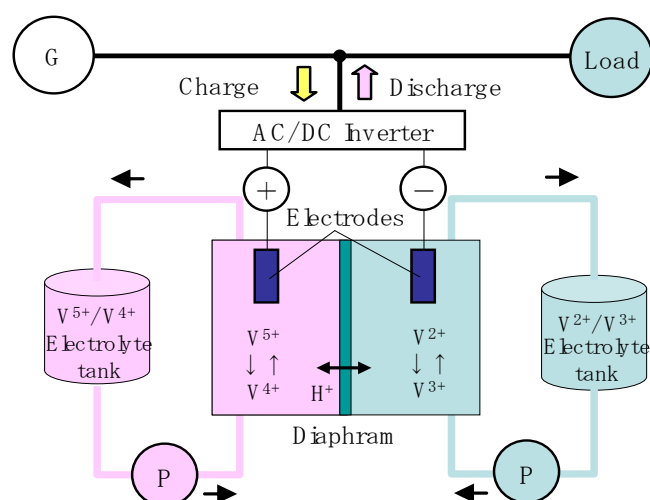
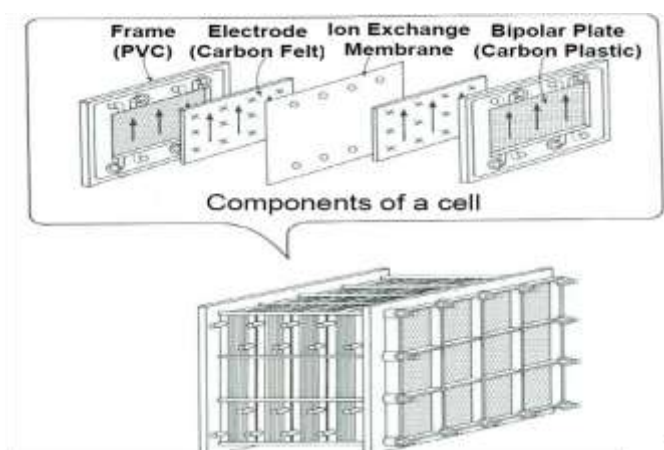


Figure A.15: Structure of redox flow cell



Source: VRB Power Systems, 2008.

Structure

The configuration of the vanadium redox flow cell is shown in Figure A.15. This example is composed of 100 cell stacks because the voltage of each stack is just 1.4 V. Pumps recirculated electrolyte between storage tanks and each cell. Since heat release is associated with charge and discharge, air or water cooling systems are required, which increases the volume and cost of the vanadium redox flow cell system.

Features

Currently produced vanadium redox flow cells achieve an energy density of about 20Wh/ℓ. This energy density is quite low compared to other rechargeable battery types, such as lead-acid (40-80Wh/ℓ), lithium-ion (140-210Wh/ℓ) and NaS (140-170Wh/ℓ) cells. Because vanadium redox flow cells operate at room temperature and atmospheric pressure, they can be operated without material deterioration due to high temperature. Since there are only two moving parts, reliability is high and operating and maintenance cost is quite low. Their current efficiency is 65-75% and life cycle is estimated to be about 12,000 charge/discharge cycles.

Technical status

Because of their less-restricted operating conditions and use of ordinary (i.e. non-hazardous) materials, redox flow cells are not technically difficult. To achieve higher efficiency, high

performance electrodes are being developed. In addition, an air-cooled cooler has been developed to decrease system volume.

Cost status

The total capital cost for vanadium redox systems is approximately 7000 - 8200USD/kW (EPRI, 2009).

Operational status

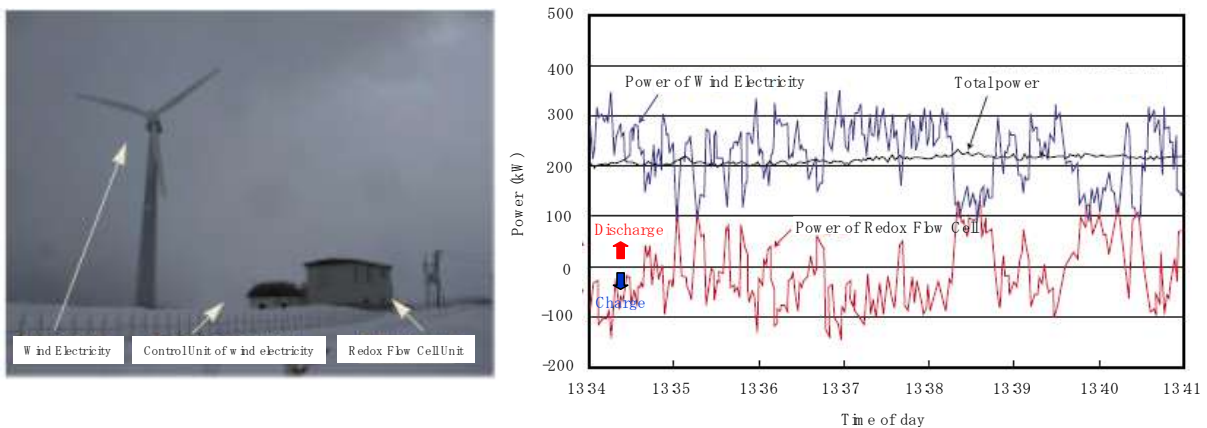
Major projects involving vanadium redox flow batteries include:

- A 1.5MW UPS system in a semiconductor fabrication plant in Japan
- A 275kW output load-leveling system in use on a wind power project on the Tomamae Wind Hills of Hokkaido, Japan
- A 200kW, 800kWh load-leveling system in use at the Huxley Hill Wind Farm on King Island, Tasmania
- A 250kW, 2MWh load-leveling system in use at Castle Valley, Utah
- A 12MWh flow battery is also to be installed at the Sorne Hill Wind Farm, Donegal, Ireland, by Sumitomo Electric Industries Inc.

A 227 kW-class system operating with a wind turbine is shown in Figure A.16. The results of stabilization of the output for this system are shown in Figure A.17, indicating that the system could stabilize the total power supplied. Figures A.24 and A.25 are photos of existing vanadium redox systems.

Figure A.16 (left): A 227-kW class system with wind power

Figure A.17 (right): Stabilization of wind power generation



Source: Sumitomo Electric Co., 2004.

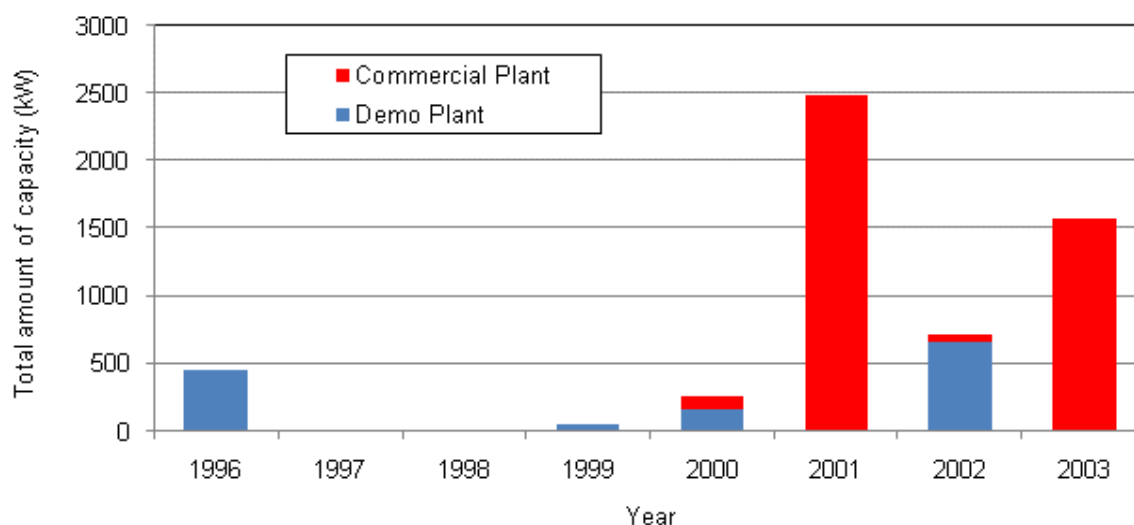
Figure A.18 (left): 1-MW class systems**Figure A.19 (right):** Electrolyte tanks

Source: VRB Power Systems, 2008.

Production status

Production trends from 1996-2003 are shown in Figure A.20. “Demo plant” refers to a plant built to evaluate fundamental features. Since 2000, the amount of production has increased gradually to handle load leveling in wind power systems, factories and buildings. Fundamental testing was done from 1996 to 1999, after which systems were launched, with their use growing gradually. Redox cell systems have experienced slower growth than NaS cell despite their similar release timing.

VRB Power Systems Inc. provides the vanadium redox flow cell systems. In May 2005, VRB Power acquired a worldwide license for SEI's patents and technology. Then, in January 2009, Prudent Energy acquired the assets of VRB Power. The company had three product lines of small systems ranging from 2.5kW to 10kW, medium-size systems of 25kW, and larger applications of 25kW-10MW. These lines appear to have been taken over by Prudent Energy.

Figure A.20: Trends in installed capacity of redox flow cells

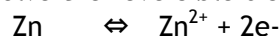
Source: IEA, based on data from Sumitomo Electric Co. and VRB Power Systems, (2004).

Regulatory status

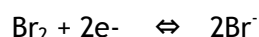
Vanadium redox flow cells are not considered hazardous goods under fire protection laws in Japan. They can be used as back-up power for fire-fighting equipment.

Future Scenarios

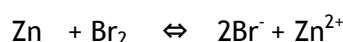
While only vanadium redox flow cells have been released as a large-scale commercial product, other types of redox flow cells are also in development. The zinc/bromine redox flow battery has received much interest as a rechargeable power source because of its good energy density, high cell voltage, high degree of reversibility, and abundant, low-cost reactants. In the cell, the negative electrode reactions involve the reversible dissolution/plating of zinc as follows:



Conversely, at the positive electrode, bromine is reversibly reduced to bromine as follows,



The overall reaction is written as:

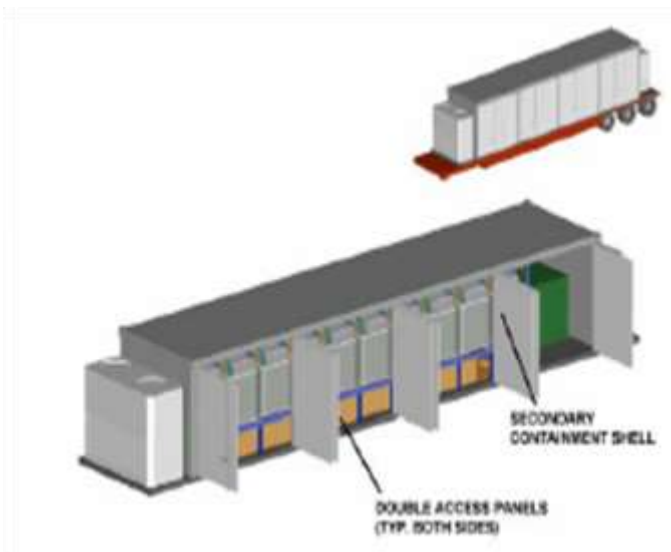


With this reaction, the potential difference is around 1.67 V per cell, and the energy density is 75 - 85Wh/kg.

ZBB Energy Corporation has released two types of products. One is a 50kW, 50kWh unit, which could power a home for approximately two days. It includes three cell stacks, each containing 60 cells. The other product consists of ten 50kWh modules electrically configured in two series strings to achieve 500kWh of energy storage.

As a demonstration system, a 2MWh (500kW × 4h) mobile energy storage system with a zinc-bromine redox flow cell is being developed by Premium Power Corporation in cooperation with EPRI (Figure A.21). The system, which includes a chiller and a power control unit, is contained in a portable and off-loadable freight container. This project aims to demonstrate the technical feasibility of lowering the peak power requirements at a substation and feeder. The estimated cost is 1.2 - 1.5 million USD over 30 months. In the project duration of 30 months, six months will be dedicated to designing and building the system, and 24 months will for on-site demonstration testing.

Figure A.21: Examples of zinc-bromine redox flow cell: a 2-MWh mobile system.



Source: EPRI, 2009.

One development challenge is to improve the durability and performance of the positive ion-exchange membrane. With continuous development of the cell and membrane, the cost reduction is important. As described above, the present cost of the redox flow cell is from 1500-3100USD/kW (EPRI, 2009). The key to reducing cost based on the experience curve is increasing future production. Compared to 150MW of production line dedicated to NaS cells, the manufacturing capacity for redox flow cells is relatively low.

Compressed Air Energy Storage (CAES)

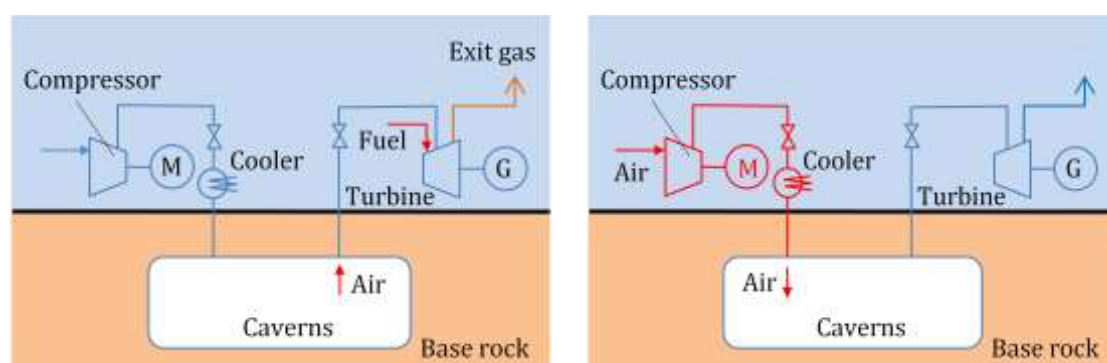
Concept

CAES is not a simple energy storage system, like other batteries. Instead, it is a peaking gas turbine power plant that consumes less than 40% of the fuel used by conventional gas turbines to produce the same amount of electric power. Unlike conventional gas turbines that consume about two-thirds of their input fuel to compress air at the time of generation, CAES pre-compresses air using low-cost electricity from the power grid at off-peak times and utilizes that energy later, along with some gas fuel, to generate electricity as needed. The compressed air is stored in appropriate underground mines or caverns, typically created inside salt rock deposits.

Structure

A CAES system consists of compressor unit with a motor unit, gas turbine, and underground compressed air storage in salt caverns, as shown in Figure A.22. When charging, usually at night, the motor unit consumes power to compress and store air in the underground chamber. The compressed air is usually cooled via a cooler unit. When discharging, usually during daytime peak loads, the compressed air is supplied to a combustor in the gas turbine to burn fuel. The combusted gas is expanded through the turbine, which drives the generator and produces electric power.

Figure A.22: Principle of the CAES system, showing daytime discharge (left) and night time charge (right).



Features

The CAES system stores electrical energy in the form of pressurized air. During periods of charging, the compressor unit compresses air into the caverns, which are at a depth of 500-800m, under a pressure of 45-70 bars. The efficiency of an ordinary CAES system, which uses the simple cycle of a gas turbine, is about 50%, which is higher than that of a conventional simple-gas turbine cycle because the CAES system is separated by the compressor unit. Efficiency is improved with the use of an advanced gas turbine cycle. CAES units can come on line within about 14 minutes. As natural gas is consumed to operate the gas turbine, it is accompanied by the production of CO₂.

To make the underground caverns used as air storage chambers, a large amount of water is injected into rock salt deposits, dissolving the salt and creating large chambers at low cost. It takes about 1.5 to 2 years to create caverns in this way. As they are most economically positioned near salt rock deposits, siting opportunities for CAES systems are limited. On the other hand, above-ground air storage, in which compressed air is stored in metal vessels or pipes, can also be used. Such systems allow CAES to be sited almost anywhere and will make it a more attractive energy storage option.

Technical status

The first commercial CAES system was a 290MW unit built in Huntorf, Germany in 1978. The second was a 110MW unit built in McIntosh, Alabama in 1991. The third CAES system, the largest yet, will be a 2700MW plant that is planned for construction in Norton, Ohio. This plant will compress air to 1500 psi in an existing limestone mine 610m underground.

Cost status

For new facilities, the current capital cost is 600 - 700USD/kW for 100-300MW, and 1500 - 1800USD/kW for 10-20MW (EPRI, 2009). With only two plants in operation, CAES plant construction remains a custom undertaking with no clear experience curve. Also note that above-ground CAES is estimated to be five times as expensive as underground salt-based compressed air storage.

Operational status

The CAES plant in Huntorf has successfully operated for more than 20 years. An aerial photo of the site is shown in Figure A.23. Its specifications are as follows:

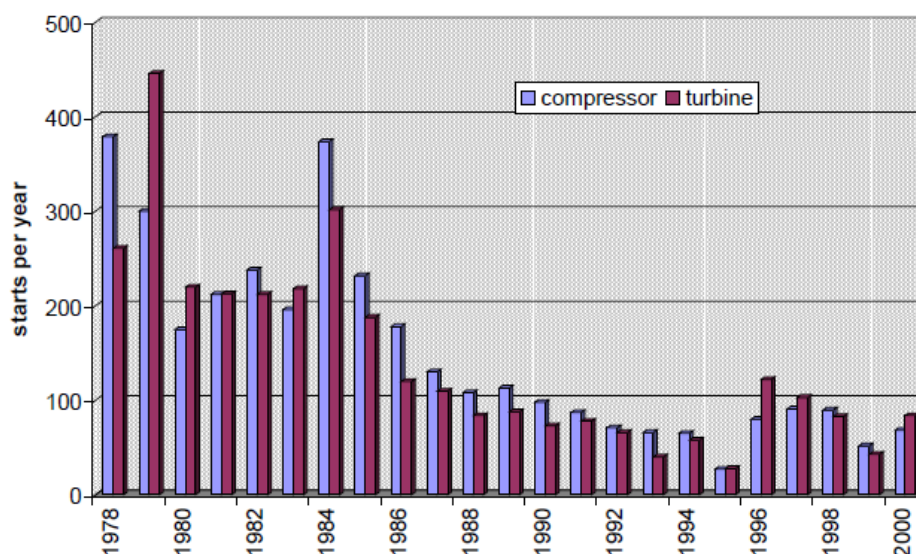
- Output: 290MW (<3 h), Compressor: 60MW (<12h)
- Air flow rate of the turbine: 427 kg/s
- Pressure of storage: 1 bar (minimum) - 70 bar (maximum)

Figure A.23: Aerial view of Huntorf



Source: F. Crotagino et al., 2001.

Figure A.24 shows the number of operational starts per year since 1978. The number of starts has decreased since 1985 due to a connection with a larger grid network that includes pumped hydro capacity. No serious problems or accidents have been reported.

Figure A.24: Operation starts per year at Huntorf

Source: F. Crotono et al., 2001.

Production status

The two plants at Huntorf and McIntosh are currently in operation, and a third plant in Ohio has been planned. The main developers and suppliers are CAES Development Company, Ridge Energy Storage, Dresser-Rand Company, and KBB.

Regulatory status

CAES systems comply with regulations similar to those governing conventional gas turbine power plants. It is felt that the main barrier to growth is the limited number of suitable sites.

Future Scenarios

A comparison of CAES systems is shown in Table A.3. In this table, the round-trip efficiencies were defined as follows:

Round-trip efficiency:

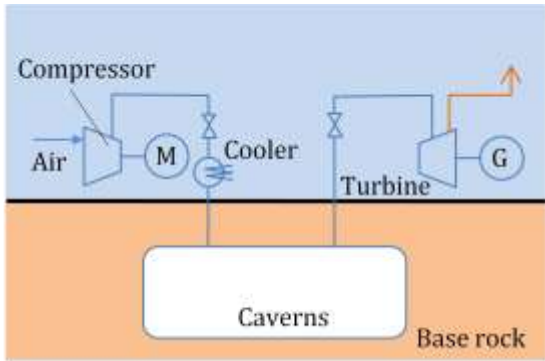
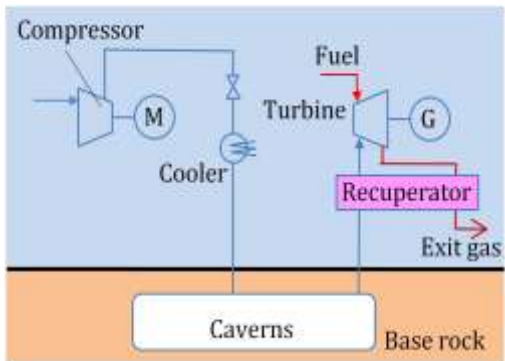
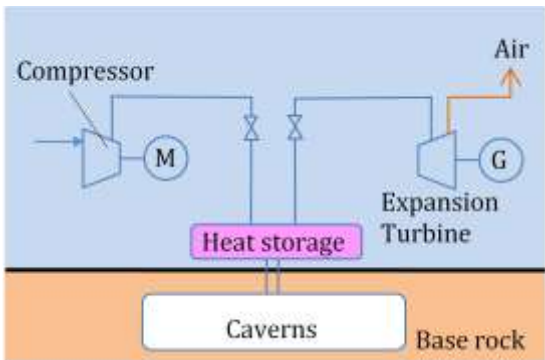
$$\eta = \frac{1.0 \text{ kWh}}{(4220/3600) * Eff_{NG} + 0.67}, \quad (\text{A.3})$$

where, Eff_{NG} is 1.00 for natural gas, 0.54 for NGCC, 0.385 for simple GT. When $Eff_{NG} = 1.00$, the round-trip efficiency is equivalent to the conventional energy efficiency. As described above, the efficiency of an ordinary CAES system is not as high as it might be because of the energy demands of the air cooler unit. Efficiency is being improved through the following approaches:

1) CAES system with recuperator

This system applies regenerative cycle technology to CAES. The heat content of the exhaust gases is recovered with a heat exchanger to preheat combustion air entering the combustor. The McIntosh plant in the U.S. adopted this cycle, which increases efficiency to about 54%.

Table A.3: Comparison of CAES systems

Systems	Specifications
 <p>Ordinary CAES system</p>	<p>Site: Huntorf</p> <p>Input:</p> <ul style="list-style-type: none"> 0.83 kWh electric energy 5322.94 Btu (=1.56 kW_r) fossil energy <p>Output: 1 kWh electric energy</p> <p>Energy Efficiency: 42% ($Eff_{NG}=1.00$)</p> <p>Round-Trip Efficiency: 60% ($Eff_{NG}=0.54$); 70% ($Eff_{NG}=0.385$)</p>
 <p>CAES system with recuperator</p>	<p>Site: McIntosh</p> <p>Input:</p> <ul style="list-style-type: none"> 0.69 kWh electric energy 3992.20 Btu (=1.17 kW_r) fossil energy <p>Output:</p> <ul style="list-style-type: none"> 1 kWh electric energy <p>Energy Efficiency: 54% ($Eff_{NG}=1.00$)</p> <p>Round-Trip Efficiency: 76% ($Eff_{NG}=0.54$) 88% ($Eff_{NG}=0.385$)</p>
 <p>Advanced adiabatic CAES system</p>	<p>Site: EU-funded R & D project</p> <p>Input:</p> <ul style="list-style-type: none"> 1.42 kWh electric energy 0.00 Btu (=0.00 kW_r) fossil energy <p>Output:</p> <ul style="list-style-type: none"> 1 kWh electric energy <p>Energy Efficiency: 70% ($Eff_{NG}=0.0$)</p>

Similar approaches with other gas turbine cycles, such as Cheng and HAT (humid air turbine) cycles, will be applicable. The Cheng cycle consists of a gas turbine capable of being injected with a large amount of superheated steam (15% - 20% of the exhaust flow) and a heat recovery steam generator (HRSG) that can generate both saturated and superheated steam with firing capability. The HAT cycle consists of a gas turbine, which is operated with highly humid air and a humidifying unit, that injects a large amount of water mist into the combustion air (15% - 20% of the exhaust flow), and a recuperator, which recovers the heat content of the exhaust gas and vaporizes the mist in the combustion air.

A second-generation CAES system is being planned in the United States. The project involves performance monitoring of two CAES systems. One will use below-ground caverns for bulk compressed air storage of 300MW for 10 hours. The other will use an above-ground air

vessel/piping system for short-term storage with a capacity of 15MW for two hours. The results of the project will provide critical information and data to make decisions about the need for energy storage solutions.

2) Advanced adiabatic CAES system

The storage efficiency of the CAES plants described above is reduced by cooling the air before it enters the cavern and reheating it prior to burning it with the fuel. In the advanced adiabatic cycle, heat energy is extracted and stored separately before the compressed air enters the cavern. When energy is required by the grid, the compressed air and heat energy are recombined, and expanded through an air turbine. This adiabatic CAES system benefits from higher storage efficiencies and, notably, zero CO₂ emissions. It is being developed through the “AA-CAES” (Advanced Adiabatic - Compressed Air Energy Storage) Project, funded by the European Union.

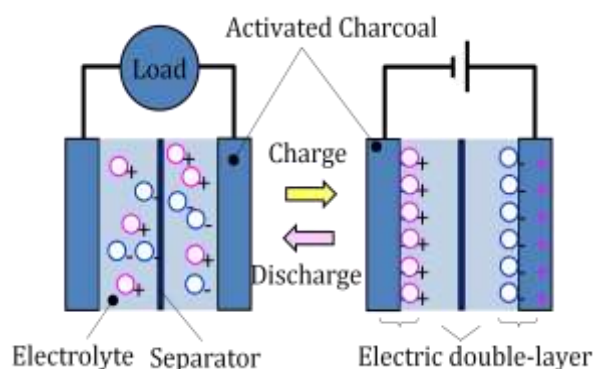
As for different approaches, a compressor with an internal cooler and water atomization cooling (WAC) might effectively reduce the power needed to drive the compressor. This power depends on the density of air, which is a function of air temperature. With an intermediate cooler, the air temperature is decreased. The WAC is a simple system that injects water mist of 10µm particle size at the compressor inlet. The water mist particles are vaporized through the compressor and the air temperature is decreased by the heat of vaporization.

Electric Double-Layer Capacitor System

Concept

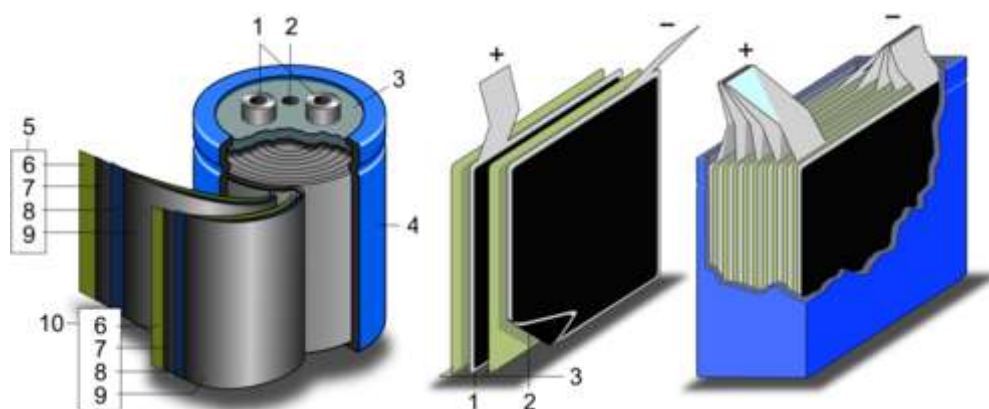
On a solid-liquid interface with a difference in voltages, a thinly-layered structure is formed that contains pairs of positive and negative charges. This phenomenon is known as the electric double-layer capacitor, and can be used to store electricity. In this technology, electricity is stored without a chemical reaction. To increase storage capacity, an activated charcoal electrode with a specific surface of 1000m²/g is used (Figure A.25). Electric double-layer capacitors are characterized by very short energy burst and limited duration.

Figure A.25: Principle of electric double-layer capacitor



Structure

Electric double-layer capacitor structures can be divided into two basic types: tube and box (Figure A.26). The tube type can increase the production efficiency because it is a simple structure with a rolled up sheet. The stacked version achieves a higher energy density but the production process is more difficult and costly. The internal resistance of the cylindrical type is larger than for the stacked type, which results in higher energy losses. Water or high molecular weight compounds are used for electrolytes in both types of capacitors.

Figure A.26: Structures of capacitors: tube type (left) and box type (right).

Source: M. Okamura, 2001.

Key to tube capacitor diagram (left): 1: terminal, 2: Safety valve, 3: Terminal board, 4: Container, 5: Positive pole, 6: separator, 7: polarisable terminal, 8: Collector, 9: Polarization elect, 10: negative terminal.

Key to box capacitor diagram (right): 1: polarisable terminal with polarisable electrode (positive), 2: polarisable terminal with polarisable electrode (negative), 3: separator.

Features

A large current can be charged and discharged through the absorption and desorption of ions. Because of the activated charcoal electrodes, capacitance is larger than that of ordinary condensers. The power density is 100 - 2000W/kg. Capacitors have a lower energy density than NaS cells or lead acid batteries, typically 1-5Wh/kg. As a consequence, they are only applicable for short discharge periods of 1 second to 1 minute. The discharge time is inversely related to the output power level, as shown in Table A.4. Since the charge and discharge processes are performed without any chemical reactions, wear is low and the system can be operated for hundreds of thousands of charge-discharge cycles. Typical system life is longer than 15 years. Furthermore, since the electrolyte does not include heavy metals, the environmental acceptability is high.

Table A.4: Example of the relationship between power and discharge time

Output (W)	Discharge time (s)
9000	0.5
5000	4
4000	6
3000	10
2000	17
1000	38

Source: Meiden Co., 2009.

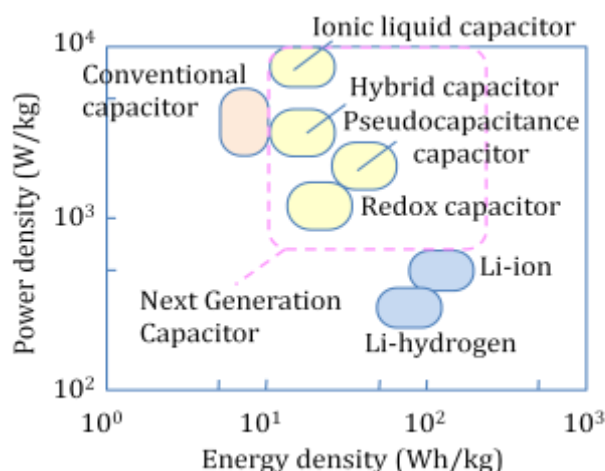
Technical status

The efficiency of the electric double-layer capacitor is about 84%. While small electrochemical capacitors are well developed, larger units with energy densities greater than 20kWh/m³ are still under development. The larger units are expected to be used for hybrid and electric vehicles, electric railway systems, UPSs, energy storage systems for short periods, and industrial systems. The energy density of the electric double-layer capacitor can be calculated by the formula

$$E = \frac{1}{2} CV^2, \quad (\text{A.4})$$

where E is the energy density, C is the capacitance (F/g), and V is the voltage (V). To increase the energy density, higher capacitance or higher voltage is effective. To increase the capacitance and the voltage of the capacitor, several approaches have been proposed. Characteristics of typical next-generation capacitors are compared with ordinary capacitors and batteries in Figure A.27. Note that lithium-ion and lithium-hydrogen batteries have generally lower power density and higher energy density.

Figure A.27: A comparison of specifications for capacitors and batteries



Source: K. Naoi, 2004.

The specifications for commercial ultracapacitors by Maxwell Technologies are illustrated in Table A.5. These specifications are already comparable to those of next-generation capacitors.

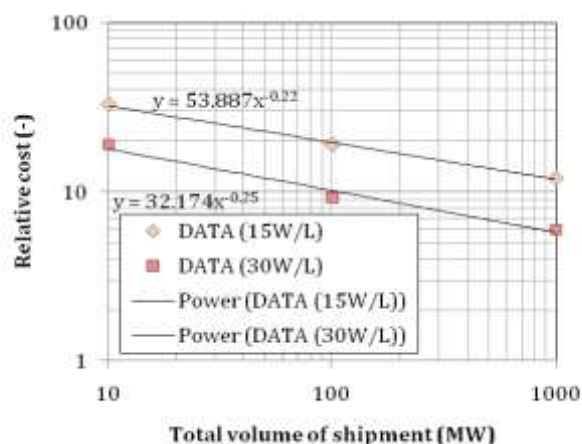
Table A.5: Specifications of commercial ultracapacitors

Energy density (Wh/kg)	Power density (W/kg)
2.91	6200
3.81	7900
3.98	6800
2.53	5200

Source: Maxwell Technologies, 2009.

Cost status

Current target capital costs for advanced capacitors are estimated to 1500 - 2500USD/kW (EPRI, 2009). The experience curve concept may be applied to small-scale electric double-layer capacitors. According to existing data, the learning rate is only 14% -15%. Figure A.28 shows how cost depends on the total volume of shipments and the capacitor size; there is roughly a factor 6 difference between low-capacity/low-cost/small-volume and high-cost shipments.

Figure A.28: Experience curve of advanced capacitors

Source: Source: M. Okamura, 2001.

Meiden Co. in Japan has expanded its production line to 15,000 units per year for load-leveling systems. Further expansion of production capacity will result in further cost reductions.

Operational status

Electric double-layer capacitors are especially applicable as energy storage systems for instantaneous voltage compensators because of their high power density and low energy density. A 10,000kVA system is shown in Figure A.29. The efficiency is more than 99%, and the compensable time is 1 second.

Figure A.29: 10,000kVA system for instantaneous voltage drop compensator

Source: Meiden Co., 2004.

To apply to them to load leveling with renewable power systems, they must be used with secondary batteries such as NaS cells. With such a combination, the short-term variations of renewable power output can be eliminated by the capacitor, while long-term variations can be eliminated by the secondary batteries. In such a configuration, the capacitors complement other energy storage technologies.

Advanced capacitors are also being considered for transportation system applications such as electric trains and road vehicles, where they can be used for regenerative braking. Already, modern train motors operate as generators during braking. The regenerated electric power can be used by nearby trains. However, when there are no nearby trains, the regenerative brake does not operate adequately. In that event, capacitors are being considered. In a similar application, 144 Maxwell Technologies ultra capacitors were used to capture regenerative

braking power and improve acceleration for transit buses in Long Beach, California. The systems have functioned reliably at temperatures from -25°C to 45°C.

Production status

The main developers and suppliers of advanced super capacitors and ultra capacitors are SAFT, NESS, ESMA, Maxwell Technologies, ELIT, Power System Co. and Meiden Co.

Regulatory status

The electrode composition varies between the different manufacturers, and organic solvent are often used to increase the voltage, hence there is some environment issues. The improvement of the environmental suitability is the key.

Future Scenarios

Storage energy depends on the voltage and capacitance (c.f. equation (6)). There are two strategies for improving the performance of capacitors: increasing capacitance, and increasing voltage. The latter is very effective, since voltage influences the storage energy as a squared value (c.f. equation (6)).

1) Higher capacitance

To increase capacitance, different electrode materials are being developed as shown in Table A.6. Doubled to tripled capacitances are obtained.

Table A.6: *Relationship between materials and capacitances*

Materials	Capacitances (F/g)
Next generation nano-carbon <ul style="list-style-type: none"> • Carbon nanotube • Mesoporous carbon • Activated charcoal nano fiber 	60-283
Metallic oxides <ul style="list-style-type: none"> • Ruthenium oxide • Mangum oxide • Nickel oxide 	300-1220
Conducting polymers <ul style="list-style-type: none"> • Polyaniline • 1,5-diaminoanthraquinone • Cyclic indole trimer polymer 	135-250

2) Higher voltage

To increase the voltage, electrolytes and structures are being developed as shown in Table A.7.

Table A.7: Relationship between electrolyte, structure and capacitance

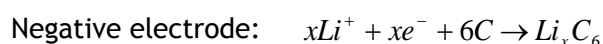
Electrolytes and electrodes	Voltages (V)
Ionic liquids (electrolytes) <ul style="list-style-type: none"> • Imidazolium salt • Pyridinium salt • Aliphatic ammonium salt 	3.0
Asymmetrical hybrid electrodes <ul style="list-style-type: none"> • Activated charcoal (+) & graphite (-) • Activated charcoal (+) & amorphous carbon(-) • Activated charcoal (+) & $\text{Li}_4\text{Ti}_5\text{O}_{12}$ (-) 	4.2

Li-ion Batteries

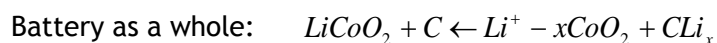
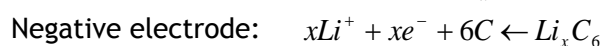
Concept

The Li-ion battery consists of a positive electrode made of LiCoO_2 and negative electrode made of specialty carbon. During the charging process, lithium in LiCoO_2 is ionized and moves to the negative electrode. During discharge, lithium ions move to the positive electrode. The main chemical reactions in the battery are given below.

1) Charge:

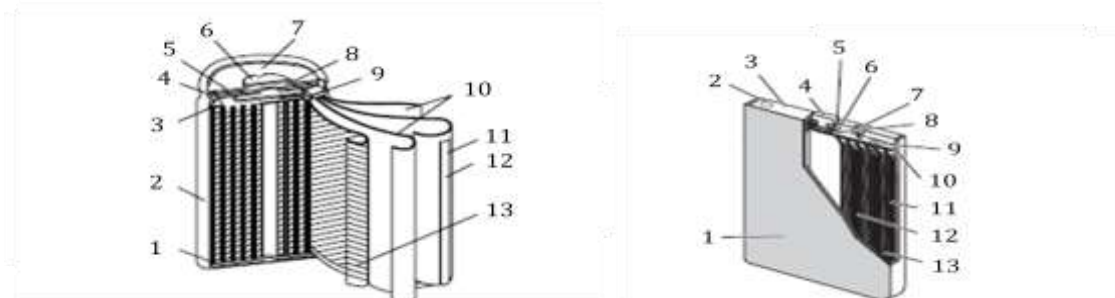


2) Discharge:



Structure

The two Li-ion battery structures, cylindrical and prismatic, are shown in Figure A.30. Each structure consists of four layers: a positive electrode of LiCoO , a negative electrode of special carbon, and two separators. The battery also has a relief valve, which discharges internal gas, to avoid accidents due to over-pressurization during overcharging. New Li-ion batteries are being developed that use manganese instead of cobalt, which avoids the problem of bursting. In addition, new types of ferro-alloys are being tested that would enable rapid charging.

Figure A.30: Structure of Li-ion battery

Key to cylindrical battery structure (left): 1: insulating plate, 2: housing, 3: insulating plate, 4: insulating gasket, 5: PIC element, 6: positive electrode, 7: exhaust gas hole, 8: relief valve, 9: positive electrode lead, 10: separator, 11: negative electrode, 12: negative electrode lead, 13: positive plate.

Key to prismatic battery structure (right): 1: housing, 2: relief valve, 3: plate, 4: electrode, 5: upper insulating gasket, 6: lower insulating gasket, 7: sealing plug, 8: internal electrode, 9: positive lead, 10: insulating frame, 11: separator, 12: positive plate, 13: negative plate.

Source: Panasonic, 2007.

Features

Because nonaqueous electrolyte is used, Li-ion battery voltages are higher than those of batteries with aqueous electrolyte. Their energy density is also higher, around 100-200 Wh/kg and 300-400 kWh/m³. Cycle efficiency is nearly 100%. Because of their reliable performance, Li-ion batteries are widely used for laptop computers and mobile phones.

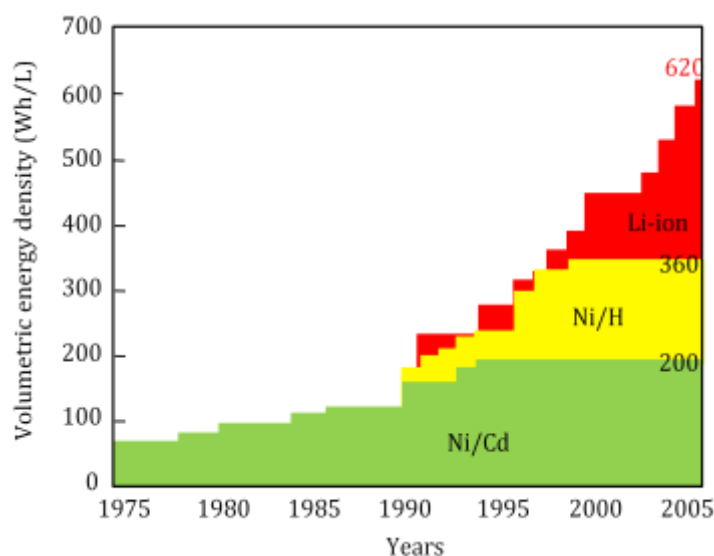
The Li-ion batteries do not experience a memory effect, which is an undesirable phenomenon in which a battery's apparent discharge capacity is reduced when it is incompletely discharged and then recharged. Li-ion batteries also have a low self-discharge rate of approximately 5% per month, compared with over 30% per month for common nickel metal hydride batteries and 10% per month for nickel cadmium batteries. Furthermore, their most important advantage is that they are free from the dendrite problem, the phenomenon of lithium precipitation that causes a short circuit at the electrodes.

Li-ion batteries require a protection circuit to monitor the charge and discharge, because the greatest weakness of this type of batteries is that their operating range is close to the hazardous range. In the case of overcharging, metallic lithium separates out at the negative electrode or oxidative tendency is heightened at the positive electrode. Both phenomena generate an abnormal amount of heat. In the case of over-discharging, cobalt is formed at the positive electrode or copper is formed at the negative electrode. These phenomena also generate abnormal amounts of heat. Vaporization of the flammable organic solvent-electrolyte in the case of overheating poses a fire hazard. In addition, short-circuiting is a hazard related to their high energy density.

Technical status

Li-ion batteries have higher volumetric energy density than other batteries (Figure A.31). Their energy density has been increasing annually. However, more development is needed to enhance the stability and reliability of large-scale systems. In particular, Li-ion batteries can rupture, ignite, or explode when exposed to high temperature environments. Short-circuiting of Li-ion batteries can cause them to ignite or explode. Development is focused on alternative materials that would not allow such effects to occur.

Figure A.31: Raising the volumetric energy density



Source: <http://www.go.jp/report/data/g60824bj.html/>

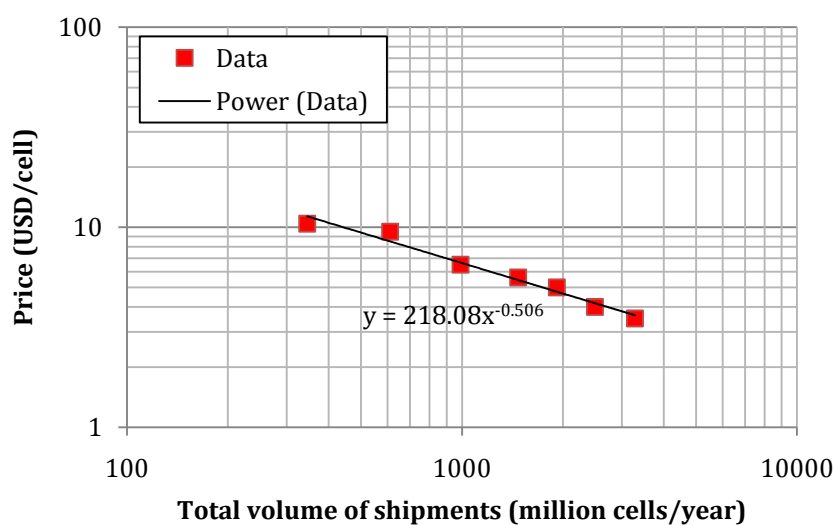
Cost status

The total capital cost of Li-ion batteries is estimated to be 4000 - 5000USD/kW (EPRI, 2009). It is expected that near-term uses will continue to be limited to small telecommunication equipment applications and other portable systems. The experience curve concept applies to Li-ion mass production technology. Based on data for cost and shipment volumes of small-scale Li-ion batteries from 1997 to 2003, an experience curve was constructed and is provided in Figure A.32. The regression model is expressed as:

$$C = 218.08n^{-0.506}, \quad (\text{A.5})$$

where C is relative cost in the n-th period. The exponent is 0.506, which implies a learning rate of 30%.

Figure A.32: Experience curve for Li-ion batteries



Source: IEA, based on data from MITI, 2004.

Operational status

While Li-ion batteries have claimed 50% of the small portable device market in just a few years, there are some challenges to making large-scale Li-ion batteries. The main hurdle is their high cost (above 600USD/kWh) due to special packaging and internal overcharge protection circuits.

In efforts to deploy Li-ion batteries with wind power systems, several companies are working on developing large-scale Li-ion energy storage systems. For example, Hokuriku Electric Power Company and Enax are testing wind and solar power generators with Li-ion batteries. This storage system consists of 336 stacked Li-ion batteries and has a capacity of 25.5kWh (Figure A.33). The project target is to produce a 100kWh system by 2010. In addition, Mitsubishi Heavy Industry and Kyushu Electric Power Company are planning large-scale Li-ion battery modules with capacities of 100kWh. SAFT is also developing UPS systems that are based on 100kW, 15kWh Li-ion batteries (Figure A.35).

Figure A.33 (left): 6.4kW modules

Figure A.34 (right): 100-kW, 15-kWh Li-ion batteries for UPS



Source: Hokuriku Electric Power Co., 2008.

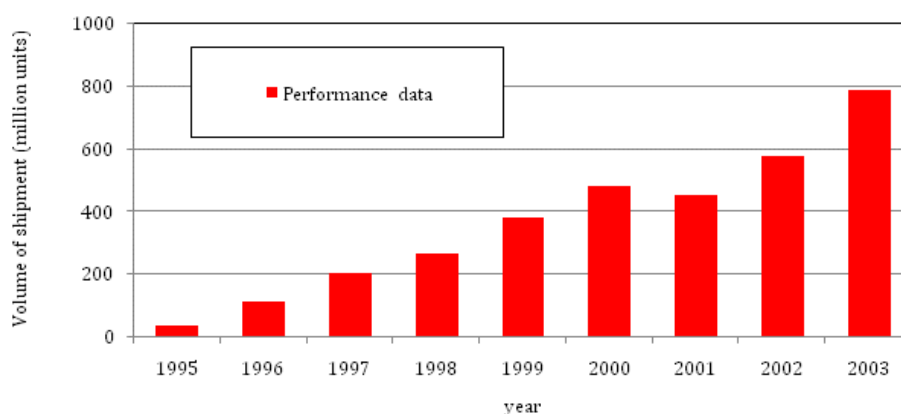


Source: Electricity Storage Association, 2009.

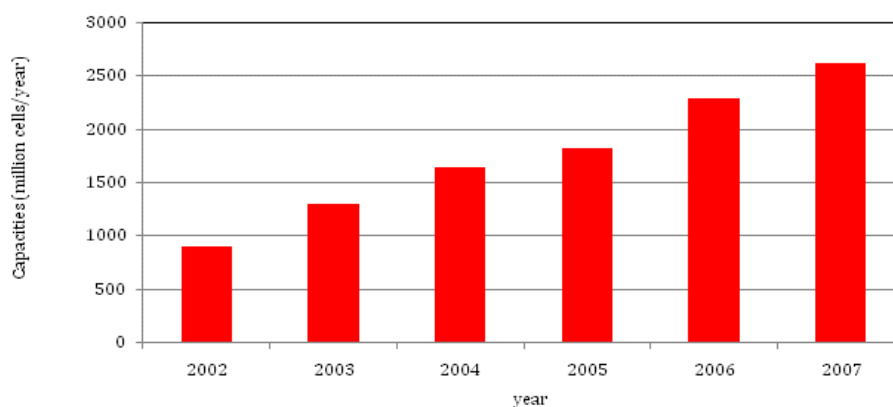
Production status

In 2003, the production of small Li-ion batteries reached 800 million units (Figure A.35), and production roughly doubled between 2003 and 2007. The production and material procurement experience obtained from these small batteries will be applied to the larger sized Li-ion batteries. However, the structure and especially materials used in small and large Li-ion batteries differ. It will be difficult to extend existing production facilities to allow production of large batteries in the same plants. The trend in production capacities for small Li-ion batteries is shown in Figure A.36. The growth rate in capacity is 20%-25% per year. Even large-scale Li-ion batteries are expected to have production potential. In particular, Li-ion batteries will be used in electric vehicles, whose volume production may help reduce costs.

In terms of materials, cobalt is a scarce metal. Three countries account for 56% of the world's production: Congo (19%), Zambia (19%), and Australia (18%). Deposits for future production are concentrated in Congo, a politically unstable country.

Figure A.35: Shipment growth of Li-ion batteries

Source: IEA, based on data from MITI, 2004.

Figure A.36: Production capacity growth of Li-ion batteries

Source: IEA, based on data from MITI, 2008.

Regulatory status

For small-scale Li-ion batteries, Underwriters Laboratory standard UL1642 is the regulation governing defects, and many tests have been established as part of UL1642 (Table A.8). However, definite regulations have not yet been determined for large-scale batteries.

Future Scenarios

The performance, stability and application of Li-ion batteries depend on the materials. Further development of Li-ion batteries for electric and hybrid vehicles is being promoted. However, Li-ion batteries for automotive and large-scale energy storage applications have few or no materials in common, and results in one area can not always be scaled up or down and applied to others.

For small batteries, a number of developments are progressing:

Materials for the positive electrode

- 1) Laminated positive electrode
 - Large capacity positive electrode
 - $\text{LiNi}_{1/3}\text{Mn}_{1/3}\text{Co}_{1/3}\text{O}_2$
- 2) Spinel type positive electrode

Materials for the negative electrode

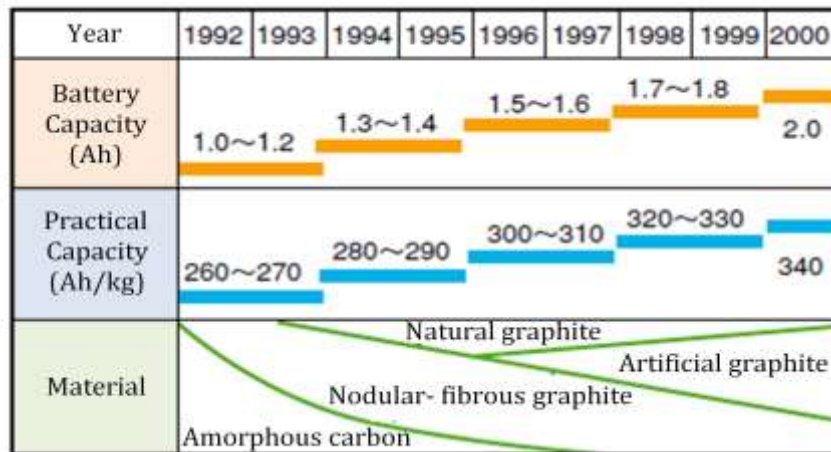
Trends in materials for the negative electrode are shown in Figure A.37. Artificial graphite improves the practical capacity from 260Ah/kg to 340Ah/kg, which is close to the theoretical maximum. Different concepts of negative electrode materials are being developed that should increase the storage capacity further, including negative electrodes made of new alloys and nitrides.

Table A.8: Contents of UL1642

Contents	Details
CONSTRUCTION	General <ul style="list-style-type: none"> • Casing • Electrolyte • Use
PERFORMANCE	General <ul style="list-style-type: none"> • Technician-replaceable batteries • User-replaceable batteries • Multi-cell installations Samples Conditioning of Samples <ul style="list-style-type: none"> • Discharge • Charge-discharge cycling Important Test Considerations Temperature Measurements
TESTS FOR TECHNICIAN-REPLACEABLE AND USER-REPLACEABLE BATTERIES	Electrical Tests <ul style="list-style-type: none"> • Short-Circuit Tests • Heating Test • Abnormal Charging Test • Forced-Discharge Test
	Mechanical Tests <ul style="list-style-type: none"> • Crush Test • Impact Test • Humidity Test • Shock Test • Vibration Test • Drop Test • Forced-Discharge Test
	Environmental Tests <ul style="list-style-type: none"> • Heating Test • Temperature Cycling Test • Low-Pressure (Altitude Simulation) Test
TESTS FOR USER-REPLACEABLE LITHIUM BATTERIES	Fire-exposure Test Test for Flaming Particles Projectile Test Explosion Test

Source: UL 1642, ISBN 1-55989-829-1, *Lithium Batteries*, 1999.

Figure A.37: Trends in negative electrode materials



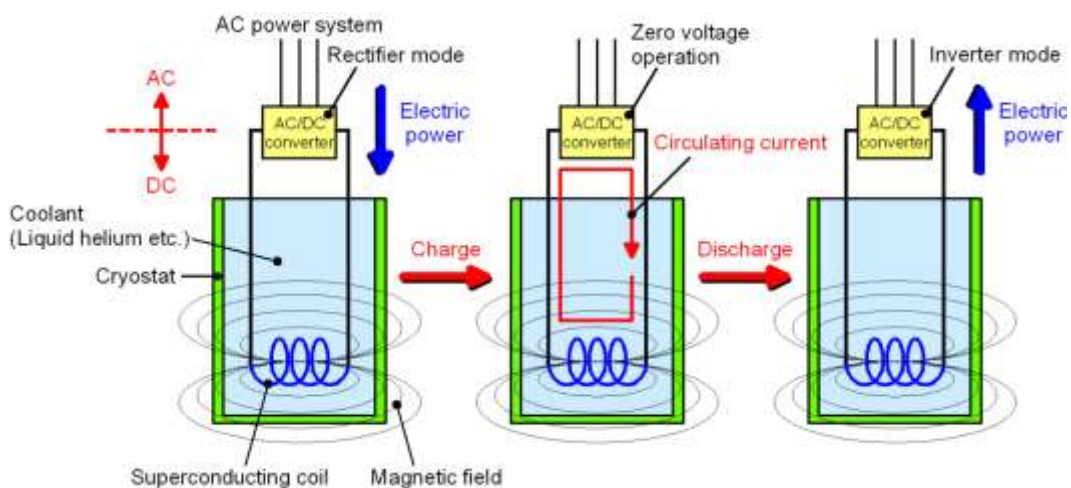
Source: Y. Ishii et al., 2006.

Superconducting Magnetic Energy Storage (SMES)

Concept

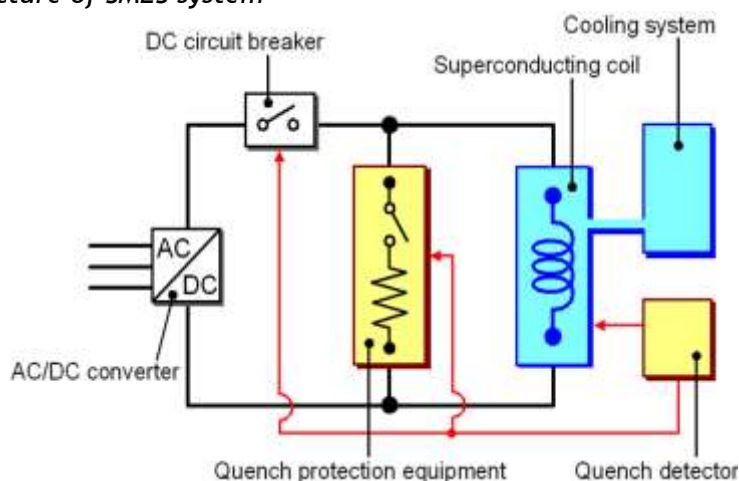
As its name states, the concept of SMES is based on the storage of magnetic energy. In order to reach superconductivity, a superconducting material that makes use of NbTi or Nb₃Sn must be operated at a temperature of around 4° K (Figure A.38).

Figure A.38: Principle of SMES



Structure

A SMES system consists of a superconducting coil, permanent current switch, quench protection equipment, DC circuit breaker, AC/DC converter, and, cooling system (Figure A.39).

Figure A.39: Structure of SMES system

The superconducting coil, made of NbTi or Nb₃Sn, stores magnetic energy. To keep the temperature at 4°K, immersion chilling or forced cooling systems are applied. Problems include achieving higher dielectric strength and lower AC loss, with quenching protection. When the superconductor coil is quenched, the coil generates heat due to Joule heating. The quench protection equipment consumes electric power in the coil based on the same principle as a resistance heating device. A DC circuit breaker cuts the electricity supply in case of erratic behaviour of the coil. The AC/DC converter connects the SMES and the electric grid. One main challenge confronting SMES is increasing its conversion efficiency (>95%).

Features

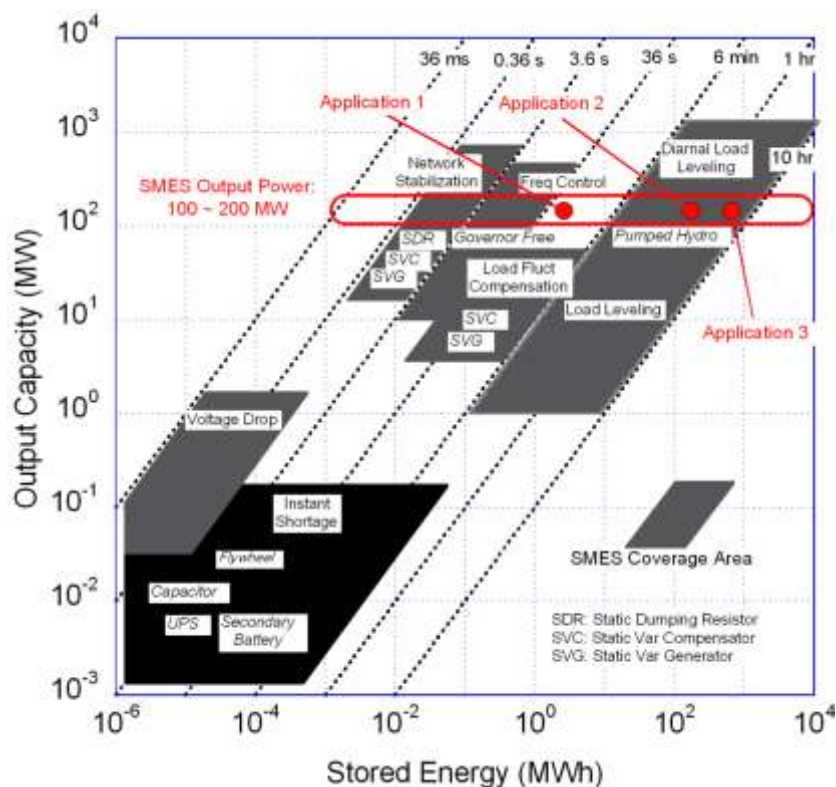
In the charge process, electric energy is transformed to magnetic energy through the coil. In the discharge process, the magnetic energy is transformed back to electric energy. Therefore, SMES systems are expected to have large energy and power densities, high storage efficiency (>90%), and quick response time (near zero), because of the characteristics of the superconducting coil. Other energy storage systems, such as pumped hydro or compressed air, have a substantial time delay associated with converting stored mechanical energy back into electricity, as well as lower efficiency. SMES is applicable to a wide range of capacity and end uses, including load levelling and grid stabilizing, as well as applications as a power compensator and frequency regulator.

Technical status

SMES systems can store electric energy as magnetic energy without conversion to other forms of energy. Therefore, it has high efficiency (>90%) and an extremely fast response time. Commercially, small-scale superconducting magnets have been applied to MRI and NMR. Additionally, large-scale superconducting magnets have been developed for fusion power plants such as Tokamak type and particle detectors. Furthermore, high-content T_c oxide high-temperature superconducting materials have been demonstrated. With these materials, coils of greater than 20 Tesla (T) can be kept below 20°K. In strictly technical terms, it seems that the breakthrough technologies needed for SMES, such as large-scale coils, superconducting materials and cryogenic cooling, are available.

Assuming a unit capacity of 100MW to 200MW per system, three application areas can be identified according to the stored energy as shown in Figure A.40. They are summarized in Table A.9.

Figure A.40: Relationship between applications, output capacity and stored energy in SMES systems



Source: RASMES (Research Association of SMES), Japan 2009.

Table A.9: Comparison of the applications of SMES systems

	Several MWh size	100 MWh size	GWh size
Applications	Frequency regulator Power compensator	Load leveling for peak demand	Daily load leveling
Capacity	100-200 MW		
Compensable Time	100 sec	0.5-1 hr	5-10 hr
Storage Energy	3 - 6 MWh	50 - 100 MWh	0.5 - 2 GWh
Estimate of necessary coil numbers for one SMES system, when half of the total stored energy is available. These numbers are not the product of SMES coils by 2050.			
Unit coil: 100kWh	60-120	-	-
Unit coil: 1 MWh	6-12	100-400	-
Unit coil: 10 MWh	-	10-40	100-400

Source: RASMES (Research Association of SMES), 2009.

1. Application 1 as a frequency regulator and power compensator (period of a few minute): The small-scale SMES systems of several MWh will be applied as a frequency regulator and power compensator to stabilize the power grid. Such systems are effective to mitigate power variation of 30s to several minutes from renewable power sources. To be used instead of governor-free operation of hydro power plants.
2. Application 2 for load levelling (period of a 30 min to 1h): The SMES systems will stabilize networks affected by introducing large numbers of wind power generation plants for a

period up to 1h. Load levelling for more than 1h will be performed by output power control of high-efficiency thermal power plants.

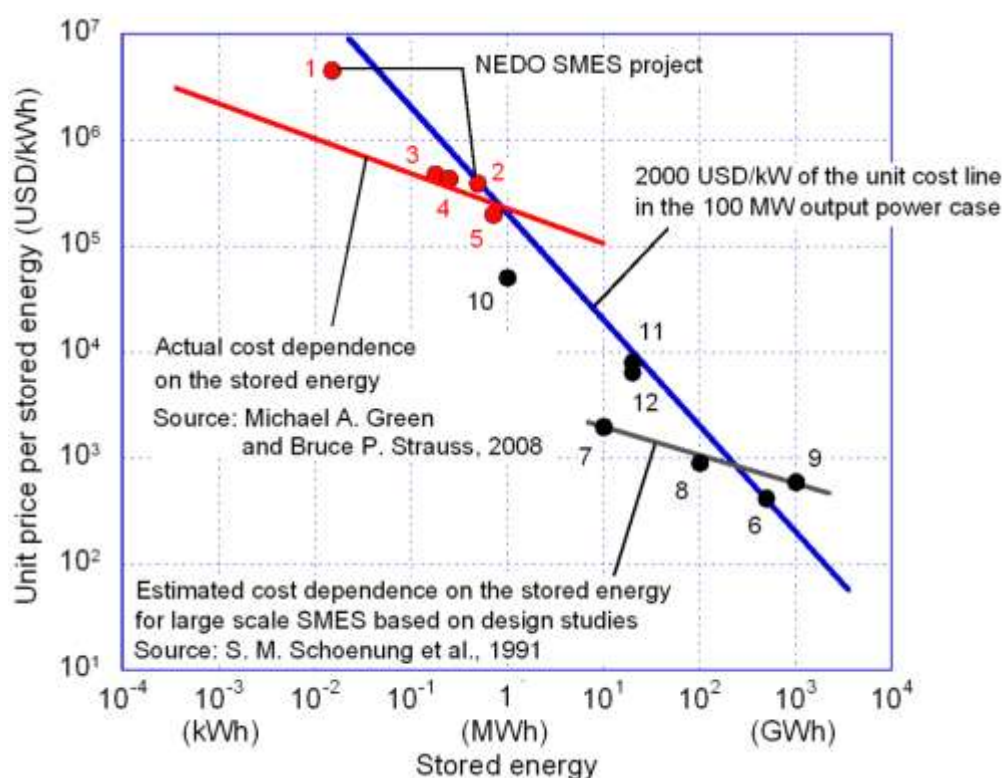
- Application 3 for daily load levelling (5 to 10h): The large-scale SMES systems of GWh size will be applied to daily load levelling. Usually, the daily start and stop operation of a thermal power plants is associated with energy loss. If the unit price per kW of SMES is lower than the price of thermal power plants, SMES would be installed instead in the interest of CO₂ reduction.

Cost status

Total capital cost is evaluated to be 380 - 490USD/kW for a 1-MW SMES system (EPRI, 2009). On the other hand, according to NEDO projects during 1993-2003, the projected future costs of SMES for grid stabilization (100 MW/15kWh) and power compensation (100 MW/500kWh) are 690 USD/kW and 1970 USD/kW, respectively.

Figure A.41 shows the relationship between CAES storage energy and unit price as predicted by NEDO, assuming development of practical coils. Based on those results, if the output power of SMES system is 100 MW, the target cost, including capital cost and operating cost for 30 years, will be 2000USD/kW. This target was successfully achieved in field tests of a 10-MVA/20-MJ SMES prototype. However, in the case of large-scale SMES systems, since cost estimates for SMES systems larger than 1MWh are based on conceptual design studies, the unit cost per kWh should also be evaluated.

Figure A.41: Cost estimation of SMES as a function of stored energy



Source: RASMES (Research Association of SMES), Japan, 2009.

Operational status

As an example of commercial SMES uses, D-SMES (Distributed SMES) and PQ-IVR (Power Quality Industrial Voltage Regulator) systems were deployed by ACCEL in the United States. The former is for grids and the later is for end users. The specifications of the D-SMES system are:

stored energy of 2.1MJ; average power of 200 kW; maximum power of 800 kW; carry-over time >8s. The D-SMES system was installed in a facility operated by Wisconsin Public Service Co., and has been successfully operated to accept a voltage reduction due to a ground discharge.

In the United States and Japan, several demonstration SMES plants have been tested. As an example, the specifications and photo of mid-scale SMES uses for grid stabilization by Chubu Electric Power Company are shown in Table A.10 and Figure A.42. This system was built and installed at the Nikko Plant of Furukawa-Nikko Power Generation Inc. for a field test. Basic design data for larger-scale SMES systems will be evaluated based on the performance test results of this system.

Figure A.42: Photo of 20-MJ SMES



Source: NEDO, 2008.

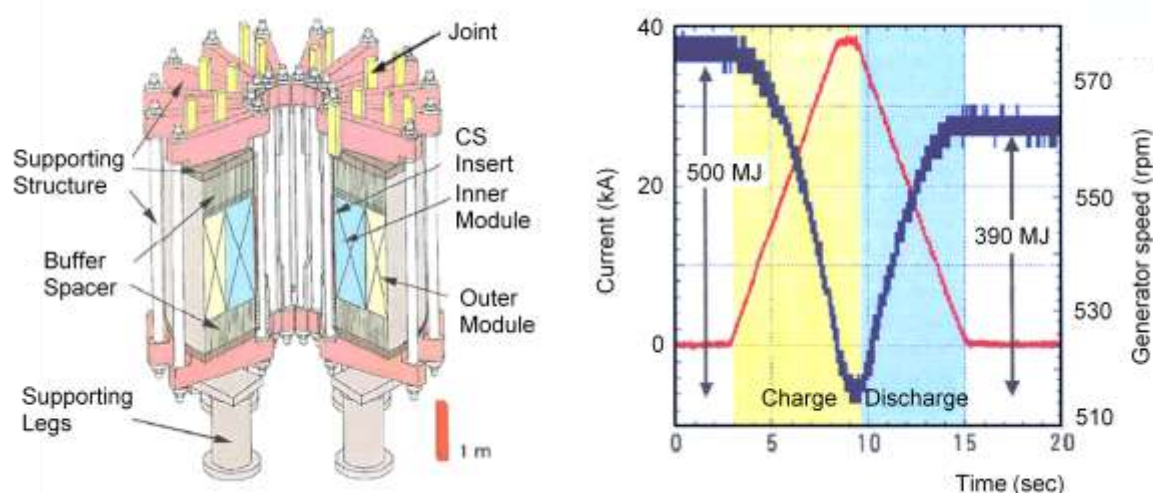
Table A.10: Specifications for mid-scale SMES

Parameters	Specifications
Installed capacity	10 MW
Stored energy	20 MJ
Superconductor material	NbTi
Coolant inlet temperature	4.17 K
Operation current value	1350 A
Operating voltage	1.1 kV
Maximum magnetic field	4.4 T

The central solenoid model coil (CSMS), which was developed as one of the technical design activities for the International Thermonuclear Experimental Reactor (ITER) Project, is 3.6m in diameter and 2.8m in height, generates magnetic induction of 13T at a current of 46kA, and has stored energy of 641MJ. The solenoid is a CIC conductor made of Nb₃Sn. The Naka Laboratory of the Japan Atomic Energy Research Agency (formerly the Japan Atomic Research Institute) successfully carried out an energy transfer experiment between the coil and a flywheel generator (P-MG, 500MVA - 1300MJ) for JT-60 using the JT-60 poloidal field coil power supply. A schematic of CSMS is shown in Figure A.43 left. Energy totalling 450 MJ was transferred back and forth in 12s, as shown in Figure A.43 right.

The transfer efficiency was estimated as 87% one way and 78% round-trip based on the change of the rotational speed of the flywheel generator, higher than that of pumped hydro storage. The main purpose of the experiment was development of the superconducting pulse coil for ITER. However, the experiment also verified that the both SMES and flywheel technologies are practical for use in a large electric power system and offer high efficiency. On the other hand, the large-scale superconducting magnet, which is a key technology of SMES, has much experience in nuclear fusion devices and particle detectors (Table A.11). The superconducting magnet of ITER represents the mid-size SMES system of 10MWh.

Figure A.43: Large electric power transfer experiment between the CSMC and the JT-60 flywheel, with schematic illustration of CSMC (left) and results of large electric power transfer (right).



Sources: T. Ando, H. Tsuji, 2001 (left); T. Terakado et al. (right).

Table A.11: Passed results and developing plans of the superconducting magnet

Projects	Magnet type	Energy (GJ)	Year of the completion	Applications
BEBC	Solenoid	0.8	1973	Particle detector
LCT	Toroid	0.9	1985	Fusion device
LHD	Helical	0.9	1997	
CSMC	Solenoid	0.64	2000	
ATLAS	Toroid	1.1	2007	Particle detector
CMS	Solenoid	2.6	2007	
LHC	Dipole and Quadrupole	8.8	2008	Particle accelerator
ITER	Toroid	41	2014	Fusion device

Production status

Commercial small-sized SMES systems have been released by ACCEL in the United States. Larger-scale SMES systems are not yet available commercially.

Regulation status

The shielding required for the intense magnetic field is a limiting factor in siting. Niobium is mainly mined in Brazil and Canada, and is in stable supply.

Future Scenarios

The forecast for SMES and the related applications cited above are summarized in Figure A.44.

1) The Present to 2020

The 1GJ class large superconducting coils have been sufficiently developed for use in particle detectors used in high-energy physics experiments and nuclear fusion. Moreover, a 10MVA/20MJ SMES system for electric power network stabilization has been developed in a Japanese government project managed by NEDO. It is possible at present to introduce SMES systems for frequency control, load variation compensation, and power generation variation compensation (Application 1).

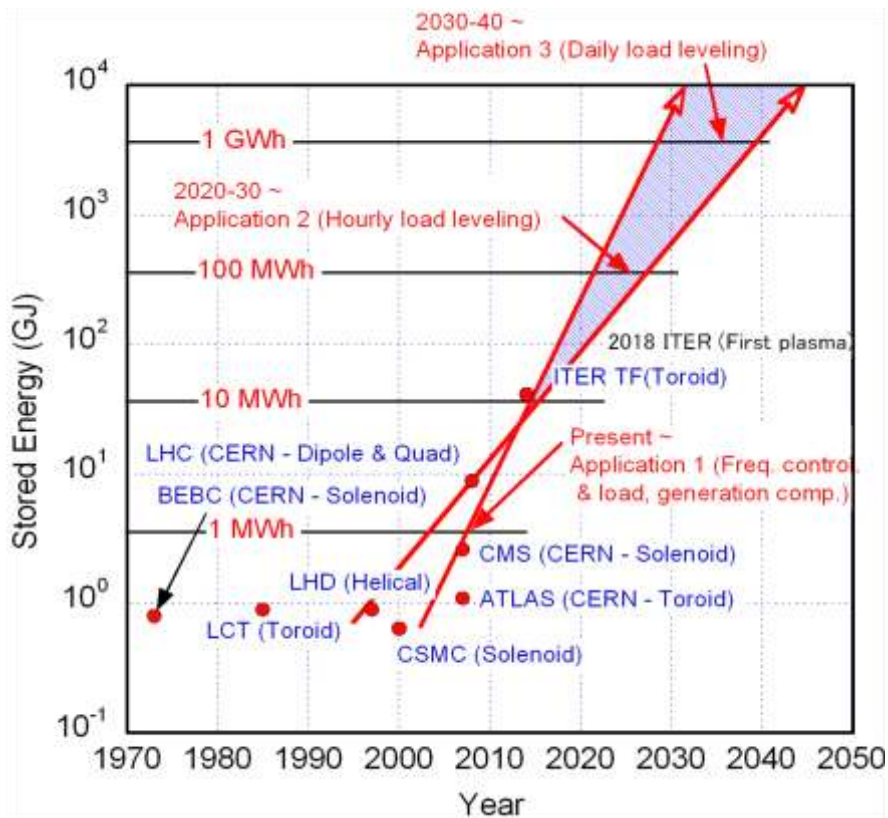
2) 2020 to 2030

Since the first plasma experiment of ITER is planned for 2018, the technologies for refrigeration and electric power conversion systems will be established for large superconducting coil systems. Therefore, it is expected that 100MWh class SMES systems for load levelling (peak cut) can be introduced during 2020-2030.

3) 2030 to 2040

By this decade, sufficient operating experience with the ITER superconducting coil will be available, and the development of 100-MWh class SMES systems for Application 2 will also have been achieved. It is expected that 1GWh class SMES systems for daily load levelling (Application 3) can be installed during 2030-40.

Figure A.44: Past results of large size superconducting magnet and road map of SMES



Source: RASMES (Research Association of SMES), Japan, 2009.

Flywheel Systems

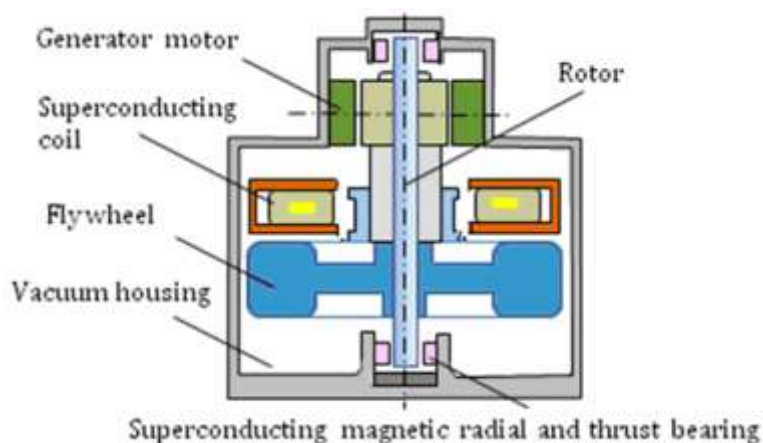
Concept

With a flywheel, electrical energy is stored as rotating energy. To reduce mechanical losses due to the bearings, a magnetic bearing—ideally a superconducting magnetic radial and thrust bearing—is used in current fly wheel storage systems. During charging, the rotating speed of the flywheel increases to 30,000 to 40,000RPM. During discharging of electric power, the rotating speed of the flywheel decreases as the spinning mass of the flywheel turns a generator that produces electricity.

Structure

Flywheel storage systems consist of the flywheel, superconducting magnetic radial and thrust bearing, superconducting coil, and generator motor. To reduce energy loss, which is caused by friction between air and the flywheel, a vacuum housing is used (Figure A.45). In advanced systems, a superconducting magnetic radial and thrust bearing supports the flywheel. In the vertical direction, the flywheel is magnetically levitated by the superconducting coil, which generates a strong magnetic field that keeps the flywheel spinning without friction.

Figure A.45: Principle and structure of flywheel



Features

During charging of flywheel systems, electric energy is transformed to rotating energy through the flywheel; during discharging, the rotating energy is transformed back to electric power. Generally, the rotational energy is proportional to the flywheel's diameter cubed. Note that because losses such as windage loss and bearing loss are generally proportional to the diameter or the square of the diameter, a larger flywheel has a theoretical advantage and higher efficiency of energy storage. To reduce the windage loss, the housing is maintained in a vacuum. In a recent advance to reduce the bearing loss, superconducting bearing technologies are being applied to the flywheel. Small flywheels have already been released as commercial products, especially for UPS systems.

Technical status

The rotating energy stored by a flywheel can be calculated as:

$$E = \frac{1}{2} I \omega^2, \quad (\text{A.6})$$

where E is the energy (J), I is moment of inertia for the thin-rim cylinder (H), and ω is the angular velocity (rad/s). Since the moment inertia I is proportional to the mass of the flywheel, achieving larger storage capacities requires higher angular velocities.

Additionally, the energy of the flywheel may be expressed as:

$$E = K_s \sigma V, \quad (\text{A.7})$$

where K_s is shape factor (-), σ is the maximum circumferential stress influencing the flywheel (N/m^2), and V is the volume of the flywheel (m^3). In addition, the bearing is influenced by the weight W of the flywheel, which is written as

$$W = \gamma V, \quad (\text{A.8})$$

where γ is the bulk density. To reduce the bearing load, light weight is preferred. In terms of the mechanical properties of the flywheel material, a larger specific intensity σ / γ is preferable per equations A.7 and A.8. Recently, glass fibre reinforced plastic (GFRP) and carbon fibre reinforced plastic (CFRP), which have higher and larger specific intensities than titanium alloy, are being used (Table A.12).

Table A.12: Mechanical properties of flywheel materials

Parameters	γ (kg/m^3)	σ (N/m^2)
Titanium alloy	4500	10.2×10^6
GFRP	2000	14.8×10^6
CFRP	1600	31.6×10^6

Cost status

Investment costs based on existing flywheel UPS systems are 800 - 2700USD/kW and 2.2-22USD/kWh (Table A.13). The cost of a 10-MW class flywheel system was estimated to be 3695 - 4315USD/kW by EPRI (2009).

Table A.13: Comparison of investment costs in some actual flywheel UPS systems

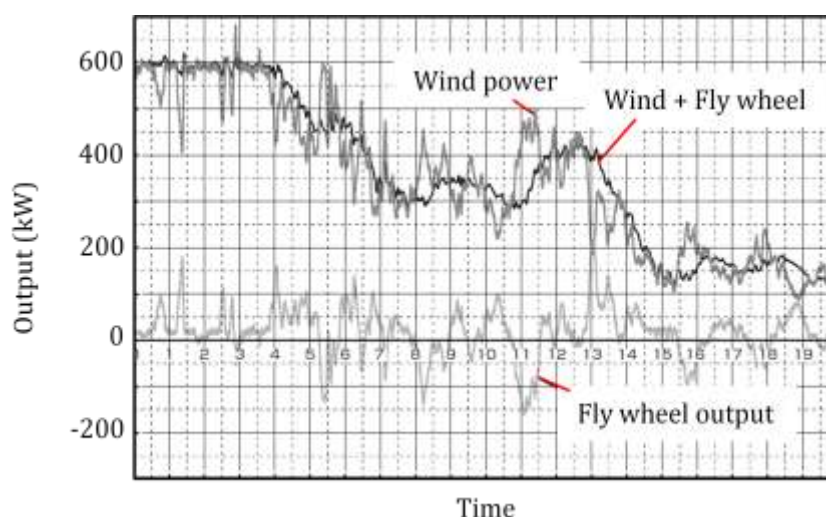
Specifications	Cost (USD/kW)	Cost (USD/kWh)
1670 kVA \times 10 s	800	2.2
250 kVA \times 15 s	988	4.1
15 kVA \times 30 s	2667	22.2
45 kVA \times 30 s	1778	14.8

Operational status

Table A.14 compares the specifications of some actual flywheel products. Several hundred kilowatt-class flywheels have been released commercially. Fuji Electric demonstrated wind power operation with a 250kWh flywheel system manufactured by Beacon Power. Figure A.46 shows operational results of that demonstration, in which variations in wind power output were mitigated with the flywheel. Flywheels at least appear to be useful for mitigating wind power variations for individual wind turbines. Beacon Power estimated that with a matrix of flywheels, better output stabilization at the megawatt level would be feasible.

Table A.14: Comparison of specifications of existing flywheel UPS systems

Manufactures	Countries	Specifications
Satcon	USA	2200kVA × 12 sec
Hitec	Netherlands	2000kVA × 10 sec
Piller	Germany	1100kVA × 15 sec
Caterpillar/Active Power	USA	240kW × 14 sec
Pentadyne	USA	120kW × 20 sec
Trinity	USA	100kW × 15 sec
Beacon Power	USA	2kW × 3 hours
		100kW × 15 min
		250kW × 25 sec
		250kW × 6 min

Figure A.46: Operational results of wind power with flywheel

Source: Fuji Electric, 2007.

The world's largest flywheel is shown in Figures A.55 and A.56. The flywheel consists of six disks that have each a diameter of 6.6m and a thickness of 0.4m. One disk weights over 107 tones. During charging, which lasts 6 min, the rotating speed is increased from 70% to 100% with a thyristor system of 19MW. The energy discharge time is approximately 30s. During this period the flywheel supplies up to 160MW of power. The system has been in operation since 1985.

More than 10,000 charge-discharge cycles, and 5000h of operation were achieved with this flywheel. After 5 years operation, no mechanical deterioration of the system was observed. In this system, the energy density of the flywheel body was $50\text{J}/\text{cm}^3$, which would correspond to the energy density of a pumped hydro system with a 5000m drop head. Even for the whole system, the energy density was $19.5\text{J}/\text{cm}^3$, which corresponded to a pumped hydro system with a 2000m drop head. Thus, the flywheel is a high-performance energy storage system with high energy density.

Figure A.47 (left): Cut-away model of the system
Figure A.48 (right): Photo of world's largest flywheel



Source: R. Shimada, 1994.

Okinawa Electric Power Company and Toshiba have developed and installed a flywheel system called ROTES. It is used in the Okinawa power grid for frequency control. It has a 23MW capacity with rotational speeds of 600 ± 15 RPM, and has been in operation since 1996. Frequency in a grid is influenced by a balance between electric demand and supply. In a grid with a small capacity, such as the Okinawa grid, frequency is very sensitive to that balance. The flywheel system has contributed to good frequency control, particularly since the system is equipped with an exclusive processor operation similar to that seen in a voltage regulator with SVC (Static Var Compensator).

As an example of a commercially available flywheel system, Beacon Power has released a frequency regulator called the Smart Energy Matrix, based on a concept for a multi-flywheel-based energy storage system comprised of 100kW/25kWh units. The first commercial 20MW Smart Energy Matrix is under development in Stephentown, New York. Figure A.49 shows the facility at Beacon headquarters and the concept of a megawatt-class system. The flywheel is designed for 20 years of operation, and 12 parameters of flywheel and system performances can be monitored remotely. The discharge time of 0.25 hrs seems to be adequate to regulate both electricity frequency and short-term variations of wind power output.

Figure A.49: Matrix flywheel system, showing test facilities at Beacon headquarters (left) and an illustration of the basic concept of a megawatt-scale flywheel-based energy storage system (right).



Source: Beacon Power, 2009.

As a different example, the flywheel systems are also applied to 100-500kVA medical-grade power systems by Pentadyne Power Corporation and Mission Critical power Solutions. This system consists of UPS system with flywheel system. The new system is designed to deliver premium-grade power for CT scanners, linear accelerators and MRIs, as well as radiography, mammography and angiography equipment.

Production status

The production of small-scale flywheel systems is increasing gradually, in parallel with increasing UPS needs. The flywheel UPS has a major advantage over lead-acid battery UPSs because it is virtually maintenance free while conventional batteries must be exchanged every few years, so that maintenance costs equal 70% of the initial cost. Also, the efficiency of a flywheel UPS is higher than that of a lead battery UPS. Because of these advantages, the use of small-scale flywheel UPS should grow significantly in the future. At least five manufacturers sell small-scale flywheels. Increasing production volumes will result in a gradual cost reduction.

Regulatory status

Flywheels do not include hazardous materials covered under fire safety laws. There is a possibility that a flywheel may be damaged by stress fatigue. Also, noise and vibration are concerns.

Future Scenarios

With commercial applications in UPS system and individual wind turbines, flywheel systems are at a practical stage of development. To promote their installation, it is important to put larger flywheel systems to practical use. Several efforts are underway to improve their efficiency.

As described above, the main energy losses of the flywheel are due to windage loss and bearing loss. The latter limits flywheel applications to short-term storage. With the development of high-temperature superconducting materials, superconducting bearing technologies can be applied to flywheels.

The Railway Technical Research Institute in Japan has developed and evaluated a superconducting flywheel bearing for use with trains. The bearing consists of a superconducting magnet and a superconducting bulk body. Under a static load, a levitation force of 10kN has been achieved. With the body of revolution with 5kN thrust, stable magnetic levitation of the body was confirmed at a rotational rate of 3000RPM.

ANNEX 2: NUMERICAL ALGORITHMS

Details of Simulation Models

In this Annex, details of the simulation algorithm are described.

1) Daily Demand Curve in Western Europe

The empirical formula for the daily demand was estimated as follows based on the actual data summarized in Figure 14:

$$D.D(T) = -0.0000001653T^6 + 0.0000125483T^5 - 0.0003441792T^4 + 0.0039132322T^3 - 0.0140985124T^2 - 0.0051670654T + 0.8326553942, \quad (\text{A.9})$$

where T is the number of each hour (e.g. 18:00 is 18, etc.). Equation (A.9) was normalized with the maximum daily demand defined as 1.0.

2) Annual Demand Curve in Western Europe

The empirical formula for the annual demand was estimated as follows based on the actual data:

$$A.D(M) = 0.3075 \times \left(\cos\left(\frac{2\pi((M-1))}{11}\right) + 5.5 \right). \quad (\text{A.10})$$

where M is the number of each month (e.g. January is 1, etc.). Equation (A.10) was normalized with the maximum monthly demand defined as 1.0. Applying the equation, the average annual demand is 0.86. In Western Europe, the summer months of June and July experience the minimum demand, as shown in Figure 15.

There is a possibility that daily and annual demand curves would vary across the years. Strictly speaking, such a variation should also be considered. On the other hand, the prediction of demand curves for the future is quite difficult. In this paper, the present demand curves were applied.

3) PV Operation Curve Model

PV output depends strongly on available daylight and weather conditions. In this working paper, the following empirical model was developed based on actual PV operational experience:

For $6 < T < 18.5$ (daytime):

$$f_{PV}(T) = -0.0000323955T^5 + 0.0012949488T^4 - 0.0133779943T^3 - 0.07745311T^2 + 2.0436509568T - 7.9849739044 \times W.F \quad (\text{A.11})$$

For $T < 6$ and $18.5 < T$ (night time):

$$PV(T) = 0$$

where T is the number of each hour (e.g. 18:00 is 18, etc.) and W.F is a factor due to the weather. It is defined as:

$$\begin{aligned} \text{Fine weather: } W.F &= 1.0, \\ \text{Cloudy weather: } W.F &= 0.65, \end{aligned}$$

Rainy weather: $W.F = 0.16$.

The PV operation curve shown in Figure 17 was estimated based on equation (A.11). In this simulation, the effect of power variations due to variable PV output was omitted. Strictly speaking, the empirical formula should be different for different regions, but in this paper equation (A.11) was applied to all regions considered.

4) Wind Speed Model

From the actual wind speed data shown in Figure 18, the probability density distribution was simulated well with the Weibull distribution, expressed as:

$$f(V) = \frac{k}{c} \left(\frac{V}{c}\right)^{k-1} \exp\left(-\left(\frac{V}{c}\right)^k\right) \quad (\text{A.12})$$

where k is a profile coefficient, c is a scale coefficient, and V is the wind speed. When $k=2$, then the distribution $f(V)$ is a Rayleigh distribution:

$$f(V) = \frac{\pi}{2} \left(\frac{V}{\bar{V}^2}\right) \exp\left(-\frac{\pi}{4} \left(\frac{V}{\bar{V}}\right)^2\right), \quad (\text{A.13})$$

where \bar{V} is the average of the wind speed. In this working paper, this Rayleigh distribution was used to represent the distribution of the wind speed. The probability function was given as an integrated equation.

$$F(V) = \int_0^V f(V) dV = 1 - \exp\left(-\frac{\pi}{4} \left(\frac{V}{\bar{V}}\right)^2\right) \quad (\text{A.14})$$

When \bar{V} is changed from 0 to 1 with a uniform random number X , the random number V , which obeys the Rayleigh distribution, is given as:

$$V = \frac{2\bar{V}}{\sqrt{\pi}} (-\ln(1-X))^{0.5}. \quad (\text{A.15})$$

The wind speed and distribution shown in Figure 19 were calculated with equation (A.15).

5) Wind Turbine Operation Model

As is well known, the output of a wind turbine may be estimated as:

$$P_w = \frac{C_w \rho A}{2} V^3 = \frac{C_w \rho \pi R^2}{2} V^3, \quad (\text{A.16})$$

where A is the cross-sectional area of an individual wind turbine's blades, ρ is the density of the air, C_w is the efficiency, R is the radius of the wind turbine, and V is the wind speed. In actual operation, output is usually regulated under high wind speed conditions, as shown in Figure 20. Due to variations in wind speed, the actual wind power is usually lower than the theoretical output. The ratio of the actual power to the theoretical maximum power throughout a year is called the capacity factor, which is usually 20%-40%. In this simulation, the estimated capacity factor was approximately 35%, close to the actual value.

To simulate the actual output shown in Figure 20, the following operation curve was applied:

$$\begin{aligned}
 0 < V < \text{Cut-in speed:} & \quad f_w = 0 \\
 \text{Cut-in speed} < V < \text{Base load speed:} & \quad f_w = C_0 \cdot V^3 \\
 \text{Base load speed} < V < \text{Cut-out speed:} & \quad f_w = C_{base}
 \end{aligned} \tag{A.17}$$

In equation (A.19), the following should be satisfied:

$$C_0 \cdot (V_{base})^3 = C_{BASE}, \tag{A.18}$$

where V_{base} is the minimum speed in the regulation operation.

In the simulation, the procedures described in models 1) and 2) concerning daily and annual load curves were applied for other areas. In addition, the procedures described in models 3) through 5) concerning PV and wind power were applied for the appropriate technologies.

Simulation Algorithm

Using the equations and methods described above, Figure A.50 summarizes the flowchart used in this working paper.

Figure A. 50: Flowchart used in the simulation



The Electricity Generation Mix in Various Countries

To evaluate the results depicted in Figure 34, the following conditions based on BLUE Map scenario were used:

Table A.15: Comparison of the share of PV and wind power

Area	Shares(2010)		Shares(2050)	
	PV Power (%)	Wind Power (%)	PV Power (%)	Wind Power (%)
AFR	0	0.8	9.0	4.0
AUS	0.4	2	0	27.7
CAN	0	0.6	1.3	13.6
CHI	0	0.8	3.2	16.8
CSA	0	1.3	5.3	15.7
EEU	0	0.1	0	4.3
FSU	0	0.8	0.7	5.3
IND	0	1.8	10.7	3.6
JAN	0.7	0.5	9	9.7
ODA	0	1.2	8	5.3
USA	0.1	1.6	11.3	8.7
WEU	0.1	9.8	4.6	25.4

Recommendations for Future Work

In this working paper, only the effect of short-term power variation was estimated. Estimation of long-term power variation should be a future task. To consider the long-term variation of wind speed, the average of the wind speed in Equation (A.13) should also vary across time. As a rational assumption, the average of wind speed during a long time scale should satisfy the Weibull distribution. With double Weibull distributions for the short- and long-term periods, the effect of long-term power variation should be estimated.

In this working paper, each geographical area was treated as a point approximation. Strictly speaking, the structure and status of the power grid should be considered. In the present simulation, each area has sufficient grid resources to transmit excess power generated by the renewable resources within it. If there is a shortage in the capacity of the power grid in particular areas, then the necessary capacity of energy storage should be increased further. Also, grid losses should be considered. To account for actual grid capacities and losses, larger-scale simulation based on the grid network simulation should be applied to enable an effective analysis of grid stability.

In this working paper, power variations based on PV generation were also omitted. Including them would increase the necessary capacity of energy storage. There is currently little statistical data on PV power variations. Over large areas, it might be close to a kind of white noise, in which case, after the magnitude of the power variations were estimated, it could be simulated well with uniform random numbers. In the case of PV power, the smoothing effect observed with wind power is not as distinct. These issues are important topics for future work.

ANNEX 3: COMPARISON WITH OTHER SCENARIOS

This working paper focused on the BLUE Map scenario in which contribution of 4.6% for PV and 25.4% for wind power are assumed for 2050. On the other hand, recent analysis (Solar Europe Industry Initiative: SEII) presented by Mr Anton Milner, CEO of Q-Cells, at the EU Sustainable Energy Week (Brussels, 11.02.2009) suggests the prospects of a much higher solar PV contribution to energy generation. In the SEII scenarios, PV contributes 12% of the European electricity demand by 2020, and 20% by 2030. Sensitivity analysis will play an important role in comparing the results of such discrepancies. This simulation and Annex assume a 12% share in 2020.

Analysis Conditions

Table A.16 shows the analysis conditions in WEU in 2020. In the SEII scenarios, components of the power generation mix in 2020 other than the 12% PV share were not indicated. Therefore, two analytical conditions based on the BLUE Map scenario were estimated. Assuming a constant 12% PV share, Case 1 assesses the impact of a smaller share of wind power, while Case 2 assesses the impact of a smaller share of middle power. Annual electricity demand was assumed to be 3072TWh, based on the BLUE Map scenario.

Table A.16: Analysis conditions in WEU in 2020

Power generation type	BLUE Map scenario	SEII scenarios	
		Case-1	Case-2
Base load (%)	41.3		41.3
PV power (%)	0.6		12.0
Wind power (%)	27.1	15.7	27.1
Middle load (%)	31.0	31.0	19.6

Simulation results

The present simulation model was applied to the SEII scenarios in 2020, and the balance of demand and supply calculated for the minimum load conditions observed in June. The influence of a high share of variable renewable power is most pronounced under the minimum load. The net variation ratio was assumed to be 15%.

Figure A.51 compares the daily balances of demand and supply in each scenario. Figures A.51 left and right show the balances during a typical day, and time-averaged balances during 30 days, respectively. In Cases 1 and 2, the adjustability of the middle load clearly decreases with increasing shares of PV. In particular, in Case 2, since the (PV + wind) output exceeds demand from 06:00 to 18:00, curtailment should be required. This represents a situation similar to the case of the United States in 2050 (Figure 33).

Table A.17 compares the necessary energy storage capacities for each scenario. In Case 1, since the wind share is less than that in the BLUE Map scenario, the necessary energy storage capacity is also lower. On the other hand, in Case 2, as the adjustability of the middle power decreases, the necessary capacity increases. In particular, a great deal of energy could be dumped due to curtailment.

In a future work, the effect of power variations due to PV power should be considered, and could increase the amount of energy storage capacity required. In addition, the extent to which PV power benefits from the smoothing effect must be studied. Employing demand-side management with smart grids might be an effective way to utilize the damped energy.

Measurement and analysis of wind and PV power will allow the amount of storage capacity needed to maximize their benefits to be estimated with great accuracy.

Figure A. 51: Comparison of BLUE Map and SEII scenarios in WEU for 2020, showing results in one day (left column) and time-averaged results (right column).

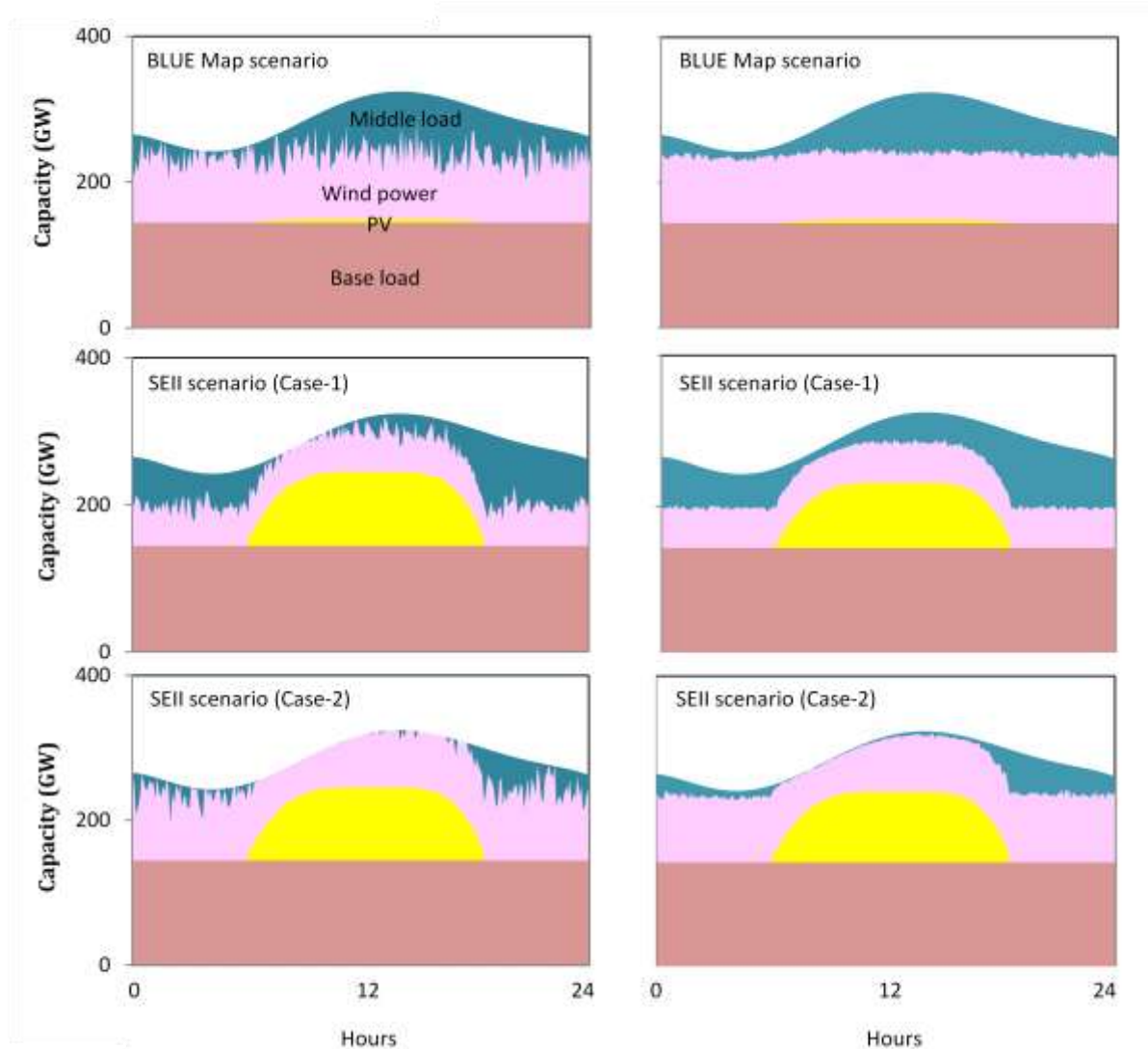


Table A.17: Comparison of necessary energy storage capacities in WEU in 2020 under different scenarios

Scenarios	BLUE Map	SEII (Case 1)	SEII (Case 2)
Capacities (GW)	39.8	31.3	42.8



International
Energy Agency

Online bookshop

Buy IEA publications
online:

www.iea.org/books

PDF versions available
at 20% discount

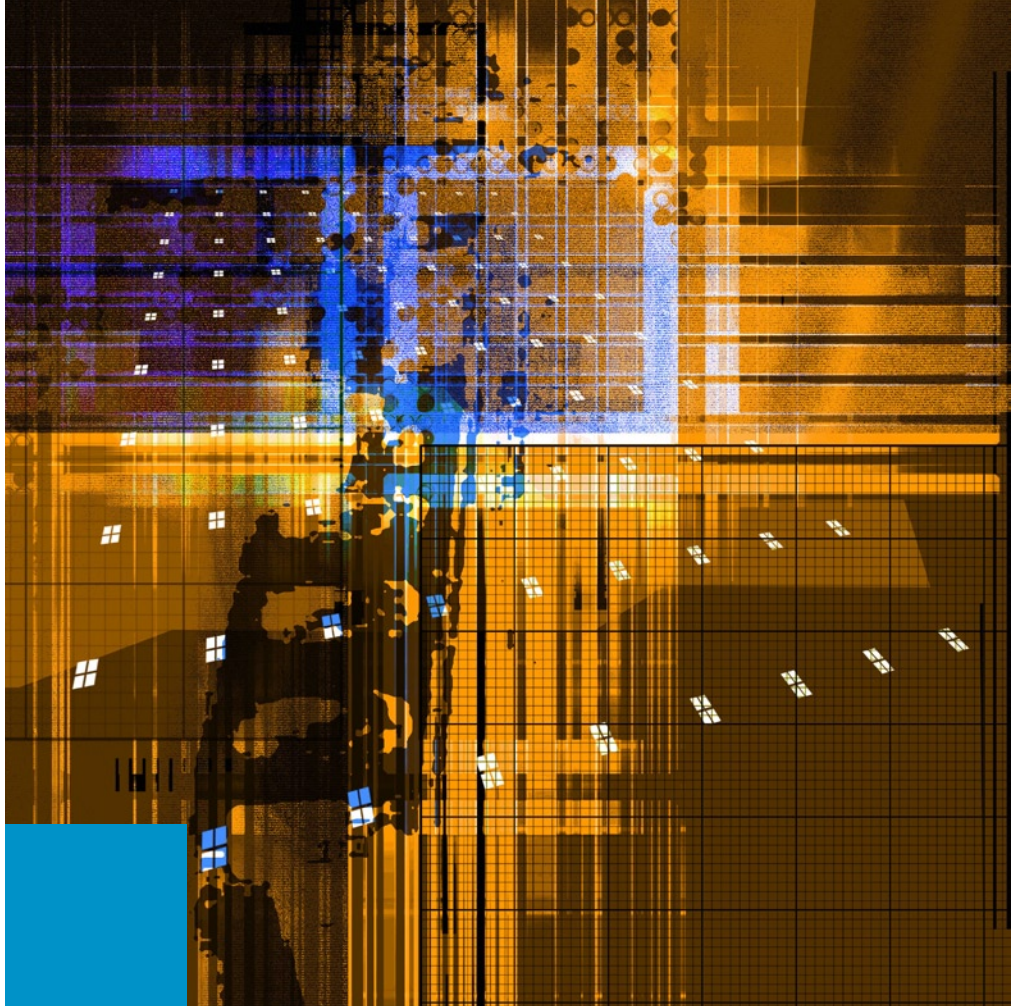
Books published before January 2008
- except statistics publications -
are freely available in pdf

International Energy Agency • 9 rue de la Fédération • 75739 Paris Cedex 15, France

iea

Tel: +33 (0)1 40 57 66 90

E-mail:
books@iea.org



INTERNATIONAL ENERGY AGENCY

9 RUE DE LA FÉDÉRATION
75739 PARIS CEDEX 15

www.iea.org